ADDIS ABABA UNIVERSITY

SCHOOL OF GRADUATE STUDIES

INSTITUTE OF TECHNOLOGY

ELECTRICAL AND COMPUTER ENGINEERING DEPARTMENT

Low Complexity MIMO−OFDM Receivers for Achieving Near Optimal Performance

By

Nadew Adisu

Advisor

Dr.-Ing Hailu Ayele

A Thesis Submitted to Addis Ababa University, School of Graduate Studies, Institute of Technology, in Partial Fulfillment of the Requirements for the Degree of Masters of Science in Electrical Engineering

July, 2011

Addis Ababa, Ethiopia

ADDIS ABABA UNIVERSITY SCHOOL OF GRADUATE STUDIES

INSTITUTE OF TECHNOLOGY

ELECTRICAL AND COMPUTER ENGINEERING DEPARTMENT

Low Complexity MIMO−OFDM Receivers for Achieving Near Optimal Performance

By

Nadew Adisu

Approval by Board of Examiners

_____	_____
Chairman, Dept. Graduate Committee	Signature
Dr.-Ing Hailu Ayele	_____
Advisor	Signature
_____	_____
Internal Examiner	Signature
_____	_____
External Examiner	Signature

Declaration

I, the undersigned, declare that this thesis is my original work, has not been presented for a degree in this or any other university, and all sources of materials used for the thesis have been fully acknowledged.

Nadew Adisu _____

Name Signature

Place: Addis Ababa

Date of Submission: _____

This thesis has been submitted for examination with my approval as a university advisor.

Dr.-Ing Hailu Ayele _____

Advisor's Name Signature

Dedicated to Isayas Arusi

Acknowledgements

First and foremost, I would like to express my sincere gratitude to my respected advisor **Dr.-Ing Hailu Ayele** for his invaluable advice, incessant guidance and continuous encouragement throughout the course of my study and research. His ample knowledge, rigorous working attitude, honest personality and eagerness for new technology are always inspiring me as a model to follow in my future study and work.

As well, I would like to thank all the people of ECED for providing such an excellent education and research environment.

Finally, I would like to express my deepest appreciation to my family and colleagues. My special thanks go to a friend of mine **Isayas Arusi,** to whom this thesis is dedicated, for his constant encouragement, support and unconditional friendship.

Contents

Acknowledgements i

List of Figures v

List of Tables vii

Acronyms and Abbreviations viii

Abstract x

Chapter 1: Introduction 1

1.1 Motivation and Background 1

1.2 Problem Statement 3

1.3 Literature Review 3

1.4 Objective of the Thesis 6

1.4.1 General Objective 6

1.4.2 Specific Objectives 6

1.5 Major Assumptions Considered in the Thesis 6

1.6 Notations used in the Thesis 7

1.7 Organization of the Thesis 7

Chapter 2: Multiple−Input−Multiple Output (MIMO) System Model 8

2.1 Introduction 8

2.2 MIMO System Model Description 8

2.3 MIMO Channel Model 10

2.3.1 Wideband MIMO Channel Model 12

2.3.2 Quasi−Static Discrete Time Channel Model 14

2.3.3 Narrowband MIMO Channel Model 16

2.4 Spatial Correlation 17

2.5 MIMO−OFDM systems 18

Chapter 3: Conventional MIMO Signal Detection Techniques 21

3.1 Introduction 21

3.2 Linear Detection Schemes 21

3.2.1 Zero Forcing (ZF) Linear Detector 22

3.2.2 Minimum Mean Square Error Method (MMSE) 23

3.3 Non-linear Detection Schemes 24

3.3.1 SIC –Successive Interference Cancellation Detection Method 25

3.3.1.1 SIC with V−BLAST 25

3.3.1.2 SIC with QR Decomposition 27

3.4 Complexity Analysis 29

3.4.1 Complexity of Zero Forcing (ZF) Algorithm 30

3.4.2 The Complexity of MMSE Algorithm 30

3.4.3 Complexity of ZF with V−BLAST 31

3.4.4 Complexity of MMSE with V−BLAST 32

3.4.5 Complexity of Sorted QR Decomposition Detection Method (SQRD) 33

Chapter 4: State−of−the Art MIMO Detection Techniques 34

4.1 Introduction 34

4.2 Maximum Likelihood Detection Method 35

4.3 Sphere Decoding Algorithms (SDAs) 37

4.3.1 Search Radius Setting Strategies 40

4.3.2 Depth First Sphere Decoding (DF SD) 42

4.3.3 Breadth First Sphere Decoding (BF SD) 43

4.4 Hybrid Sphere Decoding Algorithm (H−SDA) 46

4.5 Complexity Analysis 50
4.5.1 Complexity of Maximum Likelihood Detection (MLD) 50
4.5.2 Complexity of Sphere Decoding Algorithms 51
4.6 Summary of Complexity Analysis 54
Chapter 5: Simulation Results and Discussion 58
5.1 Introduction 58
5.2 Simulation Setup 58
5.3 Performance Comparison for Conventional MIMO Detection Schemes 61
5.3.1 Effect of Spatial Correlation 64
5.3.2 Complexity Comparison 66
5.4 Performance Comparison for the state−of−the Art MIMO Detection Schemes 68
5.4.1 Performance of DF SDA 68
5.4.2 Performance Comparison for k−best SDA 70
5.4.3 Performance Comparison for Layer Reordered k−best SD 71
5.4.4 Performance Comparison for Dynamic k−best SD 72
5.5 Performance Comparison for the Proposed Hybrid SD 74
5.6 Performance Comparison of MIMO detection schemes in wideband systems 79
Chapter 6: Conclusions and Recommendations for Future Work 82
6.1 Conclusions 82
6.1 Recommendations for Future Work 84
Appendix A General Rules of Complexity Analysis 86
Appendix B.1 QR Decomposition Algorithm 87
Appendix B.2 Sorted QR Decomposition Algorithm 88
References 89

List of Figures

Figure 2.1 General block diagram of MIMO system model with N_t transmit and N_r receive antennas 9

Figure 2.2 A MIMO communication systems operating in a scattering environment 11

Figure 2.3 Tapped delay line channel model for time−variant channels 13

Figure 2.4 Exponentially decaying power delay profiles 16

Figure 2.5 a) Simplified block diagram of MIMO-OFDM systems b) OFDM modulation per antenna c) OFDM demodulation per antenna d) addition of cyclic prefix 19

Figure 3.1 Block diagram of linear detection schemes 22

Figure 3.2 Illustration of V−BLAST detection process for 4X4 MIMO system 27

Figure 3.3 Block diagram of SQRD based SIC 4X4 MIMO system 29

Figure 4.1 A two dimensional geometric representation of the sphere decoding 37

Figure 4.2 Search tree diagram of sphere decoding algorithm 39

Figure 4.3 Search sequence in which nodes are explored in DF SDA for a 4X4 MIMO system 42

Figure 4.4 Search order in which nodes are explored in BF SDA for a 4X4 MIMO system 43

Figure 4.5 Block diagram of the proposed hybrid Sphere Decoding Scheme 48

Figure 5.1 Simulation set up for MIMO−OFDM systems 60

Figure 5.2 BER performances of conventional MIMO detection schemes for 2X2, QPSK modulation 61

Figure 5.3 BER performance of conventional MIMO detection schemes for a 4X4, QPSK modulation 63

Figure 5.5 BER performance of conventional MIMO detection schemes for a 4 X 4, operating in a correlated (r=0.6), flat Rayleigh fading, 16−QAM modulation 65

Figure 5.9 BER performance versus SNR per receive antenna of DF SD and MLD for a 4X4, 16-QAM modulation 68

Figure 5.10 Complexity of DF SD (number of parent nodes) versus SNR per receive antenna for the two radius setting strategies 69

Figure 5.11 BER performance of k−best SDA (k=6, 8 and 10) for a 4 X 4, 16−QAM, flat Rayleigh fading channel (MMSE with SIC and DF SD are included as a reference) 70

Figure 5.12 BER comparison of normal k−best SDA and layer reordered k-best SDA for a 4 X 4, 16−QAM, flat fading Rayleigh channel 71

Figure 5.13 Computational complexity comparisons (E_{ADDs}/Symbol vector) for k−best SDA (k=6, 8 and 10), MLD and MMSE with SIC as a function of number of antennas.....72

Figure 5.14 BER comparison of normal k-best, dynamic k−best, layer reordered k−best and combined k−best SDAs for a 4X4, 16−QAM modulation 73

Figure 5.15 BER performance comparison of hybrid SD scheme with k-best SD schemes for a 4X4, 16-QAM (k=8 for normal and layer reordered, and k=11, 8 and L=2 for hybrid schemes) ...74

Figure 5.16 Average number of parent nodes for the proposed scheme as compared to the number of parent nodes for k−best SDAs for a 4X4, 16−QAM modulation.....75

Figure 5.17 Throughput versus SNR per receive antenna of the proposed hybrid scheme and the conventional k−best SDA for a 4X4, 16−QAM systems. 76

Figure 5.18 Performance comparison of hybrid SDA for different values of parameter L and k for a 4X4, 16-QAM system 77

Figure 5.19 Average throughput (Mbps) comparison of the hybrid sphere decoding for different values of L for a 4X4, 16−QAM systems (The throughput of k-best SDA included for reference) 78

Figure 5.20 BER performance comparisons of MIMO−OFDM signal detection schemes for 4X4, 16−QAM systems and wideband Rayleigh fading channel 80

List of Tables

Table 4.1 Summary of the complexity of preamble processing for MIMO detection schemes…..56

Table 4.2 Summary of the complexity of payload processing of MIMO detection schemes……..57

Table 5.1 Basic simulation parameters for narrowband MIMO systems…….59

Table 5.2 Main parameters of OFDM used in the simulation…….....79

Acronyms and Abbreviations

ADC	Analog to Digital Converter
AWGN	Additive White Gaussian Noise
Bw	Band width
BER	Bit Error Rate
BF SD/A	Breadth First Sphere Decoding/Algorithm
bpcu	Bits per channel use
bps	Bits per second
bps/Hz	Bits per second per Hertz
BPSK	Binary Phase Shift Keying
CP	Cyclic Prefix
CSCG	Circular Symmetric Complex Gaussian
CSI	Channel State Information
DAC	Digital to Analog Converter
D-BLAST	Diagonal Bell Labs Layered Space-Time
DF SD/A	Depth First Sphere Decoding/Algorithm
Eb/No	Energy per bit to Noise spectral density ratio
E_{ADDs}	Equivalent Additions
F−P	Fincke−Pohst
GI	Guard Interval
i.i.d	independent identically distributed
I/DFT	Inverse/Discrete Fourier Transforms
I/FFT	Inverse/Fast Fourier Transforms
ISI	Inter Symbol Interference
LOS	Line of Sight
Mbps	Mega bits per second
MGS	Modified Gram-Schmidt
MIMO	Multiple−Input Multiple−Output
ML	Maximum Likelihood

MLD	Maximum Likelihood Decoding
MMSE	Minimum Mean Square Error
MMSE−SIC	Minimum Mean Square Error−Successive Interference Cancelation
NLOS	Non Line of Sight
OFDM	Orthogonal Frequency Division Multiplexing
Pdf	Probability density function
PDP	Power Delay Profile
PED	Partial Euclidean Distance
QAM	Quadrature Amplitude Modulation
QoS	Quality of Service
QPSK	Quadrature Phase Shift Keying
R_{ADDs}	Real Additions
R_{MULs}	Real Multiplications
RX	Receiver
SDA/s	Sphere Decoding Algorithm/s
SDM	Spatial Division Multiplexing
S−E	Schnorr−Euchnerr
SIC	Successive Interference Cancelation
SINR	Signal to Interference plus Noise Ratio
SISO	Single-Input Single-Output
SM−MIMO	Spatial Multiplexing Multiple−Input Multiple−Output
SNR	Signal-to-Noise Ratio
SQRD	Sorted QR Decomposition
TX	Transmitter
V−BLAST	Vertical Bell Labs Layered Space-Time
WLAN	Wireless Local Area Networks
ZF	Zero Forcing
ZF−SIC	Zero−Forcing Successive Interference Cancelation

Abstract

Since the useable frequency spectrum is a scarce resource, future wireless systems should focus on new technologies that provide high spectral efficiency and improved link reliability. The combination of Multiple−Input Multiple−Output (MIMO) wireless communication with Orthogonal Frequency Division Multiplexing (OFDM) is a very promising technology to meet these requirements.

Although MIMO−OFDM systems have demonstrated very high spectral efficiency, the available capacities of these systems are not fully exploited due to lack of low complex and, at the same time, optimal signal detection scheme. To this end, after reviewing the available detection techniques, this thesis proposes a low complex MIMO signal detection technique which has near optimal performance.

It is found that among the MIMO signal detection techniques the Maximum Likelihood Decoding (MLD) has optimal performance; however, the corresponding computational complexity grows exponentially with the number of antennas and/or constellation size. The conventional detection schemes such as ZF, MMSE, ZF with SIC and MMSE with SIC have relatively manageable complexity; however, in general their BER performance is poor especially for large MIMO sizes.

The sphere decoding algorithms (SDAs), specifically the depth first sphere decoding (DF SD), achieves similar performance to MLD at relatively reasonable complexity, but it has very large variation of computational throughput. In order to reduce the complexity of DF SD, initial radius setting strategy is introduced in this thesis and, with this, enormous computational complexity is saved. Fixed throughput SDAs, namely k−best SDAs, are also analyzed and as a result, it is obtained that these schemes have performance degradation compared to the MLD. So, a hybrid sphere decoding which combines the desirable features of the two SDAs is proposed in this thesis and simulation results show that the proposed scheme can achieve performance very close to the MLD at very high computational throughput which is more than twice of that of k−best SDAs.

Key words: **MIMO−OFDM Signal Detection, Sphere Decoding Algorithms, Hybrid Sphere Decoding**

Chapter 1

Introduction

1.1 Motivation and Background

The demand for high data rate wireless communications at high quality of service (QoS) is constantly growing. Consequently, future wireless applications are characterized by flexible and ubiquitous connectivity with significantly higher link throughput and significantly reduced cost per transmitted bit. Traditionally, higher bit rates have been obtained using higher symbol rates and larger modulation constellations, resulting in a larger signal bandwidth which in turn results in increased inter symbol interference (ISI) and reduced energy per bit to noise ratio (Eb/No). Combined with the fact that the available frequency spectrum is limited and the propagation conditions are hostile due to multipath fading, the traditional wireless systems cannot meet the demands of future wireless communications. Therefore, considerable research efforts have been directed at designing communication systems that are capable of handling high data rates while maintaining sufficient BER performance and without increasing the bandwidth [1−2].

Multiple−Input Multiple−Output (MIMO) wireless technology is one possible solution that can meet the demands of future generation wireless communications and hence, has come to be a hot research area over the recent past. In contrast to traditional wireless systems, in which there is one transmitting and one receiving antenna, MIMO systems use array of multiple antennas at both ends of the wireless link, all operating at the same frequency and at the same time. Besides, MIMO systems make use of multipath effects of the propagation environment, which is regarded as an impediment to accurate data transmission in traditional wireless systems. Rather than combating the multipath signals, MIMO systems make them carry more information. Thus, MIMO systems are paradigm shifts, changing perceptions of and responses to multipath propagation [2].

Basically, MIMO schemes can be split into two, depending on the aim to be achieved. The first is *spatial diversity*, which is aimed at increasing the robustness/performance of the wireless communication by transmitting different representations of the same data stream on different

transmitter antennas. This is realized through space time coding and is attractive when compared to time and frequency diversities as it does not incur additional transmission time and bandwidth, respectively. The second and the focus of this thesis is *spatial multiplexing* MIMO, which achieves spectral efficiency by transmitting independent data streams on different transmit branches simultaneously and at the same carrier frequency. Thus, it yields extra ordinary capacity increase compared to single antenna systems at no additional power and bandwidth expenditures. The corresponding capacity gain is available if the propagation channel exhibits rich scattering where multipath characteristics are exploited [1−3].

Spatial multiplexing MIMO (SM−MIMO) is known to increase the spectral efficiency significantly [7]. For high data rate transmissions, the multipath characteristic of the environment causes the MIMO channel to be frequency selective. Orthogonal Frequency Division Multiplexing (OFDM) is a technique that can transform such a frequency selective MIMO channel into a set of parallel frequency flat MIMO channels, and therefore, decrease receiver complexity. The combination of the two powerful techniques, MIMO and OFDM, is very attractive, and has become a promising broadband wireless access scheme [4−5].

Additionally, the SM−MIMO systems have even better performance than the traditional Single Input Single Output (SISO) systems operating within the same bandwidth and power constraints. As long as there are sufficient scattering objects in the propagation environment, the performance of MIMO systems keep growing with increasing number of antennas. In other words, MIMO systems operating in rich scattering environment demonstrate more reliability even with increasing spectral efficiency [11]. However, this simultaneous increase in performance and spectral efficiency of MIMO systems is not achievable with all the available MIMO signal detection schemes. Those which achieve this have an associated computational complexity which increases exponentially with the number of antennas. Hence, among the number of issues that constrain the exploitation of the enormous capacity of MIMO systems, MIMO signal detection schemes need to be investigated for fast implementation and deployment to meet the demands of the future wireless communications.

1.2 Problem Statement

Despite the fact that MIMO systems take the spectral efficiency to a new level, there are challenges accompanying this system. One of the main challenges is the computational complexity of the receiver algorithms, which increase with number of antennas employed. This is due to the fact that independent data streams transmitted from each transmit antenna occupy the same frequency spectrum and therefore, interfere with one another in addition to the effects of system related noise. Hence, the challenge is to develop MIMO receiver algorithm (MIMO detection technique) which has high performance and, simultaneously, has low and manageable computational complexity. In this regard, this thesis focuses on the development of the MIMO signal detection scheme with reasonable computational complexity and performance closer to the maximum likelihood bound which is optimal MIMO signal detector.

1.3 Literature Review

Because of its extra ordinary increase in data throughput and link reliability without expending additional bandwidth and transmit power, MIMO−OFDM systems have attracted a wide research attentions in wireless communications since the last decade. Some of the researches conducted on the area of MIMO systems are reviewed below.

The first breakthrough to MIMO systems was made by Gerard J. Foschini and M. J. Gant in [1], where they used information theoretic approach to investigate the ultimate limits of the spectral efficiency achievable when using MIMO systems. Besides, they have hinted the need of inventing a new MIMO detection scheme to realize a hefty portion of the great capacity promised.

In [2], Gerard J. Foschini showed that enormous spectral efficiency up to 42 bps/Hz can be achieved when using MIMO systems with 8 antennas both at the transmitter and receiver, which is more than 40 times that of the SISO systems. However, he used D−BLAST (diagonal−BLAST) architecture which suffers from certain implementation complexities which make it inappropriate to realize in hardware.

P. W. Wolkiansky et al in [7] introduced V−BLAST (Vertical BLAST) which uses ordered successive interference cancellation (OSIC) as MIMO detection technique. In their laboratory test bed, they achieved spectral efficiency up to 40 bps/Hz at practical SNRs.

In [8, 10] the Zero Forcing (ZF) based V−BLAST of [7] was extended to MMSE based V−BLAST to improve system performance. However, the main drawback of MMSE V−BLAST is that it requires accurate estimate of the noise level in the system which is practically difficult to obtain. In [8] D. Wübben et al obtained the same performance as MMSE V−BLAST using MMSE−SQRD which has lower complexity compared to MMSE V−BLAST. This also requires knowledge of statistical information of noise level within a system to maintain high performance.

The work of A. V. Zelst in [10] revised the above MIMO detection schemes and compared the performance results of these schemes with the Maximum Likelihood Detection (MLD) scheme. In this paper it was shown that MLD outperforms the other detection methods. Furthermore, the performances of these detection algorithms for broadband MIMO systems were analyzed in [13] where OFDM is coupled with MIMO systems to combat the ISI resulting from high data rate. In either case, the performance of the traditional MIMO detection schemes is far inferior to that of maximum likelihood detection method especially for higher MIMO sizes. However, the MLD scheme has a complexity which increases exponentially with the number of antennas and/or the constellation orders.

Moreover, the performances of the traditional MIMO detection schemes deteriorates under ill−conditioned channels resulting from spatial correlations and fall below acceptable threshold for certain applications requiring significant transmission accuracy [44]. The works reported in [11, 14] try to reduce the complexity of MLD by using approximations, but the complexity reduction they achieved is not satisfactory for higher modulation orders and large MIMO sizes.

Sphere decoding algorithms introduced in [32, 35−37] are the state−of−the art MIMO detection techniques which can substitute the MLD algorithm. These algorithms use iterative search based on a tree structure, either breadth first search or depth first search, to perform MIMO signal detection. In [33] B. Hassibi and H. Vikalo used sphere decoding to obtain MLD performance and

reported that SDAs have, in general, variable complexity under different channel conditions and SNRs and hence, have variable computational throughput.

To resolve the issue of variable complexity in regular sphere decoders, k−best sphere decoding algorithm is introduced in [38, 43]. It is shown that using k−best sphere decoding, fixed complexity (constant throughput) can be achieved, but this has performance degradation compared to the MLD.

Improvements to the k−best SD have been introduced by Q. Li and Z. Wang in [39] by incorporating layer reordering of the tree levels and dynamically varying the k values and obtained significant performance improvements. There are a lot of works done to improve the performance of k−best SD with negligible additional complexity as in [41−43]. In general, the performance of the k−best SD is poor especially when the k value is small.

Even though there are plenty of works done in the literature to reduce the complexity and/or improve the performance of the two SD schemes separately, little attention has been paid to the combination schemes which can take the advantage of both schemes. To this end, authors in [45] introduced staggered SD where the search is simultaneously performed along the depth and breadth of the tree. However, this requires a number of independent processing units to perform the search along the different dimensions of the tree. Nevertheless, they claimed that they achieved better throughput than the pure depth first SD.

In [46], H. L. Chiang and S. G. Chen, incorporated DF SD into k−best SD to reduce its complexity. They also used MMSE−SQRD based layer reordering and obtained performance similar to the layer reordered k−best SD with reduced complexity. However, they used S−E enumeration of [31], which requires specific ordering of the tree branches according to their distance.

In this thesis, the hybrid SD scheme, which collects the desirable features of the two SDAs, k−best and DF SDAs, is proposed to achieve performance very close to that of MLD. Moreover, initial radius setting technique, which can reduce the complexity without using any enumeration technique, is introduced.

1.4 Objective of the Thesis

1.4.1 General Objective

In general, the objective of this thesis is to develop a MIMO signal detection scheme which has near optimal performance with much reduced computational complexity. The optimal MIMO detection scheme referred is the maximum likelihood detection (MLD), which has prohibitively large computational complexity.

1.4.2 Specific Objectives

Specifically the aim of this thesis is to:

- Extensively study the available MIMO signal detection schemes, analyze and evaluate the computational complexities of these schemes in conjunction with their performances under different channel conditions and antenna configurations.
- Develop a MIMO signal detection scheme which exploits the desirable features of the sphere decoding algorithms with new radius setting technique.
- Analyze and investigate the best combination of the two sphere decoding schemes considering the computational complexity and BER performance.
- Evaluate and compare the BER performance and throughput enhancement of the proposed scheme with the existing detection techniques.
- Finally, evaluate these detection schemes in combination with OFDM in order to verify the applicability of the proposed detection scheme for wideband systems.

1.5 Major Assumptions Considered in the Thesis

- Perfect channel state information at the receiver but not at the transmitter: Since the aim of the thesis is to analyze and investigate the performances of different MIMO detection algorithms, perfect channel state information is assumed at the receiver for simplicity.
- Indoor like channel environment with rich scattering objects is assumed.
- Sufficient antenna spacing $(\geq \lambda/2)$ so that the path gain of each antenna is uncorrelated with others.

- The transmitter and the receiver antennas are assumed to be placed far apart so that there is no mutual coupling between the two.

1.6 Notations used in the thesis

Throughout the thesis the following notations are used. Matrices are represented by boldface, italic capital letters, vectors by boldface, italic lower case letters. The superscripts $(\,)^T, (\,)^H$ and $(\,)^+$ stand for transpose, conjugate transpose and pseudo−inverse respectively. We write $a_{i,j}$ for entry in the i^{th} row and j^{th} column of the matrix **A,** and b_i for the i^{th} entry of vector $\boldsymbol{b} = [b_1\ b_2, \cdots, b_N]^T$. Likewise, $\boldsymbol{a}^{(i)}$ and $\boldsymbol{a}_i$ represent the i^{th} row and i^{th} column of matrix $\boldsymbol{A}$, respectively**.** $\boldsymbol{I}_N$ and $\mathbf{0}_N$ denotes the N X N identity and zero matrices respectively. (N_t, N_r) stands for a MIMO system with N_t transmit and N_r receive antennas. $E[\cdot]$ represents the expectation operation. In general, the MIMO system architecture considered in this thesis is spatial multiplexing and hence, MIMO refers to SM−MIMO throughout this document.

1.7 Organization of the thesis

The remainder of the thesis is organized as follows: In chapter two MIMO system model is described and detailed mathematical analysis of the MIMO channel models to be used in the thesis is provided. Chapter three presents brief discussion of conventional MIMO detection schemes along with their complexity analysis. Similarly, Chapter four provides the state−of−the art MIMO detection schemes including the proposed MIMO detection scheme of this thesis. Besides, complexity analysis of the described schemes and summary of the complexity analysis of all MIMO detection techniques is made towards the end of this chapter.

In Chapter five simulation results of all the detection schemes considered in Chapters three and four are provided. Most of the simulation results are BER versus SNR characteristics, which are used to compare performance of different MIMO detection schemes, while there are also complexity and throughput comparisons. Finally, in Chapter six, conclusions based on the results obtained and recommendations to future works are given.

Chapter 2

Multiple−Input−Multiple Output (MIMO) System Model

2.1 Introduction

In the previous chapter, introduction and literature reviews of works related to MIMO systems were briefly discussed. In this chapter, general MIMO system model and basic concepts behind MIMO systems are discussed. The chapter is organized as follows.

In Section 2.2 general description of MIMO system model and brief discussion of its operation principle are provided. In Section 2.3 MIMO channel models along with necessary parameters affecting the MIMO system design are described. Narrowband and wideband MIMO channels which are part of this thesis are defined. A spatial correlation, which is impairment specific to MIMO systems, is an important issue worth considering when designing MIMO systems and it is briefly described in Section 2.4. Finally, OFDM in combination with MIMO systems is discussed in Section 2.5.

2.2 MIMO System Model Description

A high level block diagram of MIMO system is shown in the Figure 2.1 below. It consists of multiple antenna systems with N_t transmit and N_r receive antennas. The source data stream is modulated into M−ary constellations and then de−multiplexed into N_t sub-streams called "layers". Before modulation, the source data may be channel coded, but for the work of this thesis no channel coding is included.

The MIMO encoder (De−Mux) in the block diagram performs a simple de−multiplexing operation so that N_t consecutive data symbols are transmitted simultaneously (i.e. V−BLAST architecture), [7−11]. Similarly, MIMO decoder performs detection of the transmitted data based on the received information. Mathematically, a MIMO transmission scheme can be seen as a set of equations (the recordings on each receive antenna) with a number of unknown variables (transmitted signals). If every equations represent a unique combination of the unknown variables,

then there exists a solution to the problem only if the number of equations is greater than or equal to the number of unknowns and hence, $N_r \geq N_t$.

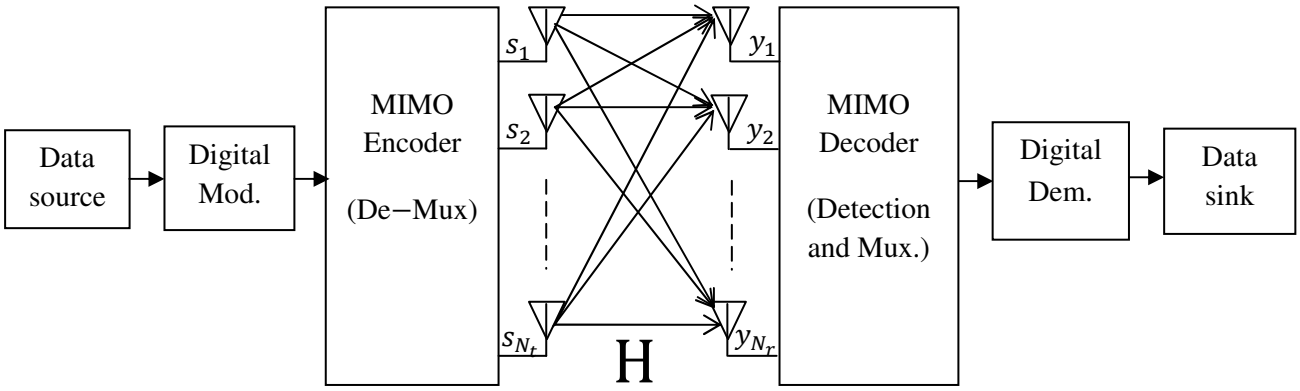

Figure 2.1 General block diagram of MIMO system model with $\boldsymbol{N_t}$ transmit and $\boldsymbol{N_r}$ receive antennas

The basic idea of spatial multiplexing MIMO systems is to transmit different streams of data on different transmit antennas, but on the same carrier frequency and at the same symbol rates. The collection of transmitters comprises, in effect, a vector valued transmitter, where the components of each N_t −dimensional vectors are symbols drawn from M−ary constellation, [7]. Let the stream on the p^{th} transmit antenna as a function of time t, be denoted by $s_p(t)$. When a transmission occurs, the transmitted signal from the p^{th} transmit antenna might find different paths to arrive at the q^{th} receive antenna i.e. through a direct path and indirect paths (multipath) (see Section 2.3 for detail). Suppose that the bandwidth Bw of the system is chosen such that the time delay between the first and the last arriving path at the receiver is considerably smaller than$1/Bw$. In this case, the system is called a narrowband system. For such a system, all the multipath components between p^{th} transmit and q^{th} receive antenna can be summed up to one term, say $h_{qp}(t)$. Since the signals from all the transmit antennas are sent at the same carrier frequency, the q^{th} receive antenna will not only receive signals from the p^{th} transmit antenna, but also from all the N_t transmitters and this can be written as in the following equation [18]:

$$y_q(t) = \sum_{p=1}^{N_t} h_{qp}(t)s_p(t) + v_q \quad \cdots\cdots\cdots\cdots\cdots\cdots\cdots\cdots\cdots\cdots\cdots\cdots\cdots\cdots (2.1)$$

To capture all the N_r received signals into one equation, the matrix notation can be used as follows

$$\boldsymbol{y}(t) = \boldsymbol{H}(t)\boldsymbol{s}(t) + \boldsymbol{v}(t) \cdots\cdots\cdots\cdots\cdots\cdots\cdots\cdots\cdots\cdots\cdots\cdots\cdots\cdots\cdots (2.2)$$

where the elements of these matrices are defined in Equation (2.3) below

$$\boldsymbol{s}(t) = \begin{bmatrix} s_1(t) \\ s_2(t) \\ \vdots \\ s_{N_t}(t) \end{bmatrix}, \boldsymbol{y}(t) = \begin{bmatrix} y_1(t) \\ y_2(t) \\ \vdots \\ y_{N_r}(t) \end{bmatrix} \text{ and } \boldsymbol{H}(t) = \begin{bmatrix} h_{11}(t) & h_{12}(t) & \cdots & h_{1,N_t}(t) \\ h_{21}(t) & h_{22}(t) & \cdots & h_{2,N_t}(t) \\ \vdots & \vdots & \ddots & \vdots \\ h_{N_r,1}(t) & h_{N_r,2}(t) & \cdots & h_{N_rN_t}(t) \end{bmatrix} \cdots\cdots (2.3)$$

where $h_{i,j}$, is the complex channel gain from the j^{th} transmit antenna to the i^{th} receive antenna and $\boldsymbol{v}(t)$ is additive white Gaussian noise. The detailed description of the channel gains is provided in Section 2.3.

In order to make a fair comparison between MIMO systems and SISO systems, the power radiated by each transmit antenna is proportional to $1/N_t$ and, thus the total power at the transmitter side remains the same as the power that would be utilized by SISO systems irrespective of the size of N_t.

2.3 MIMO Channel Model

In the ideal case, the data rate of MIMO systems grow linearly with the number of transmit antennas, [2, 7, 11, 18]. However, the maximum transmission rate in a given bandwidth (i.e., the spectral efficiency) that can be exploited when using MIMO systems depends on a number of parameters observed at the receiver, including the average received power of the desired signal, thermal and system related noise, as well as co−channel interference. Therefore, it is important for the designer of a MIMO communication system to have an appropriate MIMO channel simulation model [18, 19].

Consider a wireless MIMO system described in Section 2.2 with N_t transmit (T_X) and N_r receive (R_X) antennas that are operating in a rich scattering environment. The channel behavior is modeled as follows. Since in MIMO systems all the T_X antennas transmit simultaneously and on the same carrier frequency, the received signal on a given R_X antenna q consists of a linear combination of contributions from the N_t transmitters. Furthermore, when considering the contribution of the p^{th} transmit antenna, due to multipath, the q^{th} receive antenna records a sum of scaled and phase shifted versions of the original T_X signal, where the i^{th} copy received at time t, experienced a time delay of $\tau_{i,qp}(t)$ which is clearly shown in Figure 2.2. So, at time t, for a MIMO system operating at a carrier frequency f_c, the equivalent baseband transfer function from p^{th} T_X to q^{th} R_X antenna is, in time domain, defined by [21].

$$g_{qp}(t) = \sum_{i=0}^{N_m(t)-1} \gamma_{i,qp}(t) exp\left(-j\varphi_{i,qp}(t)\right) \delta\left(\tau - \tau_{i,qp}(t)\right) \dots\dots\dots \dots (2.4)$$

where $N_m(t)$ is the number of resolvable multipath components at time t and, $\gamma_{i,qp}(t)$ and $\tau_{i,qp}(t)$ are the gain and delay, respectively, of a signal travelled through the i^{th} path from p^{th} T_X to q^{th} R_X and received at time t. Furthermore, $\delta(t)$ represents the Dirac delta function and $\varphi_{i,qp}(t) = 2\pi f_c \tau_{i,qp}(t)$.

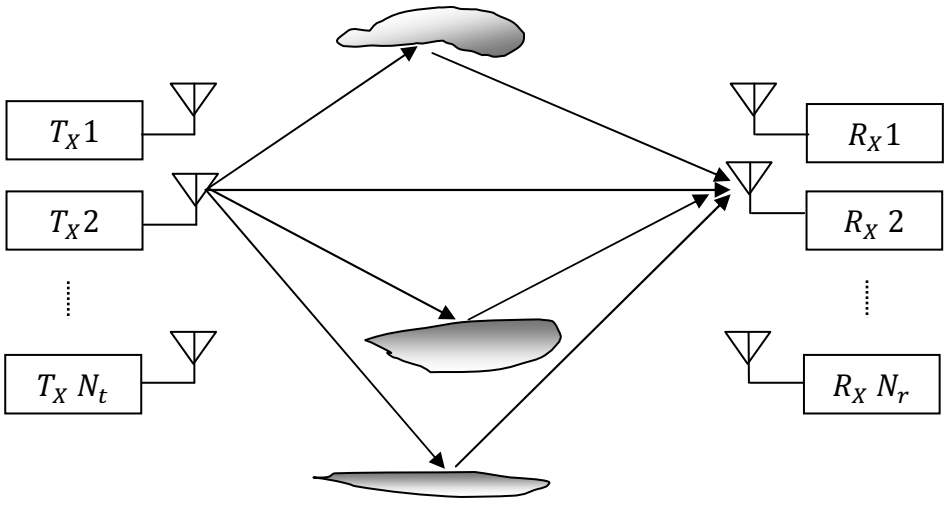

Figure 2.2 A MIMO communication systems operating in a scattering environment

When the system bandwidth is limited, most likely the system is not able to distinguish every multipath component, but the receiver observes (weighted) summations of multipath components. This can be explained by the fact that transmit and receive filters, which form part of any practical communication system, perform an integrating function and as a result rake together the multipath components. Thus, for convenience and without loss of generality, the multipath components within one sampling interval (T_s) are linearly combined. Then the coefficients of the FIR channel can be written as in [18, 21, 22]

$$g_{qp}(nT_s, lT_s) = \sum_{i=N_{min}(nT_s)}^{N_{max}(nT_s)} \gamma_{i,qp}\,(nT_s) exp\left(-j\varphi_{i,qp}(nT_s)\right) \dots\dots\dots\dots (2.5)$$

where $N_{min}(nT_s)$ and $N_{max}(nT_s)$ are chosen such that the paths observed at time nT_s with indices i, with $N_{min}(nT_s) \leq i \leq N_{max}(nT_s)$ and with an encountered delay $\tau_{i,qp}(nT_s)$, stem from the l^{th} sampling interval of the time-variant channel impulse response, i.e.

$$lT_s \leq \tau_{i,qp}(nT_s) \leq (l+1)T_s \dots\dots\dots\dots\dots\dots\dots\dots\dots\dots\dots\dots\dots\dots\dots (2.6)$$

Note that the above channel model can be represented by a tapped delay line as shown in Figure 2.3, and that l denotes the channel tap index, with $l = 0, \dots, L_{qp}(nT_s) - 1$. $L_{qp}(nT_s)$ is the channel length and equals the number of channel taps that are required to also include the last path with index $N_m(nT_s) - 1$, i.e.,

$$L_{qp}(nT_s) = \left\lceil \frac{\tau_{N_m(nT_s)-1,qp}(nT_s)}{T_s} \right\rceil \dots\dots\dots\dots\dots\dots\dots\dots\dots\dots\dots\dots\dots (2.7)$$

where $\lceil x \rceil$ provides the lowest integer value larger than or equal to x.

2.3.1 Wideband MIMO Channel Model

Let the transmitted discrete-time complex baseband signal on the p^{th} T_X antenna as a function of the sampling index n be $u_p(nT_s)$, with a bandwidth $Bw \leq 1/T_s$. Furthermore, under the assumption that the T_X antennas are co-located and that this also holds for the R_X antennas, it is reasonable to assume that $L_{qp}(nT_s)$ is equal for all p and q, with $p = 1, \dots, N_t$ and $q = 1, \dots, N_r$,

and set to $L(nT_s)$. Then, when omitting the additive noise at the receiver, the baseband signal $r_q(nT_s)$ recorded at the q^{th} receiver is given by [18]

$$r_q(nT_s) = \sum_{p=0}^{N_t} \sum_{l=0}^{L(nT_s)-1} g_{qp}(nT_s, lT_s) u_p(nT_s - lT_s) \quad \cdots\cdots\cdots\cdots\cdots\cdots\cdots (2.8)$$

Moreover, to capture all the N_r received signals into one equation, the matrix notation can be used such that

$$\boldsymbol{r}(nT_s) = \sum_{l=0}^{L(nT_s)-1} \boldsymbol{G}(nT_s, lT_s)\boldsymbol{u}(nT_s - lT_s) \cdots\cdots\cdots\cdots\cdots\cdots\cdots\cdots\cdots (2.9)$$

where,

$$\boldsymbol{u}(t) = \begin{bmatrix} u_1(t) \\ u_2(t) \\ \vdots \\ u_{N_t}(t) \end{bmatrix}, \boldsymbol{r}(t) = \begin{bmatrix} r_1(t) \\ r_2(t) \\ \vdots \\ r_{N_r}(t) \end{bmatrix} \text{ and } \boldsymbol{G}(t,\tau) = \begin{bmatrix} g_{11}(t,\tau) & g_{11}(t,\tau) & \cdots & g_{1,N_t}(t,\tau) \\ g_{21}(t,\tau) & g_{22}(t,\tau) & \cdots & g_{2,N_t}(t,\tau) \\ \vdots & \vdots & \ddots & \vdots \\ g_{N_r,1}(t,\tau) & g_{N_r,2}(t,\tau) & \cdots & g_{N_r,N_t}(t,\tau) \end{bmatrix}$$

This can be represented using tapped delay line as shown in figure below.

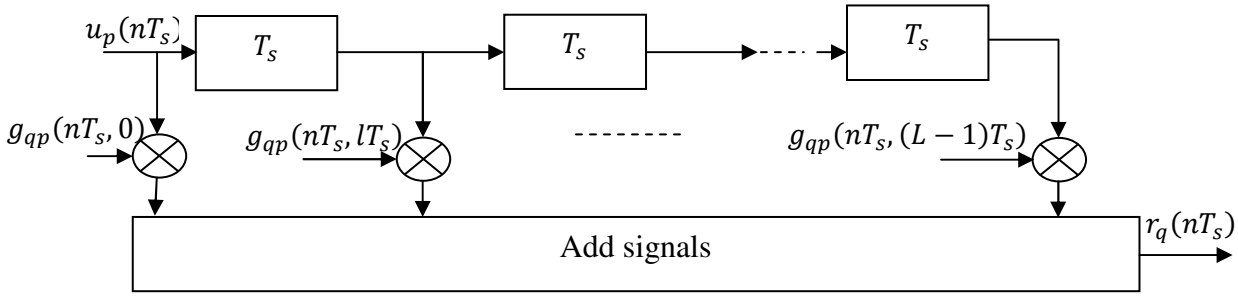

Figure 2.3 Tapped delay line channel model for time−variant channels

To simplify the notations and without loss of generality T_s is dropped and the discrete time-domain MIMO channel model is defined by

$$\boldsymbol{r}(n) = \sum_{l=0}^{L-1} \boldsymbol{G}(n,l)\boldsymbol{u}(n-l) \cdots\cdots\cdots\cdots\cdots\cdots\cdots\cdots\cdots\cdots\cdots\cdots\cdots\cdots\cdots\cdots (2.10)$$

2.3.2 Quasi−Static Discrete Time Channel Model

When the user and/or objects hardly move during a packet transmission, the MIMO radio channel can be considered constant for the respective time interval. Such a channel is called *quasi−static* channel. In other words, the packet duration is assumed less than the coherence time, i.e., the time in which the communication channel can be considered static.

Under the quasi−static assumption, $\boldsymbol{G}(n,l)$ is independent of n during a packet transmission. So, Equation (2.10) can be rewritten as in [15, 18]

$$\boldsymbol{r}(n) = \sum_{l=0}^{L-1} \boldsymbol{G}(l)\boldsymbol{u}(n-l) \cdots\cdots\cdots\cdots\cdots\cdots\cdots\cdots\cdots\cdots\cdots\cdots\cdots\cdots\cdots\cdots (2.11)$$

For indoor environments, measurement campaigns have indicated that the amplitudes of the elements of $\boldsymbol{G}(l), |g_{qp}(l)|$, are approximately Rayleigh distributed [15−19]. This can be understood intuitively from the reasonable assumption that an indoor environment contains a large number of scatters and, as a result, a channel tap consists of a large sum of multipath components (see Equation 2.5). When the multipath components have similar gains and the phase is uniformly distributed between 0 and 2π, then, according to the Central Limit Theorem [21], the resulting complex channel coefficients are complex Gaussian distributed (and their amplitude is Rayleigh distributed). This results in a stochastic channel model which allows direct modeling of the components of $\boldsymbol{G}(l)$ instead of fully describing the physical geometric propagation paths, thus, resulting in more convenient and faster channel modeling.

Although the channel is assumed static for a packet transmission, it is commonly known that the multipath characteristics change over time, due to movement of the user, movement of objects in the environment, etc. This is modeled by changing $\boldsymbol{G}(l)$ on a packet by packet basis according to a given fading statistics (block fading).

To simplify the channel modeling, it is furthermore assumed that the average power of all transmission coefficients for a given tap, i.e., of all elements of $\boldsymbol{G}(l)$ is identical for a given tap, so

$$E\left[\left|g_{qp}(l)\right|^2\right] \equiv P(l) \quad \cdots\cdots (2.12)$$

for all $p = 1,2, \ldots, N_t$, and $q = 1,2, \ldots, N_r$, $P(l)$ with $l = 0, \ldots, L-1$, is the discrete−time power delay profile (PDP) which is defined as the power of the channel impulse response as a function of delay τ. The total power of the discrete−time PDP, i.e., the large−scale channel gain encompassing distance-dependent decay, is given by

$$P_c = \sum_{l=0}^{L-1} P(l) \quad \cdots\cdots (2.13)$$

From fundamental works in [15, 17, 18] and many other measurements reported in the literature, it is deduced that the average received multipath power of a transmitted impulse in an indoor-like environments tends to fall off exponentially (see Figure 2.4). Moreover, assuming fixed number of taps with equidistant delays, the wideband MIMO channel model is [18]

$$\boldsymbol{r}(n) = \sum_{l=0}^{L-1} \sqrt{P(l)}\boldsymbol{G}(l)\boldsymbol{u}(n-l) \quad \cdots\cdots (2.14)$$

where $\boldsymbol{G}(l)$ is $N_r \mathrm{X}\, N_t$ matrix of i.i.d CSCG (independent identically distributed, circularly-symmetric complex Gaussian) variables with zero mean and unit variance, with an independent realization for all $l, l = 0, 1, \ldots, L-1$. Considering the quasi-static property of the channel, an independent realization of $G(l)$ is generated on a packet by packet basis.

The PDP can be modeled as follows considering the above discussions

$$P(l) = \begin{cases} \dfrac{p_c \exp(-l/\tau_d f_s)}{\sum_{l=0}^{L-1} exp(-l/\tau_d f_s)}, & \text{for } \tau_d > 0 \text{ and } l = 0,1, \ldots, L-1 \\ p_c, & \text{for } \tau_d = 0 \text{ and L} = 1 \end{cases} \quad \cdots (2.15)$$

where, τ_d represents rms delay spread which is defined as the second moment of PDP (see [18]) and $f_s = 1/T_s$ denotes the sampling frequency.

Besides the propagation characteristics, the receiver also observes thermal and system related noise. Thermal noise is modeled as AWGN [21], and considering this, the MIMO signal model under noisy system is:

$$\boldsymbol{r}(n) = \sum_{l=0}^{L-1} \sqrt{P(l)}\boldsymbol{G}(l)\boldsymbol{u}(n-l) + \boldsymbol{v}(n) \quad \cdots\cdots\cdots\cdots\cdots\cdots\cdots\cdots\cdots\cdots (2.16)$$

where $\boldsymbol{v}(n)$ represents AWGN at the n^{th} sample with N_r i.i.d zero mean, CSCG elements with variance σ_v^2.

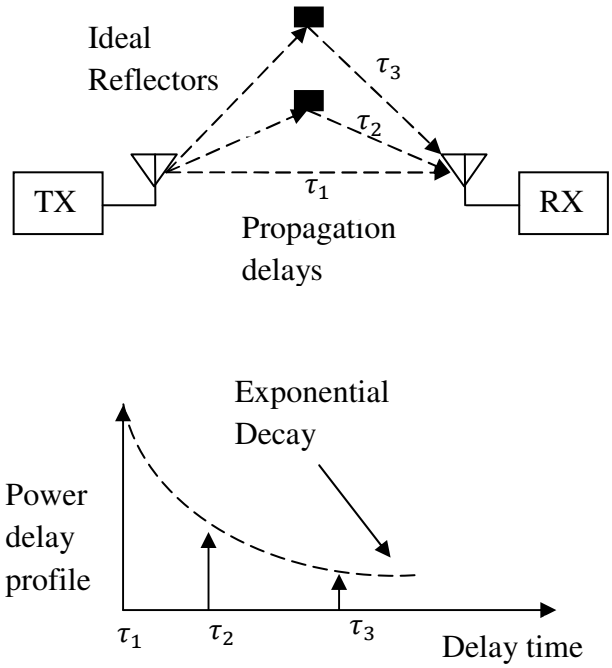

Figure 2.4 Exponentially decaying power delay profiles

2.3.3 Narrowband MIMO Channel Model

Now, the wideband channel model described above can be extended to narrowband systems since the narrowband systems are special cases of the wideband systems. For narrowband systems the

channel is flat over frequency i.e., no ISI. Thus, only the first tap of Equation (2.14) is assumed to have significant contribution, i.e. the channel length L is set to one and the PDP is

$$P(l) = \begin{cases} p_c, & \text{for l} = 0 \\ 0, & \text{for l} \neq 0 \end{cases} \quad \cdots\cdots\cdots\cdots\cdots\cdots\cdots\cdots\cdots\cdots\cdots\cdots\cdots\cdots\cdots\cdots (2.17)$$

Omitting, the time index and assuming that the average path loss is normalized, such that $p_c = 1$, the narrow band signal model is [18]

$$\boldsymbol{y} = \boldsymbol{H}\boldsymbol{s} + \boldsymbol{n} \quad \cdots\cdots\cdots\cdots\cdots\cdots\cdots\cdots\cdots\cdots\cdots\cdots\cdots\cdots\cdots\cdots\cdots\cdots (2.18)$$

where, $\boldsymbol{H} = \boldsymbol{G}(0), \boldsymbol{s} = \boldsymbol{u}(n), \boldsymbol{y} = \boldsymbol{r}(n)$ and $\mathbf{n}$ is AWGN equivalent of $\boldsymbol{v}(n)$.

2.4 Spatial Correlation

Spatial correlation, which results from insufficient antenna spacing and/or lack of sufficient scattering objects, is a crucial impairment for practical MIMO wireless communication systems. This is due to the fact that the spectral efficiency that can be exploited depends strongly on the multidimensional statistical behavior of the MIMO fading channel, partly characterized by the spatial fading correlation [24−27].

When a system simulation needs to be carried out, one way to proceed is to explicitly state specific correlation matrices R_{TX} and R_{RX} covering various propagation scenarios. To obtain these specific correlation matrices, either ray tracing or correlation measurements have to be performed which is a cumbersome process to cover the best-case to worst-case scenarios. With respect to this, the works in [24, 25] obtained the correlation matrices from utmost two parameters r_{TX} and r_{RX} as shown below, assuming equally spaced linear array antennas at both sides

$$\boldsymbol{R}_{TX} = \begin{bmatrix} 1 & r_{TX} & r_{TX}^2 & \cdots & r_{TX}^{N_t-1} \\ r_{TX} & 1 & r_{TX} & r_{TX}^2 & \vdots \\ r_{TX}^2 & r_{TX} & 1 & \ddots & r_{TX}^2 \\ \vdots & \ddots & \ddots & \ddots & r_{TX} \\ r_{TX}^{N_t-1} & \cdots & r_{TX}^2 & r_{TX} & 1 \end{bmatrix} \cdots\cdots\cdots\cdots\cdots\cdots\cdots (2.19)$$

$$\boldsymbol{R}_{RX} = \begin{bmatrix} 1 & r_{RX} & r_{RX}^2 & \cdots & r_{RX}^{N_r-1} \\ r_{RX} & 1 & r_{RX} & r_{RX}^2 & \vdots \\ r_{RX}^2 & r_{RX} & 1 & \ddots & r_{RX}^2 \\ \vdots & \ddots & \ddots & \ddots & r_{RX} \\ r_{RX}^{N_r-1} & \cdots & r_{RX}^2 & r_{RX} & 1 \end{bmatrix} \quad \ldots\ldots\ldots\ldots\ldots\ldots\ldots\ldots\ldots (2.20)$$

where r_{TX} and r_{RX} represent (real-valued) correlation coefficients.

The correlated channel $\boldsymbol{H}$ is modeled as shown in the following equation [39]

$$\boldsymbol{H} = \boldsymbol{R}_{RX}^{1/2} \boldsymbol{H}_{i.i.d} \left(\boldsymbol{R}_{TX}^{1/2} \right)^H \ldots\ldots\ldots\ldots\ldots\ldots\ldots\ldots\ldots\ldots\ldots\ldots\ldots\ldots\ldots\ldots (2.23)$$

With this correlation model, it is possible to represent a fully uncorrelated scenario to a fully correlated scenario by just varying r_{TX} and r_{RX} from zero to one respectively, without performing practical measurements.

2.5 MIMO−OFDM Systems

Broadband MIMO wireless communication systems operating in a rich scattering environment usually face unacceptable inter−symbol interference (ISI) from multipath propagation and their inherent delay spread. Thus, the channel exhibits frequency selective fading.

Orthogonal Frequency Division Multiplexing (OFDM) is a powerful, multicarrier technique for combating ISI. In effect, it transforms a frequency selective channel into a set of parallel flat fading channels and hence, the signals on each subcarrier undergo narrowband fading. In order to deal with frequency selective nature of broadband wireless channels, MIMO can be combined with OFDM. Thus, the combination of the two technologies can achieve higher data rates at high quality of service [3−6].

OFDM is a multi−carrier technique that operates with specific orthogonality constraints between the sub-carriers, which enables it to achieve a very high spectral efficiency. It can be implemented

using IDFT (inverse discrete Fourier transform) at the transmitter and DFT (discrete Fourier transform) at the receiver which are in turn implemented using IFFT (inverse fast Fourier transform) and FFT (fast Fourier transform) algorithms respectively when the number of subcarriers are powers of two.

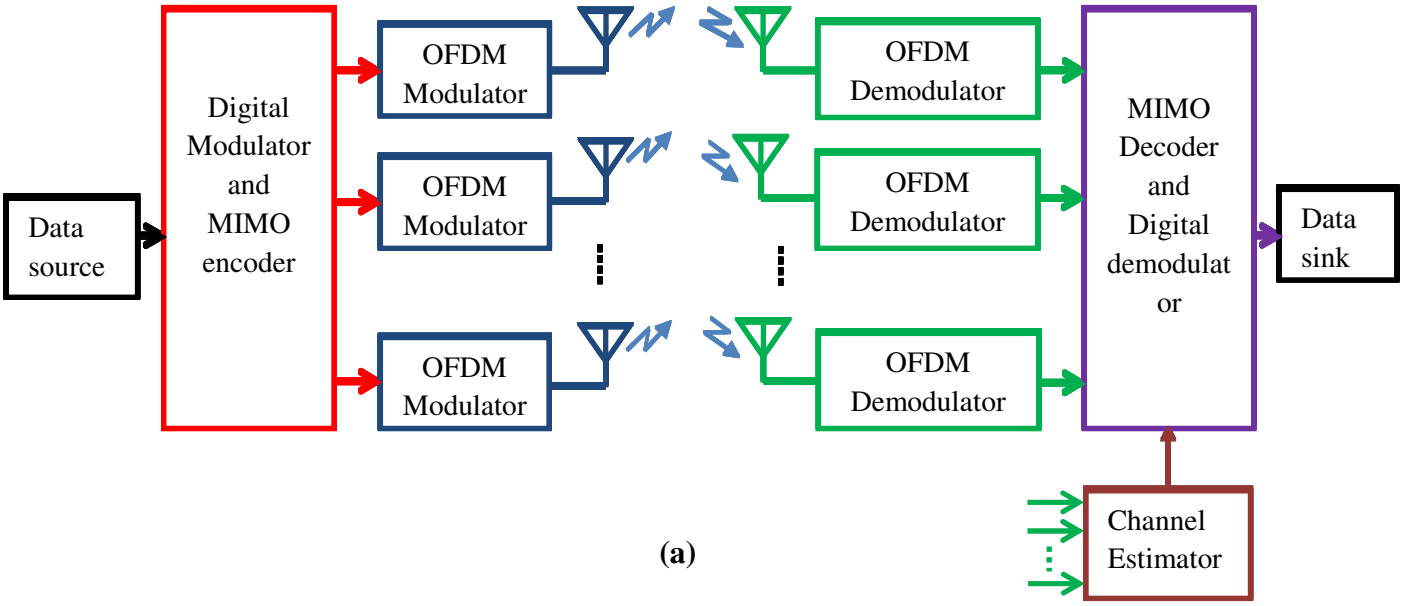

(a)

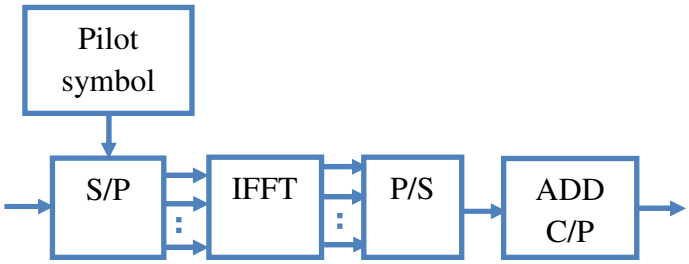

b) OFDM Modulator

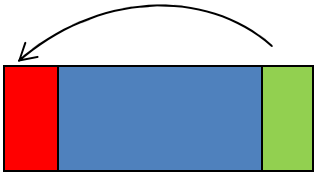

d) CP addition

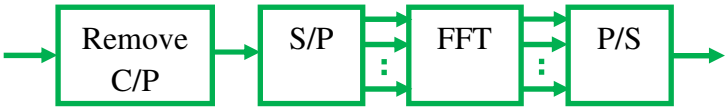

c) OFDM Demodulator

Figure 2.5 a) Simplified block diagram of MIMO-OFDM systems b) OFDM modulation per antenna c) OFDM demodulation per antenna d) addition of cyclic prefix

Note, in the block diagram DAC, ADC, pulse shaping filters, etc are not included for simplicity and clarity.

The data symbols to be transmitted are first converted serial to parallel and each N_c (N_c is the number of OFDM subcarriers) of these symbols are OFDM modulated using IFFT at the transmitter (assuming all subcarriers are utilized) as shown in the block diagram of Figure 2.5. The output of IFFT is N_c samples of a time domain OFDM symbols.

OFDM combats ISI by using guard interval, the duration of time in which the multipath components are allowed to die out. To reduce the receiver complexity, a guard symbol which is a replica of the last N_g samples (called *cyclic prefix*) of the OFDM symbol, is introduced during the guard interval. This converts a linear convolution of a signal and the channel to a circular convolution and thereby causing the FFT of the circularly convolved signal and channel to simply be the product of their respective FFTs. The guard length N_g is chosen to be greater than the maximum channel delay spread. Thus, the relative length of the cyclic prefix depends on the ratio of the channel delay spread to the OFDM symbol duration.

In the block diagram of MIMO−OFDM systems shown in Figure 2.5, for simplicity, channel coding and interleaving of the source bit streams are not included. On the transmitter side the source data bits are mapped to a constellation by digital modulator and then encoded (de−multiplexed) by MIMO encoder (de−multiplexer) on to different transmission layers. Just before transmission the symbols of each transmission layer are OFDM modulated where data symbols are serial to parallel converted, passed through IFFT filters and then in order to avoid ISI cyclic prefix (CP) is added to each OFDM symbols [6, 13].

At the receiver side, the reverse process of transmitter takes place. The received samples are OFDM demodulated where, first, CP is removed, then the remaining samples are serial to parallel converted and finally passed through FFT filters. The outputs of the FFT filters are fed to the MIMO decoders where signal detection takes place per sub-carrier [13].

Chapter 3

Conventional MIMO Signal Detection Techniques

3.1 Introduction

MIMO systems increase system capacity and spectrum efficiency by exploiting the spatial dimension through the use of multiple antennas at both the transmitter and receiver sides of the wireless link. Ideally, the data rates of MIMO systems grow linearly with the number of transmit antennas [7]. However, this increase in system capacity and spectral efficiency come at the cost of increased computational complexity in the receiver. Many algorithms have been proposed in the literature to implement efficient and less complex MIMO receivers which are broadly classified into linear and non−linear detection techniques [5−10]. This chapter briefly reviews some of the conventional narrowband MIMO signal detection algorithms along with their computational complexity assuming perfect CSI at the receiver.

The chapter is organized as follows. Section 3.2 describes the linear MIMO detection techniques while in Section 3.3 some of the non−linear MIMO detection techniques which are based on SIC (successive interference cancellation) are discussed. The computational complexity analysis of these techniques is provided in Section 3.4.

3.2 Linear Detection Schemes

Linear signal detection methods treat all the transmitted signals as interference except for the desired stream from the target transmit antenna. Therefore, interference signals from other transmit antennas are minimized or nullified in the course of detecting the desired signal from the target transmit antenna. Accordingly, the received signal vector $\boldsymbol{y}$ is multiplied by filter matrix $\boldsymbol{G}$ obtained from channel matrix $\boldsymbol{H}$ and then followed by parallel decision on all layers as shown in the block diagram of Figure 3.1 of [28]. Mathematically, using the narrowband system Equation (2.18), the linear detection process can be expressed as follows

$$\boldsymbol{s_{est}} = \boldsymbol{Gy} \quad \cdots\cdots (3.1)$$

where $\boldsymbol{G}$ is the filter matrix obtained from the channel matrix $\boldsymbol{H}$ and $\boldsymbol{y}$ is N_r X 1 vector of received signals.

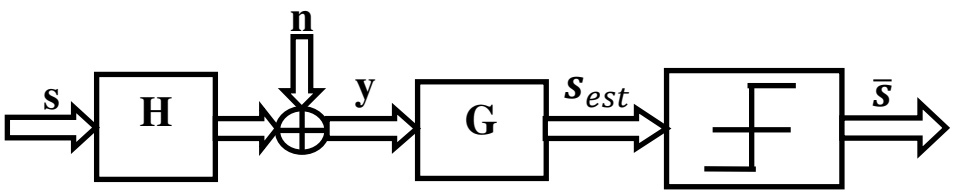

Figure 3.1 Block diagram of linear detection schemes

Depending on the design of the filter matrix $\boldsymbol{G}$, linear detectors are further classified into Zero Forcing (ZF) and Minimum Mean Square Error (MMSE) methods which are discussed below.

3.2.1 Zero Forcing (ZF) Linear Detector

With ZF the mutual interference among the layers is perfectly suppressed. This is accomplished by the filter matrix $\boldsymbol{G}_{ZF}$ which is given in the following equation [10, 13, 28].

$$\boldsymbol{G}_{ZF} = \boldsymbol{H}^{+} = (\boldsymbol{H}^{H}\boldsymbol{H})^{-1}\boldsymbol{H}^{H} \quad \cdots\cdots\cdots\cdots\cdots\cdots\cdots\cdots\cdots\cdots\cdots\cdots\cdots\cdots\cdots\cdots (3.2)$$

Where $(\cdot)^{+}$ represents a pseudo-inverse and $(\cdot)^{H}$ is the Hermitian transpose operator.

In order for the pseudo inverse to exist, N_t must be less than or equal to N_r, otherwise $(\boldsymbol{H}^{H}\boldsymbol{H})^{-1}$ is singular and its inverse doesn't exist. The signal estimation is performed as given in the following equation,

$$\bar{\boldsymbol{s}}_{ZF,est} = \boldsymbol{G}_{ZF}\boldsymbol{y} \quad \cdots\cdots\cdots\cdots\cdots\cdots\cdots\cdots\cdots\cdots\cdots\cdots\cdots\cdots\cdots\cdots (3.3)$$

$$= \boldsymbol{s} + (\boldsymbol{H}^{H}\boldsymbol{H})^{-1}\boldsymbol{H}^{H}\boldsymbol{n}$$

The decision step consists of slicing each element of the filter output vector ($\bar{\boldsymbol{s}}_{ZF}$) to the nearest constellation point by minimum distance quantization. The estimation errors of different layers correspond to the main diagonal elements of the error covariance matrix [28]

$$\boldsymbol{\Phi}_{ZF} = E\{(\bar{\boldsymbol{s}}_{ZF} - \boldsymbol{s})(\bar{\boldsymbol{s}}_{ZF} - \boldsymbol{s})^H\} = \sigma_n^2(\boldsymbol{H}^H\boldsymbol{H})^{-1} \cdots\cdots\cdots\cdots\cdots\cdots\cdots\cdots (3.4)$$

where $\boldsymbol{\Phi}_{ZF}$ error covariance matrix of ZF detection and σ_n^2 is variance of the noise in the system.

This is equivalent to the covariance matrix of the noise after the filter. The larger the p^{th} diagonal element of the error covariance matrix, the more likely erroneous the p^{th} layer is relative to the remaining layers. From the error covariance matrix, it can be seen that small Eigen values of $(\boldsymbol{H}^H\boldsymbol{H})$ will lead to large error due to error amplification as $(\boldsymbol{H}^H\boldsymbol{H})^{-1}$ would be large. Hence, the error rate performance of the zero forcing linear detectors is poor.

This can also be verified from the fact that the diversity order of MIMO systems with antenna configuration of (N_t, N_r) is $N_r - N_t + 1$ when using ZF linear detector. A diversity order of i means, the BER decreases 10^i times if the SNR increases by 10 dB [10, 21].

3.2.2 Minimum Mean Square Error Method (MMSE)

The MMSE detection method estimates the transmitted vector by minimizing the mean squared error between the actually transmitted symbol vector and the output of the linear detector as shown in Equation (3.5) [9].

$$\varepsilon^2 = E\{(\boldsymbol{s} - \boldsymbol{s}_{est})^H(\boldsymbol{s} - \boldsymbol{s}_{est})\} \cdots\cdots\cdots\cdots\cdots\cdots\cdots\cdots\cdots\cdots\cdots\cdots (3.5)$$

The estimate that minimizes the above expression is obtained from the following equation

$$\boldsymbol{s}_{est} = \boldsymbol{G}_{MMSE}\boldsymbol{y} \cdots\cdots\cdots\cdots\cdots\cdots\cdots\cdots\cdots\cdots\cdots\cdots\cdots\cdots\cdots\cdots (3.6)$$

where, the MMSE filter matrix $\boldsymbol{G}_{MMSE}$ is given by, [8, 10, 28]

$$\boldsymbol{G}_{MMSE} = \left(\sigma_n^2\boldsymbol{I}_{N_t} + \boldsymbol{H}^H\boldsymbol{H}\right)^{-1}\boldsymbol{H}^H \cdots\cdots\cdots\cdots\cdots\cdots\cdots\cdots\cdots\cdots\cdots\cdots (3.7)$$

where, $\sigma_n^2 = N_t/SNR$ and $\boldsymbol{I}_{N_t}$ is N_t X N_t identity matrix.

Thus, from equation (3.7) it can be clearly seen that the ZF solution corresponds to MMSE solution when $\sigma_n^2 = 0$. This filter represents the tradeoff between the noise amplification and interference suppression. The estimation errors of different layers correspond to the main diagonal elements of the error covariance matrix [8, 28].

$$\boldsymbol{\Phi}_{MMSE} = E\{(\boldsymbol{s}_{est} - \boldsymbol{s})(\boldsymbol{s}_{est} - \boldsymbol{s})^H\} = \sigma_n^2\left(\boldsymbol{H}^H\boldsymbol{H} + \sigma_n^2\boldsymbol{I}_{N_t}\right)^{-1} \quad \cdots\cdots\cdots\cdots (3.8)$$

The term $\sigma_n^2\boldsymbol{I}_{N_t}$reduces the noise amplification at the cost of interference suppression. The MMSE method performs better than the ZF method by incorporating the noise term in its filter design. However, this requires accurate estimation of the noise level in the system which is practically difficult to obtain.

The MMSE solution can be considered to be the ZF solution by extending the channel matrix $\boldsymbol{H}$ and the received vector $\boldsymbol{y}$ as follows [10]

$$\underline{\boldsymbol{H}} \rightarrow \begin{bmatrix} \boldsymbol{H} \\ \sigma_n\boldsymbol{I}_{N_t} \end{bmatrix} \text{ and } \underline{\boldsymbol{y}} \rightarrow \begin{bmatrix} \boldsymbol{y} \\ \boldsymbol{O} \end{bmatrix} \cdots\cdots\cdots\cdots\cdots\cdots\cdots\cdots\cdots\cdots\cdots\cdots\cdots\cdots (3.9)$$

where $\mathbf{0}$ is N_r X 1 vector of zero elements.

3.3 Non-linear Detection Schemes

The linear detection schemes described earlier are viable, but superior performance can be obtained by using non−linear detection schemes. The non−linear detection schemes exploit higher diversity order than the linear detection schemes and, as a result, they perform better than the linear detectors. Broadly, non−linear MIMO detection schemes are categorized as:

a) SIC –Successive Interference Cancellation Detection
b) MLD –Maximum Likelihood Detection
c) Sphere Decoding (SD) Algorithms (SDAs)

In this section, we describe the SIC detection scheme only while the MLD and SDAs are considered in Chapter 4.

3.3.1 SIC –Successive Interference Cancellation Detection Method

The non-linear successive interference cancellation (SIC) schemes detect the signals one after the other in a way similar to a decision-feedback equalizer [7−9]. That is, the interference of the already detected signals is subtracted from the received signal $\boldsymbol{y}$ before detecting the remaining signals. Due to the effect of error propagation, the sequence of detection has strong impact on the overall performance of the system [7]. If, somehow, first, the most reliable element of the transmitted vector $\boldsymbol{s}$ is decoded and its interference is removed from the remaining signals, the performance can be enhanced. This can be justified by the fact that after the interference of the already detected signals is removed, the diversity order of the remaining signals is increased. In other words, the remaining received signal is modified in such a way that there are fewer interferers in it.

Mathematically, SIC can be realized using two different approaches. The first approach is based on V−BLAST (Vertical Bell Labs Layered Space Time) approach [7, 29] and the other is based on QRD (QR decomposition) of the channel matrix [8, 9].

3.3.1.1 SIC with V−BLAST

V−BLAST was introduced by Foschini et al [7] for the first time and, with this architecture, they achieved spectral efficiencies of 20−40 bps/Hz under realistic SNRs. Basically, the V−BLAST uses ZF or MMSE algorithms [29] iteratively to perform symbol estimation. In general, the V−BLAST detection method involves the following iterative steps:

1. Determine filter matrix $\boldsymbol{G}$ based on Equations (3.2) or (3.7) for ZF based V−BLAST or MMSE based V−BLAST respectively
2. Choose the best channel based on post signal-to-noise ratio (post-SNR) or post signal-to interference-plus-noise ratio (post-SINR) for ZF V−BLAST or MMSE V−BLAST respectively. This can simply be known from error covariance matrices of Equations (3.4) or (3.8) which turns out to be $\boldsymbol{\Phi}_{ee} = \sigma_n^2 \boldsymbol{G}\boldsymbol{G}^H$. Thus, the smallest estimation error corresponds to the row of $\boldsymbol{G}$ with minimum Euclidean norm [28].

3. Estimate the corresponding element of $\boldsymbol{s}$ using the p^{th} row of $\boldsymbol{G}$ as a nulling vector as shown below (assuming the p^{th} row of $\boldsymbol{G}$ has minimum Euclidean norm)

$$\boldsymbol{s}_{(est),p} = \boldsymbol{g}_p \boldsymbol{y} \cdots \cdots \cdots \cdots \cdots \cdots \cdots \cdots \cdots \cdots \cdots \cdots \cdots \cdots \cdots \cdots \cdots \cdots \cdots \cdots \cdots \cdots \tag{3.10}$$

4. Slice the $\boldsymbol{s}_{(est),p}$ to the nearest constellation point using minimum distance quantization i.e. to make a symbol decision

$$\bar{s}_p = Q\big(s_{(est),p}\big) \cdots \cdots \cdots \cdots \cdots \cdots \cdots \cdots \cdots \cdots \cdots \cdots \cdots \cdots \cdots \cdots \cdots \cdots \cdots \cdots \cdots \tag{3.11}$$

   Where $Q(\cdot)$ is a minimum distance quantizer of a given constellation type

5. Cancel the interference of $\bar{s}_p$ from the receive signal vector $\boldsymbol{y}$ as shown in the equation

$$\boldsymbol{y}_{p-1} = \boldsymbol{y} - \boldsymbol{h}_p \bar{s}_p \cdots \cdots \cdots \cdots \cdots \cdots \cdots \cdots \cdots \cdots \cdots \cdots \cdots \cdots \cdots \cdots \cdots \cdots \cdots \cdots \cdots \tag{3.12}$$

   Now, if the previous detection is correct, the diversity order of the remaining receive signal increases by one since the system $(N_t \text{ X } N_r)$ reduces to $(N_t - 1 \text{ X } N_r)$ after one symbol detection and this increment continues until the last layer.

6. Go back to step one, but now by deleting the p^{th} column channel matrix of $\boldsymbol{H}$ which corresponds to the already detected symbol and replace $\boldsymbol{y}$ by $\boldsymbol{y}_{p-1}$

The above procedures hold for both ZF with V−BLAST and MMSE with V−BLAST which only differ in the design of the filter matrix $\boldsymbol{G}$ at step one. However, the detection sequence of MMSE with V−BLAST is not necessarily the same as the detection sequence of ZF with V−BLAST as the former method optimizes its detection ordering based on the signal to interference plus noise ratio (SINR) while the latter method is based on SNR [28].

Assuming correct previous decision at each layer, the diversity order of V−BLAST increases from $N_r - N_t + 1$ for the first detected signal to N_r for the last signal. However, due to error propagation this cannot be attained for all transmitted signals. Moreover, the V−BLAST algorithm described above performs both filter matrix computation and signal detection simultaneously. However, practically steps 1, 2 and 6 are performed during the preamble

processing while the remaining steps are computed during the payload processing. Hence, if the detection sequence and filter matrix weights are determined during the preamble processing, the V−BLAST detection is performed as described in Figure 3.2 for 4X4 system.

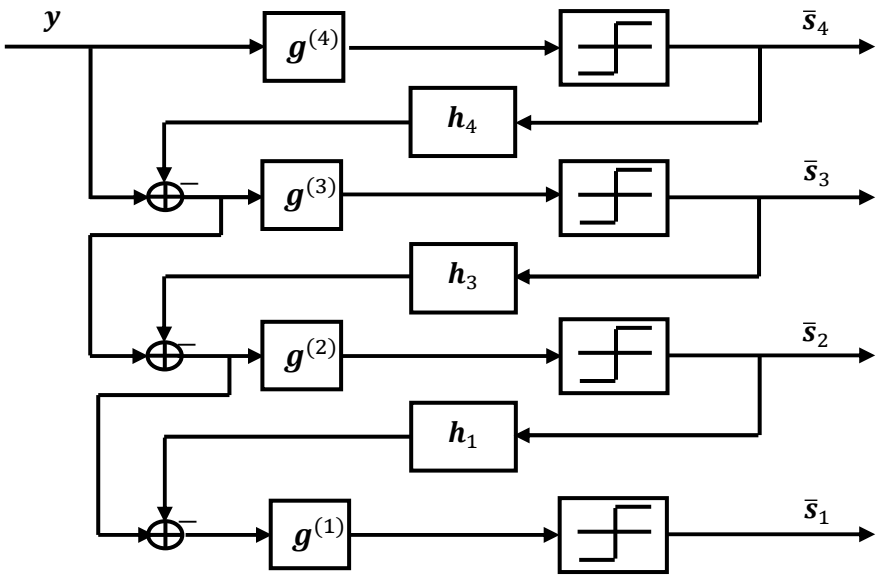

Figure 3.2 Illustration of V−BLAST detection process for 4X4 MIMO system

Even though V−BLAST performs much better than the linear detection schemes, it has the drawback of computational complexity as it requires multiple calculations of the pseudo−inverses of the channel matrix. In order to reduce this complexity, a new efficient decoding algorithm based on the QR decomposition of the channel matrix $\boldsymbol{H}$ is proposed by D. Wübben, et al [9]. Since this doesn't involve any sort of matrix inversion it attains the same performance as V−BLAST with a fraction of computational effort presented in the next section.

3.3.1.2 SIC with QR Decomposition

This, basically, is the restatement of the V−BLAST algorithm in terms of the QR decomposition of the channel matrix $\boldsymbol{H} = \boldsymbol{QR}$, where $\boldsymbol{Q}$ is N_r X N_t matrix of ortho−normal columns and $\boldsymbol{R}$ is $\mathrm{N_t}$ X $\mathrm{N_t}$ upper triangular matrix. By left multiplying the received signal vector $\boldsymbol{y}$ with Hermitian transposes of the $\boldsymbol{Q}$ matrix we obtain the modified receive signal vector as follows [9]

$$\hat{\boldsymbol{s}} = \boldsymbol{Q}^H \boldsymbol{y} \cdots\cdots\cdots\cdots\cdots\cdots\cdots\cdots\cdots\cdots\cdots\cdots\cdots\cdots\cdots\cdots\cdots\cdots (3.13)$$

$$= \boldsymbol{R}\boldsymbol{s} + \boldsymbol{\eta}$$

where, $\boldsymbol{y} = \boldsymbol{H}\boldsymbol{s} + \boldsymbol{n}$ and $\boldsymbol{\eta} = \boldsymbol{Q}^{\boldsymbol{H}}\boldsymbol{n}$. Since $\boldsymbol{Q}$ is a unitary matrix, the statistical properties of the noise term $\boldsymbol{\eta} = \boldsymbol{Q}^{\boldsymbol{H}}\boldsymbol{n}$ remains unchanged.

Due to upper triangular structure of $\boldsymbol{R}$ the k^{th} element of the $\hat{\boldsymbol{s}}$ is given by

$$\hat{s}_k = r_{k,k} s_k + \sum_{i=k+1}^{N_t} r_{k,i} s_i + \eta_{\,k} \cdots\cdots\cdots\cdots\cdots\cdots\cdots\cdots\cdots\cdots\cdots\cdots\cdots (3.14)$$

The second term of the right hand side $D_k = \sum_{i=k+1}^{N_t} r_{k,i} s_i$ represents the interference of layers $k+1, \ldots, N_t$. Hence, $\hat{s}_k$ is free from interferences of lower layers $1, \ldots, k-1$. As it can be seen from the block diagram of Figure 3.3, $\hat{s}_{N_t}$ is free from any interference and can be used to estimate s_{N_t} after appropriate scaling with $1/r_{N_t,N_t}$. Proceeding with $\hat{s}_{N_t-1}, \ldots, \hat{s}_1$ and assuming the correct previous decisions, the interference can be perfectly cancelled at each step [8, 9, 28].

$$s_k = \left(\hat{s}_k - \sum_{i=k+1}^{N_t} r_{k,i} s_i \right) \Big/ r_{k,k} \cdots\cdots\cdots\cdots\cdots\cdots\cdots\cdots\cdots\cdots\cdots\cdots\cdots\cdots (3.15)$$

From Equations (3.14) and (3.15), it follows that the SNR of layer k is determined by diagonal element $\left|r_{k,k}\right|^2$. As already mentioned, for SIC of any type, the detection sequence is crucial due to risk of error propagation. The estimation errors of the different layers in the first detection step correspond to the diagonal elements of the error covariance matrix given by [28]

$$\boldsymbol{\Phi}_{ee} = \sigma_n^2 (\boldsymbol{H}^H \boldsymbol{H})^{-1} = \sigma_n^2 (\boldsymbol{R}^H \boldsymbol{R})^{-1} \cdots\cdots\cdots\cdots\cdots\cdots\cdots\cdots\cdots\cdots\cdots\cdots\cdots\cdots (3.16)$$

From this equation, the estimation error of a given layer k after perfect interference cancellation is given by $\sigma_n^2 / \left|r_{k,k}\right|^2$. Thus, in order to reduce the risk of error propagation it is optimal to choose the permutation of $\boldsymbol{H}$ that minimizes the diagonal elements of $\boldsymbol{R}$ in the direction of detection i.e.

$(N_t, \dots, 1)$. There are algorithms that result in the permutation of $\boldsymbol{H}$ in the desired order, one of which is the Modified Gram-Schmidt (MGS) Ortho−normalization and the algorithm becomes SQRD (sorted QR Decomposition). See Appendix (B) for detailed process of MGS process

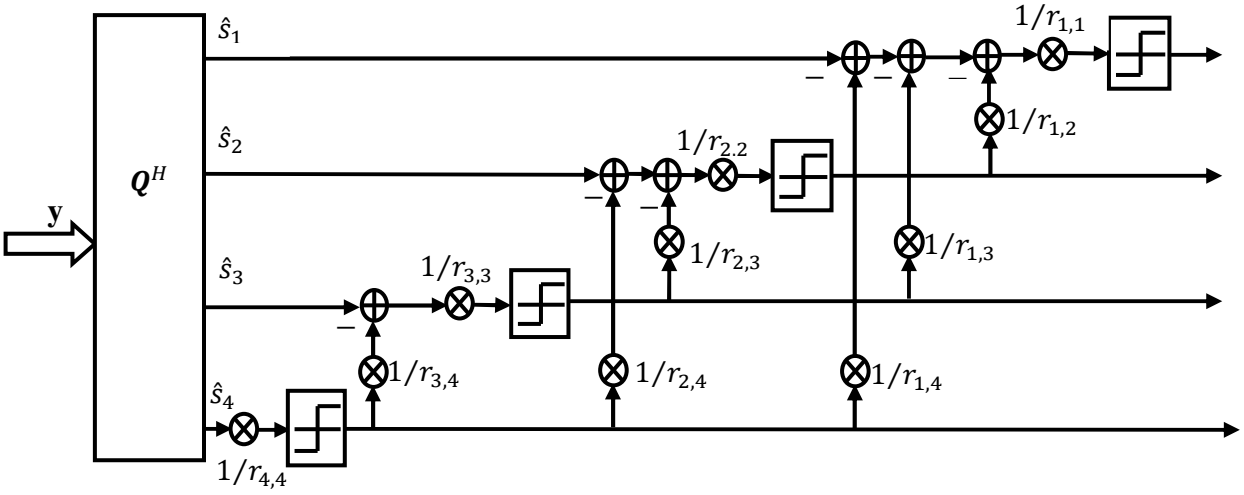

Figure 3.3 Block diagram of SQRD based SIC for 4X4 MIMO system

The QR decomposition based SIC detection described earlier is basically based on ZF criterion at each detection step. In [9], D. Wübben, et al extended the ZF based QRD method to MMSE based QRD method with only slight modifications to the channel matrix and the receive vector as indicated in equation (3.9) in [9].

3.4 Complexity Analysis

In this section complexity in terms of number of additions and number of multiplications of various MIMO detection techniques is analyzed. Since data is transferred on a packet by packet basis and the channel remains constant during packet transmission (quasi−static environment), the complexity figures are split into complexity number for the preamble processing and complexity number for the payload processing.

Before proceeding to the complexity of each detection scheme, the reader is advised to review appendix (A) which provides general rules that are used in the analysis of the complexity.

3.4.1 Complexity of Zero Forcing (ZF) Algorithm

a) Complexity in the preamble processing

In the preamble processing only the pseudo−inverse of the channel matrix $\boldsymbol{H}$ is computed using Equation (3.2). It is performed after the channel training in the preamble processing. The total complexity of the preamble processing in terms of real operations (i.e. real additions (R_{ADDs}) plus real multiplications (R_{MULs})) is found to be [18]:

$$4N_t^3 + N_t^2(8N_r - 2) - 2N_tN_r\ (R_{ADDs}) \cdots\cdots\cdots\cdots\cdots\cdots\cdots\cdots\cdots\cdots\cdots\cdots (3.17)$$

$$4N_t^3 + 8N_t^2N_r\ (R_{MULs}) \cdots\cdots\cdots\cdots\cdots\cdots\cdots\cdots\cdots\cdots\cdots\cdots\cdots\cdots\cdots (3.18)$$

b) Complexity in the payload processing

The payload processing for ZF consists of a matrix−vector multiplication followed by slicing step per transmitted signal vector as shown in Equation (3.3). The complexity of matrix−vector product is equal to $N_t(N_r - 1)\ C_{ADDs}$ and $N_tN_r\ C_{MULs}$. From appendix (A) the complexity of slicing N_t dimensional vector to M−ary constellation points is $N_t log_2(M)\ R_{ADDs}$. Thus, during the payload processing the total complexity per transmitted vector $\boldsymbol{s}$ in terms of R_{ADDs} and R_{MULs} is equal to [18]:

$$2N_tN_r + 2N_t(N_r - 1) + N_t log_2 M\ (R_{ADDs}) \cdots\cdots\cdots\cdots\cdots\cdots\cdots\cdots\cdots (3.19)$$

$$N_tN_r\ (R_{MULs}) \cdots\cdots\cdots\cdots\cdots\cdots\cdots\cdots\cdots\cdots\cdots\cdots\cdots\cdots\cdots\cdots (3.20)$$

3.4.2 The Complexity of MMSE Algorithm

The complexity of MMSE algorithm is almost the same as that of the ZF except the slight difference in preamble processing where the former method has the additional complexity of $N_t\ R_{ADDs}$ due to the addition of α to the real part of the diagonal elements of $\boldsymbol{H}^H\boldsymbol{H}$. Thus, the total complexity in the preamble processing phase is equal to:

$$4N_t^3 + N_t^2(8N_r - 2) - 2N_tN_r + N_t\ (R_{ADDs}) \cdots\cdots\cdots\cdots\cdots\cdots\cdots\cdots (3.21)$$

$$4N_t^3 + 8N_t^2N_r\ (R_{MULs}) \quad \cdots\cdots\cdots\cdots\cdots\cdots\cdots\cdots\cdots\cdots\cdots\cdots\cdots\cdots\cdots\cdots (3.22)$$

The complexity of MMSE during the payload processing is equal to that of ZF and is as given by Equations (3.19) and (3.20).

3.4.3 Complexity of ZF with V−BLAST

The complexity figures are split into preamble processing, where ordering and the weight vectors are determined, and the payload processing, where the actual detection and SIC is performed.

a) Complexity in the preamble processing

In order to obtain the weight vectors, an iterative algorithm that consists of two steps is performed.

1. Compute pseudo−inverse $\boldsymbol{G} = \boldsymbol{H}^{+}$ and find the minimum squared length row of $\boldsymbol{G}$. This row is the weight vector. Permute it to be the last row and permute the columns of H accordingly.
2. While $((N_t - 1) > 0)$ go back to step 1, but with:
   $\boldsymbol{H} \rightarrow \boldsymbol{H}^{(N_t-1)} = \left(h_1\ h_2\ \ldots\ h_{N_t-1}\right)$ and $N_t \rightarrow N_t - 1$

From the preceding sections, the complexity of calculating the pseudo−inverse is already determined as, $4N_t^3 + N_t^2(8N_r - 2) - 2N_tN_r\ R_{ADDs}$ and $4N_t^3 + 8N_t^2N_r\ R_{MULs}$

The squared length of all rows of $\boldsymbol{G}$ is obtained as

$$\boldsymbol{P} = \boldsymbol{G}(\boldsymbol{G})^H \quad \cdots\cdots\cdots\cdots\cdots\cdots\cdots\cdots\cdots\cdots\cdots\cdots\cdots\cdots\cdots\cdots (3.23)$$

This has the complexity of $N_t^2(N_r - 1)\ (C_{ADDs})$ and $N_t^2N_r\ (C_{MULs})$ and from appendix (A) finding the minimum of the diagonal elements of **P**, has the complexity of $N_t - 1(\ R_{ADDs})$. The permutation step is assumed to have negligible complexity, since it is simply swapping the memory pointers. Since the algorithm is an iterative process, and the dimensions of the used matrices are scaling down, the complexity per iteration is reducing. Hence, considering this, the total computational complexity found to be:

$$\frac{1}{6}N_t(6N_t^3 + 8N_t^2(1 + 2N_r) + 3N_t(1 + 6N_r) + 2N_r - 5)\ (R_{ADDs}) \quad \cdots (3.24)$$

$$N_t^2(N_t + 1) + \frac{4}{3}N_rN_t(N_t + 1)(2N_t + 1)\ (R_{MULs}) \cdots\cdots\cdots\cdots\cdots\cdots\cdots (3.25)$$

b) Complexity in the payload processing

In the data processing phase, steps 3−5 (shown in Figure 3.2 for 4X4 system) of V−BLAST algorithm described in section 3.3.1.1 is computed as follows

1. Estimate the best component of $\boldsymbol{s}$. Due to the permutation the corresponding weight vector equals the N_t^{th} row of the permuted $\boldsymbol{G}$. In the case of ZF with SIC:

   $$(s_{est})_k = \boldsymbol{G}^{N_t}\boldsymbol{y}$$

   Slice $(s_{est})_k$ to the nearest constellation point $\left(s_{est,sliced}\right)_k$.
2. While $(N_t - 1) > 0$ go back to step 1, but now with

   $$\boldsymbol{y} \rightarrow \boldsymbol{y} - \boldsymbol{h}_{N_t}\left(s_{est,sliced}\right)_k \text{ and } N_t \rightarrow N_t - 1.$$

Because the above steps are performed N_t times, the total complexity is, therefore, given by:

$$2N_t(4N_r - 1) + N_t log_2 M\ (R_{ADDs}) \cdots\cdots\cdots\cdots\cdots\cdots\cdots\cdots\cdots\cdots (3.26)$$

$$8N_tN_r\ (R_{MULs}) \cdots\cdots\cdots\cdots\cdots\cdots\cdots\cdots\cdots\cdots\cdots\cdots\cdots\cdots\cdots (3.27)$$

3.4.4 Complexity of MMSE with V−BLAST

The complexity of MMSE with SIC is the same as that of ZF with SIC except the slight difference in the preamble processing which is shown below

$$\frac{1}{3}N_t(3N_t^3 + 4N_t^2(2N_r + 1) + 3N_t(3N_r + 1) + Nr - 1)\ (R_{ADDs}) \quad \cdots\cdots (3.28)$$

$$N_t^2(N_t + 1)^2 + \frac{4}{3}N_tN_r(N_t + 1)(2N_t + 1)\ (R_{MULs}) \cdots\cdots\cdots\cdots\cdots\cdots\cdots (3.29)$$

3.4.5 Complexity of Sorted QR Decomposition Detection Method (SQRD)

a) Complexity in the preamble processing

In the preamble processing ordering and QR decomposition are performed using Modified Gram−Schmidt (MGS) procedure detailed in appendix (B). Considering this algorithm the sum total complexity of the SQRD during the preamble processing is obtained to be

$$4N_t^2N_r + \frac{1}{2}(N_t^2 - 5N_t)\ (R_{ADDs}) \cdots\cdots\cdots\cdots\cdots\cdots\cdots\cdots\cdots\cdots\cdots\cdots\cdots\cdots (3.30)$$

$$4N_t^2N_r + N_t^2 + 2N_tN_r\ (R_{MULs}) \cdots\cdots\cdots\cdots\cdots\cdots\cdots\cdots\cdots\cdots\cdots\cdots\cdots\cdots (3.31)$$

b) Complexity of payload processing

The pay load processing of SQRD method involves the following steps.

1. Filtering the receive signal vector $\boldsymbol{y}$ by $\boldsymbol{Q}^H$ as given in Equation (3.13)
2. The iterative successive interference cancellation performed as given in Equation (3.15). Thus, the total complexity of the payload processing for SQRD is as shown by the equations below

$$2N_t^2 + 4N_tN_R\ (R_{MULs}) \cdots\cdots\cdots\cdots\cdots\cdots\cdots\cdots\cdots\cdots\cdots\cdots\cdots\cdots (3.32)$$

$$2N_t^2 + 4N_tN_r - 4N_t + N_t.log_2M(R_{ADDs}) \cdots\cdots\cdots\cdots\cdots\cdots\cdots\cdots\cdots\cdots\cdots (3.33)$$

Chapter 4

State−of−the Art MIMO Detection Techniques

4.1 Introduction

In Chapter 3 the conventional MIMO detection techniques under the category of linear and non-linear detection methods were discussed. Even though it was said that better performances could be obtained by using non-linear SIC methods, still the performance of these methods is suboptimal when compared to the other detection techniques. Mathematically, the optimal MIMO detection scheme is Maximum Likelihood Detection (MLD) which is considered in this chapter. Furthermore, unlike the conventional MIMO detection techniques, the detection performance of the MLD algorithm grows with the number of antennas [11]. However, the main drawback of the MLD method is that its computational complexity increases exponentially with the number of the transmit antennas and/or the constellation points.

In order to reduce the computational complexity of MLD, sphere decoding algorithms (SDAs) have been proposed [30−35]. Depending on search strategies, SDAs are divided into Breadth First Sphere Decoding (BF SD) and Depth First Sphere Decoding (DF SD). In this thesis, Hybrid Sphere Decoding which is a combination of the two SDAs is proposed. Before hybridizing the two search schemes, important modifications which are aimed to improve the performance and/or reduce the complexity of SDAs, are incorporated to each search scheme and with their respective modifications, the DF SD and BF SD are combined effectively to achieve performance very close to that of MLD with very much reduced computational complexity.

This chapter is organized as follows. In Section 4.2 theoretical and mathematical analysis of the MLD is provided. Section 4.3 discusses the SDAs in detail where the two categories of SDAs mentioned earlier are thoroughly analyzed along with their respective modifications. In Section 4.4 the proposed hybrid sphere decoding is described. The complexity analysis of MIMO detection schemes discussed in this chapter are presented in Section 4.5.

4.2 Maximum Likelihood Detection Method

The MLD method estimates the transmitted vector $\boldsymbol{s}$ according to the maximum likelihood principle where the received vector is compared with the entire possible transmitted vector (which is modified by the channel $\boldsymbol{H}$). Mathematically, the idea is to find a vector $\boldsymbol{s}_j$ for which the conditional probability $P(\boldsymbol{s}_j/\boldsymbol{y})$ is maximized (with $1 < j \leq \Omega$), where Ω denotes the ensemble of the possible transmitted vectors. Considering, a MIMO system with (N_t, N_r) antenna configuration and employing M−point constellation,

$$\Omega = M^{N_t} \quad \cdots\cdots (4.1)$$

Using Baye's theorem, the probability density of the maximum a posteriori (MAP) equation ($P(\boldsymbol{s}_j/\boldsymbol{y})$) can be written as: [13]

$$P\left({}^{\boldsymbol{s}_j}/_{\boldsymbol{y}}\right) = \frac{P\left({}^{\boldsymbol{y}}/_{\boldsymbol{s}_j}\right) P(\boldsymbol{s}_j)}{P(\boldsymbol{y})} \quad \cdots\cdots (4.2)$$

where, $P(\boldsymbol{y}/\boldsymbol{s}_j)$ is the conditional probability density function (pdf) of the received vector $\boldsymbol{y}$, given that $\boldsymbol{s}_j$ is transmitted vector, $P(\boldsymbol{s}_j)$ is the probability of the j^{th} transmit vector. We assume all the vectors are equally probable, i.e. $P(\boldsymbol{s}_j) = 1/\Omega$. Furthermore, $P(\boldsymbol{y})$ is independent of $\boldsymbol{s}_j$. Consequently, finding the vector that maximizes $P(\boldsymbol{s}_j/\boldsymbol{y})$ is equivalent to finding the vector that maximizes $P(\boldsymbol{y}/\boldsymbol{s}_j)$. Thus, MAP transforms to maximum likelihood probability.

The conditional pdf $P(\boldsymbol{y}/\boldsymbol{s}_j)$ is a complex multivariate normal distribution. Based on this information, equation (4.2) can be manipulated further and results in the maximum likelihood solution given below (the reader can refer to [13] for further detail).

$$\boldsymbol{s}_{ml} = \arg \min_{s_j \in \{s_1, \cdots, s_\Omega\}} \left\| \boldsymbol{y} - \boldsymbol{H}\boldsymbol{s}_j \right\|^2 \quad \cdots\cdots (4.3)$$

Thus, the symbol decision is made in favor of vector $\boldsymbol{s_j}$ that minimizes the Euclidean distance to the received vector $\boldsymbol{y}$ as shown in Equation (4.3). Note, because finding the maximum of the conditional probability $P(\boldsymbol{s}_j/\boldsymbol{y})$ leads to minimization of symbol error, the MLD is optimal in its error rate performance [10, 11, 13]. Moreover, unlike the conventional MIMO detection schemes discussed in Chapter 3 which have a diversity order of $N_r - N_t + 1$, it is shown in [10] that the MLD method achieves diversity order of N_r which is independent of N_t. For this reason, MLD completely outperforms the conventional detection techniques. Additionally, it is due to this fact (due to diversity order) that the performance of the MLD increases with increasing number of antennas [11, 13].

From Equation (4.1), it is clearly seen that the MLD solution requires an exhaustive search through the entire transmit vectors Ω. Therefore, its complexity is proportional to Ω, which increases exponentially with N_t and/or M. This is the main disadvantage of the MLD method and hence, it is practically infeasible for large dimensional MIMO systems.

In order to reduce the computational complexity of MLD, a number of solutions have been proposed in the literature. Among these, the works of A.V. Zelst et al in [11] made MLD free of relatively complex multiplications by using approximations to norm calculations where l_2 −norm is approximated by l_1 −norm. With this modification to norm computation they obtained negligible performance penalty for QPSK and about 0.5 dB for 16−QAM constellations. These same authors in [14] further simplified the MLD by transforming the exhaustive search in to tree search in order to avoid some computational redundancies. With all these modifications, the computational complexity is found to be manageable only for small number of antennas (small data rate per channel use).

The real reduction to the computational complexity of the MLD method comes with the introduction of sphere decoding algorithms (SDAs) through the works of E. Viterbo and J. J. Boutros in [32] and M. O. Damen et al in [35]. Also it is shown in [33] that SDAs achieve similar performance to MLD with relatively acceptable computational complexity. In the sequel, the details of SDAs are provided.

4.3 Sphere Decoding Algorithms (SDAs)

As it is already mentioned, the brute force MLD is not feasible for larger number of transmit antennas and/or higher modulation schemes. A feasible option is the application of SDAs [32, 35, 36], whose computational complexity is independent of the total number of possible transmit vectors (Ω).

SDAs achieve similar performance to MLD with reasonable computational complexity. This is due to the fact that SDAs examine only the vector candidates which fall within a hyper sphere (N_r dimensional region) of a given radius C centered at the receive vector, instead of examining the entire possible transmit vectors as shown in Figure 4.1. As it can be clearly seen from this figure, the closest point inside the sphere will also be the closest point for the whole set of points.

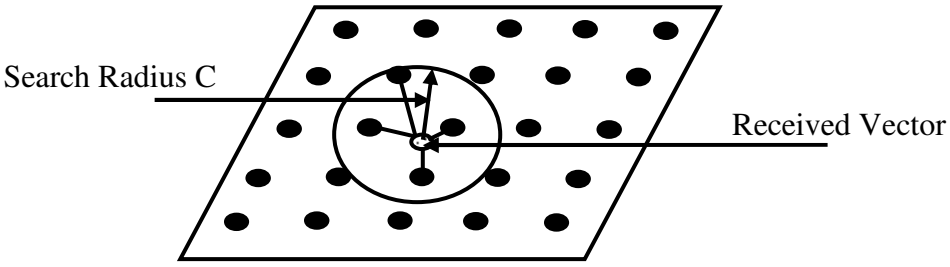

Figure 4.1 A two dimensional geometric representation of the sphere decoding

From Figure 4.1 we can see that the number of vector candidates within the sphere is significantly smaller and this makes the SD computationally efficient. The sphere decoding performs the ML search by imposing a constraint on the exhaustive search of Equation (4.3) as follows [32, 36, 37]

$$\boldsymbol{s}_{ml} = \arg \min_{\boldsymbol{s}_j \in \{\boldsymbol{s}_1, \cdots, \boldsymbol{s}_\Omega\}} \left\| \boldsymbol{y} - \boldsymbol{H}\boldsymbol{s}_j \right\|^2 \leq C^2 \cdots\cdots\cdots\cdots\cdots\cdots\cdots\cdots\cdots\cdots\cdots\cdots\cdots (4.4)$$

where C the radius of a sphere. Equation (4.4) is called sphere constraint equation.

Only imposing the sphere constraint using Equation (4.4) doesn't lead to complexity reductions as the challenge has merely been shifted from finding the closest point to identifying points that lie

inside the sphere. Hence, the complexity is only reduced if the sphere constraint can be checked other than exhaustively searching through all possible candidate vectors. Therefore, Equation (4.4) needs further processing as follows [35−37]

$$\|\boldsymbol{y}-\boldsymbol{H}\boldsymbol{s}_j\|^2=(\boldsymbol{y}-\boldsymbol{H}\boldsymbol{s}_j)^H(\boldsymbol{y}-\boldsymbol{H}\boldsymbol{s}_j)\cdots\cdots\cdots\cdots\cdots\cdots\cdots\cdots\cdots\cdots\cdots\cdots(4.5)$$

$$=(\hat{\boldsymbol{s}}-\boldsymbol{s}_j)^H\boldsymbol{H}^H\boldsymbol{H}(\hat{\boldsymbol{s}}-\boldsymbol{s}_j)$$

where $\hat{\boldsymbol{s}}=(\boldsymbol{H}^H\boldsymbol{H})^{-1}\boldsymbol{H}^H\boldsymbol{y}$ is the unconstrained solution (the ZF solution of Equation (3.3)). Moreover, after QR decomposition of the channel matrix $\boldsymbol{H}$ we obtain:

$$\boldsymbol{s}_{ml}=\arg\min_{S_j\in\Omega}(\hat{\boldsymbol{s}}-\boldsymbol{s}_j)^H\boldsymbol{R}^H\boldsymbol{R}(\hat{\boldsymbol{s}}-\boldsymbol{s}_j)\leq C^2\cdots\cdots\cdots\cdots\cdots\cdots\cdots\cdots\cdots(4.6)$$

where $\boldsymbol{R}$ is the upper triangular matrix obtained by QR decomposition of $\boldsymbol{H}$. It is this upper triangular nature of $\boldsymbol{R}$ that enables the sphere decoder to decide whether the point is inside the sphere or not, before computing the total sphere constraint equation. Besides, due to this structure of matrix $\boldsymbol{R}$, Equation (4.6) can be transformed from matrix manipulation to summation expression as follows [37]

$$\sum_{i=N_t}^{1}\left\|\sum_{l=i}^{N_t}r_{i,l}(\hat{s}_l-s_l^m)\right\|^2\leq C^2\cdots\cdots\cdots\cdots\cdots\cdots\cdots\cdots\cdots\cdots\cdots\cdots\cdots(4.7)$$

where $r_{i,l}$ is $(i,l)^{th}$ element of $\boldsymbol{R}$, $\hat{s}_l$ is the l^{th} element of $\hat{\boldsymbol{s}}$ and s_l^m is the m^{th} element of the M point constellation used at the l^{th} layer. With Equation (4.7) the exhaustive search has turned out to be an iterative tree traversal, where the leaves at the bottom level correspond to all possible symbol vectors $\boldsymbol{s}$ and, the M possible values of entry s_{N_t} define its top level (root level) as illustrated in Figure 4.2 for a single root. This enables us to uniquely describe the node at level i $(i=1,2,\cdots,\ N_t)$ by the partial vectors $\boldsymbol{s}^{(i)}=\left[s_i,s_{i+1},\cdots,s_{N_t}\right]^T$ as described in the figure.

We define branch cost function (increments) associated with nodes in the i^{th} layer as [37]:

$$e_i(\boldsymbol{s}^{(i)}) = \left|\sum_{l=i}^{N_t} r_{i,l}(\hat{s}_l - s_l^m)\right|^2 = \left|\sum_{l=i}^{N_t} r_{i,l}\hat{s}_l - \sum_{l=i+1}^{N_t} r_{i,l}s_l^m - r_{i,i}s_i^m\right|^2 \quad \cdots (4.8)$$

where $\boldsymbol{s}^{(i)}$ is the partial vector of $\boldsymbol{s}$ with $s_1 = 0, \cdots, s_{i-1} = 0$. From Equation (4.8) it can be deduced that the computation of the squared Euclidean distance is a recursive process where intermediate computations are reused.

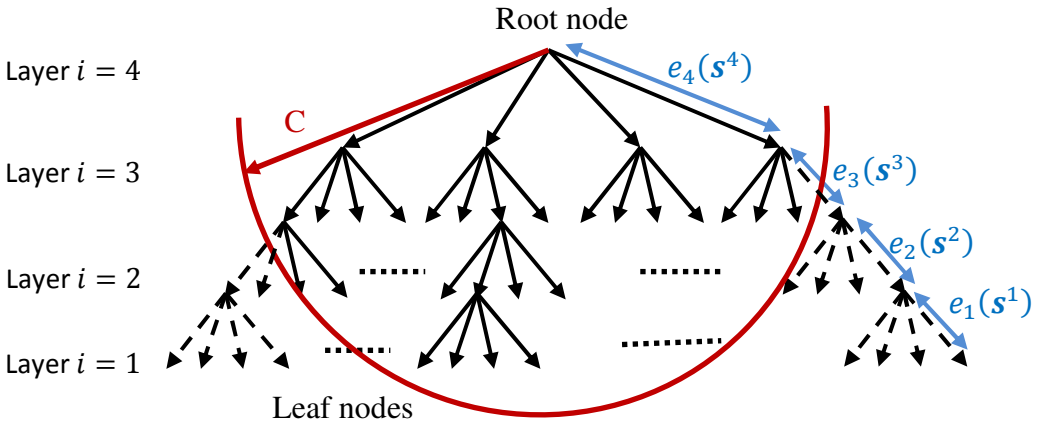

Figure 4.2 Search tree diagram of sphere decoding algorithm

We can further decompose Equation (4.8) to separate the part influenced by s_i^m as follows:

$$e_i(\boldsymbol{s}^{(i)}) = \left|b_{i+1}\boldsymbol{s}^{(i+1)} - r_{i,i}s_i^m\right|^2 \cdots\cdots\cdots\cdots\cdots\cdots\cdots\cdots\cdots\cdots\cdots\cdots\cdots\cdots (4.9)$$

$$b_{i+1}\boldsymbol{s}^{(i+1)} = r_{i,i}\hat{s}_i + \sum_{l=i+1}^{N_t} r_{i,l}(\hat{s}_l - s_l^m) \cdots\cdots\cdots\cdots\cdots\cdots\cdots\cdots\cdots\cdots\cdots\cdots\cdots\cdots (4.10)$$

It is obvious from (4.9) that $b_{i+1}\boldsymbol{s}^{(i+1)}$ is common to all the children of the node under consideration. So, the branch cost function can be obtained with minimum effort by

pre−computing $b_{i+1}\boldsymbol{s}^{(i+1)}$ and simply evaluating (4.9) for all $s_i^m \in M$. The distance of the partial vector is obtained as

$$T_i\left(\boldsymbol{s}^{(i)}\right) = T_{i+1}\left(\boldsymbol{s}^{(i+1)}\right) + e_i\left(\boldsymbol{s}^{(i)}\right) \cdots\cdots\cdots\cdots\cdots\cdots\cdots\cdots\cdots\cdots\cdots\cdots\cdots\cdots (4.11)$$

where $T_i\left(\boldsymbol{s}^{(i)}\right)$ is called partial Euclidean distance (PED) which is non−decreasing function and for $i = N_t$, $T_{i+1}\left(\boldsymbol{s}^{(i+1)}\right)$ initialized to zero. Thus, the decoding process can be regarded as descending down a tree in which each node has M branches. Since branch increments $e_i\left(\boldsymbol{s}^{i}\right)$ are non−negative, it follows immediately that whenever the PED of a node violates the sphere constraint, now given by:

$$T_i\left(\boldsymbol{s}^{i}\right) \leq C^2 \cdots\cdots\cdots\cdots\cdots\cdots\cdots\cdots\cdots\cdots\cdots\cdots\cdots\cdots\cdots\cdots\cdots\cdots\cdots\cdots (4.10)$$

the PEDs of all its descendants will also violate the sphere constraint. Consequently, the tree can be pruned below this node. This approach effectively reduces the number of vector symbols (i.e. leaves of the tree) to be checked. When the tree traversal is finished the leaf with the lowest $T_1(\boldsymbol{s})$ is chosen as corresponding to the transmitted vector (for hard decision decoding).

Depending on the tree traversal, SDA can be categorized into breadth first SD and Depth First SD. As already mentioned, the main aim of this thesis is to exploit the advantages of the two search schemes by effectively combining both schemes in order to improve performance and reduce complexity. Before we discuss the two search schemes in detail we need to address some of the challenges of utilizing SDA. One of these problems is the choice of the search radius which has a direct influence on the complexity of the system. The next subtopic discusses some of the ways in which this problem is tackled in the literature and finally introduces a new choice of this search radius.

4.3.1 Search Radius Setting Strategies

As stated in the preceding section, one of the main challenges of SDA is how to determine the search radius C of the sphere [33]. This is due to the fact that, if the chosen radius C is too large we obtain too many leaf nodes within the sphere and the search remain exponential in size, whereas,

if C is too small we obtain no leaf node inside the sphere and the search must be restarted by increasing the radius after a huge computational loss.

Schnorr−Euchner (S−E) in [31] introduced an algorithm which doesn't require initial radius estimate. The tree is explored depth−first and child nodes at level i are prioritized in the increasing order of PEDs. Furthermore, the initial search radius C is set to infinity, and is updated with the PED of each new candidate solution. The S−E enumeration finds eligible solutions faster, and is the foundation for most of SD extensions [39, 42, 43]. However, S−E algorithm requires the real−valued decomposition of the channel matrix and the receive vector, which doubles the tree depth. This in turn has negative impact on the computational throughput as shown in [33, 37]. Besides, it requires integer valued constellations such as M−QAM for ordering and cannot be used with M−PSK modulations with ease.

In this thesis the tree with complex valued constellations is considered, i.e. without performing real−valued decomposition. In order to avoid the problem of the choice of initial radius C, the ZF estimate of equation (4.5) is used to set the radius as shown in the following equation

$$\boldsymbol{s}^{ZF} = Q(\hat{\boldsymbol{s}}) \quad \cdots\cdots\cdots\cdots\cdots\cdots\cdots\cdots\cdots\cdots\cdots\cdots\cdots\cdots\cdots\cdots\cdots\cdots (4.11)$$

where $Q(\cdot)$ performs minimum distance quantization of each element of $\hat{\boldsymbol{s}}$ to the constellation points in use. Using the quantized points the initial radius is obtained as follows:

$$C = \sum_{i=N_t}^{1} \left| \sum_{l=i}^{N_t} r_{i,l}(\hat{s}_l - s_l^{ZF}) \right|^2 \quad \cdots\cdots\cdots\cdots\cdots\cdots\cdots\cdots\cdots\cdots\cdots\cdots\cdots\cdots\cdots\cdots\cdots\cdots (4.12)$$

Since the computation of $\hat{\boldsymbol{s}}$ is part of the SD, the additional complexity is limited to the complexity of Equations (4.11) and (4.12) which is negligible. Moreover, further complexity reduction can be achieved by employing the radius update strategy by setting the distance of every new candidate as a new search radius.

4.3.2 Depth First Sphere Decoding (DF SD)

Depth first search progresses by expanding the first child node of the search tree that appears and goes deeper and deeper until leaf node is reached as long as every node encountered satisfies the sphere constraint. In other words, the search descends down the tree by computing the PED of one node per layer. After reaching the leaf node, the search backtracks, returning to the most recent node it has not finished exploring as it is depicted in the Figure 4.3. Moreover, if at any layer i, the node violates the sphere constraint, then its entire descendants are pruned and the search continues with next neighbor nodes, and likewise until all leaf nodes within the search radius are explored.

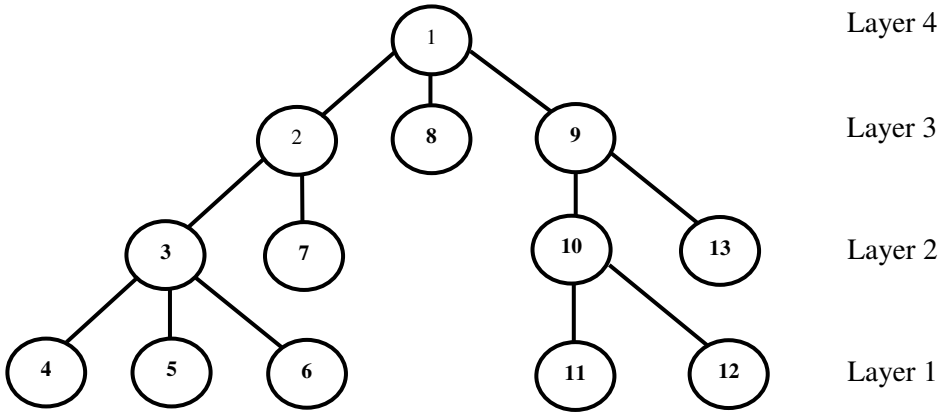

Figure 4.3 Search sequence in which nodes explored in DF SDA for a 4**X**4 MIMO system

As shown in [30−32], the DF SDA guarantees maximum likelihood solution as long as the chosen search radius includes at least one leaf node. However, this search scheme has the main disadvantage that it has non-deterministic computational complexity which varies with channel realizations and SNRs. This in turn results in variable throughput under different scenarios. It is shown in [32] that this scheme has the worst−case exponential complexity.

The work in this thesis avoids this worst case exponential complexity of DF SD by incorporating the radius setting strategy described in section 4.3.2. Moreover, radius updating technique is combined with the radius setting in order to further reduce the number of candidate nodes within the sphere. It is shown through simulations, in Chapter 5, that this scheme significantly reduces the computational complexity to a manageable level while its performance is similar to MLD.

However, it is still subject to large variations in throughput over wide range of SNRs where this is undesirable feature for hardware implementation. The average throughput can be measured as follows [37],

$$E[throughput] = \frac{N_t M}{E[D]} f_{clk}\ (bps) \quad \cdots\cdots\cdots\cdots\cdots\cdots\cdots\cdots\cdots\cdots\cdots\cdots (4.13)$$

where $E[throughput]$ is the average throughput (in bps), $E[D]$ is the average processing cycle per transmitted vector and f_{clk} is the operating clock frequency. $E[D]$ can be measured in terms of the average number of visited nodes per transmitted vector.

4.3.3 Breadth First Sphere Decoding (BF SD)

Breadth first SD begins the search at the root node and explores all the neighboring nodes before going to the branches in the next layer. In other words, it is only after visiting all the neighboring nodes (all the children of stored parents) at a given layer that the expansion to the nodes in the next layer is performed. The expansion is made only for those nodes satisfying the sphere constraint and the others are pruned. Unlike DF SD there is no backtrack in BF SD as all the candidate nodes are explored in the forward direction until leaf nodes are reached. Figure 4.4 illustrates the order of tree traversal in BF SD.

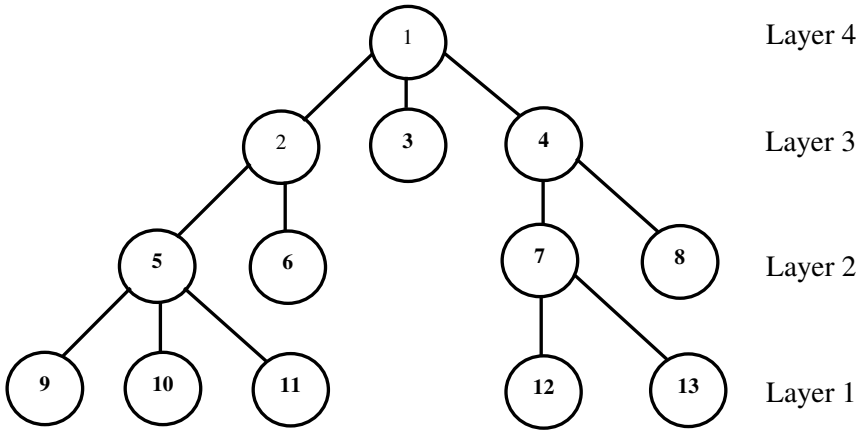

Figure 4.4 Search orders in which nodes are explored in BF SDA for a 4X4 MIMO system

Due to its level by level tree search fashion, BF SD is not suitable for radius update in the search process and hence, more complex than DF SD with radius reduction strategy. However, BF SD can be approximated by k−best SD algorithm [38, 44]. K−best SDA expands only k nodes with smallest PEDs instead of expanding all nodes at each level and finally reaches k leaf nodes with smallest PEDs. The hard decision decoder regards the leaf node with smallest accumulated distance as the detection result.

The main advantage of the k−best SDA over a full breadth first or depth first search is its uniform data path and throughput that is independent of the channel realization and the SNRs. However, the k−best SDA doesn't necessarily yield the ML solution [38, 39]. The reason why k−best SDA cannot guarantee the ML solution is analyzed in the following paragraph.

Consider symbol vectors $\boldsymbol{s}_1$ and $\boldsymbol{s}_2$ one of which say $\boldsymbol{s}_1$ is the ML solution. Obviously, at the leaf node we have $T_1(\boldsymbol{s}_1) < T_2(\boldsymbol{s}_2)$ and the k−best SDA should select $\boldsymbol{s}_1$ as the candidate instead of choosing $\boldsymbol{s}_2$. However, k−best SDA is making decision based on intermediate PEDs $T_i\left(\boldsymbol{s}_1^{(i)}\right)$ and $T_i\left(\boldsymbol{s}_2^{(i)}\right),\ i = N_t, N_t - 1, \cdots, 1$. If at some early layer $i, T_i\left(\boldsymbol{s}_1^{(i)}\right)$ is not among the k smallest PEDs (although the total sum of $e_i\left(\boldsymbol{s}_1^{(i)}\right)$ is minimum, its partial sum is not minimum at all layers), and candidate $\boldsymbol{s}_1^{(i)}$ will be discarded. In other words, even though we select the k−best PEDs at early layers, the excluded PEDs are still possible to become the minimum PED at leaf layer after accumulating the cost metrics of the remaining stages. Thus, due to the crossover of the PEDs at the intermediate layers, the error at early layer will propagate and make the decoder miss the ML solution [39].

To maintain the performance level of k−best SDA close to ML, the k value needs to be large which increases the complexity. However, it is possible to enhance the performance of k−best SDA without increasing the k value, through layer reordering and dynamic k−best SDAs, which can improve the performance with negligible computational overhead.

4.3.3.1 Layer Reordered k−best SDA

The fundamental idea behind layer reordering is to find some permutation of the columns of the channel matrix $\boldsymbol{H}$ such that the PEDs are re−distributed not to cross each other at later layers. In other words, if we can find some layer reordering scheme which can redistribute the PEDs such that the differences of PEDs of any two vectors $\boldsymbol{s}_1^i$ and $\boldsymbol{s}_2^i$ at early layer is enlarged, the possibility of the path metrics to cross each other at later layers is reduced. Mathematically, if $T_i\left(\boldsymbol{s}_1^{(i)}\right) < T_i\left(\boldsymbol{s}_2^{(i)}\right)$ and the difference is enlarged, it is less likely that after accumulating the cost metrics of the remaining layers, $T_1(\boldsymbol{s}_1) > T_1(\boldsymbol{s}_2)$ (the less likely the remaining cost metrics can change the earlier order). Hence, the k−best candidates at early layers are more likely to be the ML solution.

From Equation (4.11), the difference between the PEDs is the partial sum of the differences between the branch cost functions $e_i(\boldsymbol{s}^i)$. Hence, increasing the difference between $e_i(\boldsymbol{s}^i)$ at earlier layers is a good approach. Note, from Equation (4.9) if, by reordering the layers, we put larger $r_{i,i}$ for earlier layers and smaller $r_{i,i}$ for lower layers, the difference between PEDs at earlier layers are increased, thus the performance of SDA is improved as shown in simulation graphs of Chapter 5. In other words, if the permutation of the columns of the channel matrix $\boldsymbol{H}$ results in increasing order of the diagonal elements of the upper triangular matrix $\boldsymbol{R}$ obtained by QR decomposition of $\boldsymbol{H}$, the performance can be improved.

N. B. The order required by this layer reordering is exactly the same as the order obtained by sorted QR decomposition discussed in section 3.3.1.2 (see appendix (B) for detail). Thus, SQRD makes crucial contribution towards the improvement of the performance of the k−best SDA.

4.3.3.2 Dynamic k−best SDA

The other way to improve the performance of the k−best sphere decoding is to change the k value at different decoding layers dynamically. The objective is to reduce the possibility of excluding the ML solution at earlier layers. Therefore, it is straight forward to use larger k values at earlier

stages (layers) to ensure the ML solution is included in the k−best candidates and to use smaller k values at later stages to reduce the complexity while maintaining performance.

The idea can be further elaborated as follows. At earlier stage i, there are $i-1$ layers left and hence, the PED has another $i-1$ branch cost metrics to accumulate before reaching the final total cost. Thus, it is more likely to miss ML solution at earlier layers and increasing k here can reduce such possibilities. As the decoder descends down the tree, the PEDs are close to their final results and less likely to cross each other and therefore, we can use smaller k values at lower layers to reduce the computational complexity while maintaining the performance.

The main difficulty of dynamic k−best SDA is that there is no exact rule regarding how to fix the dynamic values of k at different detection levels [39]. It also lacks regularity which normal k−best SDA has at each stage. Despite such disadvantages, dynamic k−best method is novel and can obtain better performance or reduce computational complexity for hard decision decoding.

Moreover, dynamic k−best SD can be combined with layer reordered k−best SDA to obtain even better performance. There are a lot of modifications to the k−best SDA to either improve performance or reduce computational complexity in the literature [38−41]. However, only the two schemes just discussed are considered and used for work of this thesis.

4.4 Hybrid Sphere Decoding Algorithm (H − SDA)

The two search schemes of SDA discussed in previous sections have their own merits and demerits. The main objective of this thesis is to hybridize the two search schemes effectively by collecting the desirable features of each scheme while suppressing their non-desirable properties. Before we discuss the proposed scheme, let's briefly take a look at the advantages and disadvantages of the two search techniques independently.

Advantages of DF SDA

- It can guarantee the ML solution

- For medium to high SNRs it has better performance and higher computational throughput than the k−best SDA
- It doesn't require any sorting of node PEDs at any layer

Disadvantages of DF SDA

- It has non-deterministic computational complexity which varies with different channels and signals
- It requires search radius estimation at the beginning of the search process
- When S−E algorithm is used the tree depth is doubled. In addition, this algorithm requires sorting of candidate nodes based on their PEDs. This sorting is required whenever the symbol vector is transmitted
- Since the partial distances of most of the branch nodes at earlier layers are less than the total distance of the ML solution, it unnecessarily explores unpromising nodes at earlier layers
- Above all DF SDA has variable throughput which is undesirable feature for real time detection and hardware implementation

Advantages of k−best SDA

- It has fixed computational complexity and hence has fixed throughput for all channel realizations and SNRs
- It is suitable for parallel and pipelined hardware implementation
- Performance−Complexity tradeoff can be made by controlling the k−value

Disadvantages of k−best SDA

- It has performance degradation since it cannot always guarantee the ML solution
- It requires sorting of the PEDs which is not present in DF SDA. To select the k nodes with smallest accumulated PEDs, it requires sorting of $k \cdot M$ PEDs, which adds significant computational complexity

- It has unnecessary redundant operations required for hard decoding at the final search stages

The hybrid SDA integrates the two search strategies effectively so that the detection performance is enhanced at a reduced computational complexity. The works in [45] staggered the two SDAs, where the search is performed along the depth and breadth of a tree simultaneously, which requires multiple processing units to perform the search along the different dimensions of the tree. Another work in [46] combines the k−best SD and DF SD sequentially, where they used S−E enumeration to reduce the complexity. Moreover, they used layer reordering based on MMSE−SQRD criterion, which when combined with SDAs reduces the complexity during the search process. However, MMSE−SQRD based layer reordering in SDAs has performance degradation compared to that based on ZF−SQRD [47].

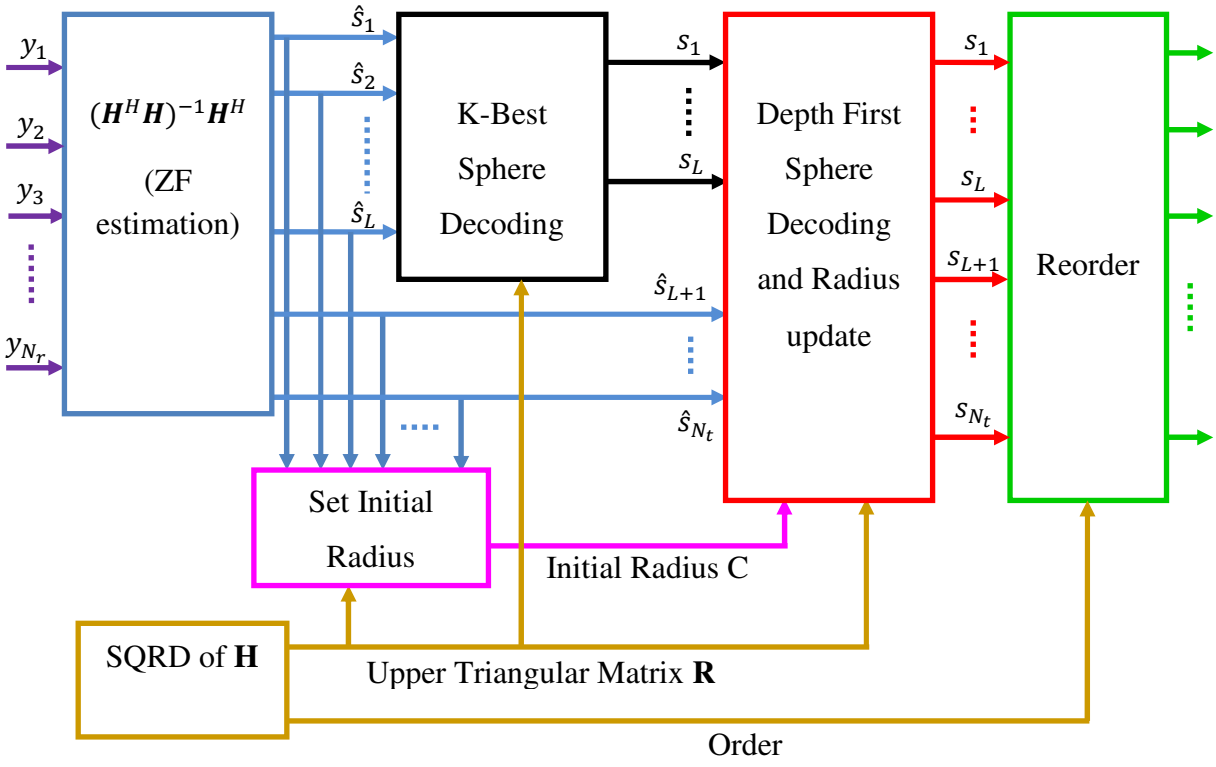

Figure 4.5 Block diagram of the proposed hybrid Sphere Decoding Scheme

In the proposed scheme the first L layers are detected using k−best SDA while the remaining $N_t - L$ layers are detected using DF SDA as shown in the block diagram of Figure 4.5. The root nodes of the DF SD are the k nodes which are outputs of the k−best SDA.

Unlike the works in the literature, the proposed hybrid scheme performs the SD search directly on complex constellations. Thus, it doesn't use S−E enumeration, which doubles the tree depth. Instead, it employs the initial radius setting and updating strategy introduced in Section 4.3.1 to reduce the complexity. In [37] it is shown that working on complex constellations is efficient for VLSI implementation as this result in higher computational throughput. Besides, the proposed scheme is suitable for any type of modulation.

Let's analyze why the hybrid sphere decoding achieve better performance at a reduced complexity. First, considering the detection performance, assume the k−best SD part consists of the ML partial vector, and since the DF SDA performs the exhaustive tree search in the remaining layers, surely it ends up with ML solution. In other words, the hybrid sphere decoder has performance at least equivalent to (if not better than) that of pure k−best SDA. The DF SD part avoids any doubt that results from crossover of the PEDs in the remaining layers which is possibly not the case for pure k−best SDA.

Second, considering the complexity, if pure DF SDA is used, a large number of nodes will be visited at earlier layers. This is due to the fact that the partial distances of most of the nodes at earlier layers are smaller than the total distance of the ML solution especially at low SNRs. Therefore, PEDs of many earlier nodes will be computed unnecessarily. Considering the case of pure k−best SDA, the number of nodes visited at any layer is fixed whereby unpromising nodes are pruned. Thus, since the hybrid SDA uses k−best SDA at its earlier layers the computational complexity is reduced at these layers. In the later layers, if pure k−best SDA is used, there is wastage of computations due to redundant operations as it expands all the k nodes even though there is significant difference in their accumulated PEDs. At lower layers, the accumulated PEDs are very close to their final values and hence, it is less likely for some of the nodes among the k−best nodes to become the final k−best solution. Therefore, k−best SDA performs unnecessary computations for these unpromising nodes. However, since the hybrid SDA uses DF SD with

initial radius setting and updating strategy, these unpromising nodes that would be considered by k−best SDA are pruned.

It is stated above that the performance of the hybrid SDA is highly dependent on the performance of the k−best SDA part. Thus, enhancing the performance of k−best SDA means enhancing performance of the hybrid scheme. Therefore, the layer reordering and dynamic k−best sphere decoding techniques discussed in the previous sections can be incorporated into the hybrid scheme, to further improve the performance.

Moreover, the parameter L, which demarcates the layers to be detected by k−best SD from the layers to be detected by DF SD, can be varied from N_t to 0. As this parameter varies from N_t to 0 the hybrid SD scheme varies from pure k−best SD to pure DF SD. Thus, the scheme can be made adaptive based on SNRs. Therefore, by using larger value of parameter L at lower SNRs and smaller value at higher SNRs, the hybrid SD scheme provides additional flexibility to the MIMO detection schemes while enhancing the performance at low computational complexity.

4.5 Complexity Analysis

4.5.1 Complexity of Maximum Likelihood Detection (MLD)

The search in the MLD goes over all the possible transmitted vectors $\boldsymbol{s}_i$ with $i = 1, 2, \ldots, M^{N_t}$; thus, the complexity of MLD is proportional to the number of candidates M^{N_t}. Furthermore the search is performed in the '$\mathbf{y} -$ space' and therefore each candidate $\boldsymbol{s}_i$ has to be multiplied by the channel matrix $\boldsymbol{H}$. The matrix−vector product of the i^{th} candidate can be written as:

$$\sum_{p=1}^{N_t} h_p (\boldsymbol{s}_i)_p \cdots\cdots\cdots\cdots\cdots\cdots\cdots\cdots\cdots\cdots\cdots\cdots\cdots\cdots\cdots\cdots (4.14)$$

Where h_p denotes the p^{th} column of H, $(\boldsymbol{s}_i)_p$ is the p^{th} element of $\boldsymbol{s}_i$.

Since all elements of $\boldsymbol{s}_i$ are taken from the set of M constellation points and thus, a given element is taken from the set $\{s_1, s_2, \cdots, s_M\}$, we can obtain all the MLD candidates. Assuming the quasi−static channel, it is efficient to store all the candidates in memory during the preamble

processing and use them in the payload processing. The amount of available memory determines the amount of complexity during the preamble and payload processing. Assuming just enough memory is available to store all the possible combinations of $\boldsymbol{Hs}_i$ with $1 \leq i \leq I$ where $I = M^{N_t}$ during training phase, complexity is analyzed as follows.

a) Complexity in the preamble processing

First, the products of every column of H with constellation points should be determined. This has a total complexity $2MN_rN_t\ R_{ADDs}$ and $4MN_rN_t\ R_{MULs}$. After that the additions corresponding to every candidate is performed. Thus, the total complexity during the preamble processing is

$$2M^2N_r\frac{M^{N_t-1}-1}{M-1} + 2MN_rN_t\ (R_{ADDs}) \cdots\cdots\cdots\cdots\cdots\cdots\cdots\cdots\cdots\cdots\cdots\cdots (4.15)$$

$$4MN_rN_t\ (R_{MULs}) \cdots\cdots\cdots\cdots\cdots\cdots\cdots\cdots\cdots\cdots\cdots\cdots\cdots\cdots\cdots\cdots\cdots\cdots (4.16)$$

b) Complexity in the payload processing

During the payload phase the vector subtraction $\boldsymbol{y} - \boldsymbol{Hs}_i$ and the squared Euclidean norm of the result have to be determined for the I possible S vectors. Then obtain the minimum of the squared norms. These operations have a total complexity of

$$(4N_rI - 1)\ (R_{ADDs}) \cdots\cdots\cdots\cdots\cdots\cdots\cdots\cdots\cdots\cdots\cdots\cdots\cdots\cdots\cdots\cdots\cdots\cdots (4.17)$$

$$2N_rI\ (R_{MULs}) \cdots\cdots\cdots\cdots\cdots\cdots\cdots\cdots\cdots\cdots\cdots\cdots\cdots\cdots\cdots\cdots\cdots\cdots\cdots (4.18)$$

4.5.2 Complexity of Sphere Decoding Algorithms

a) Complexity of the preamble processing

The preamble processing for the SD schemes basically consists of two computations

i) Computation of pseudo-inverse of the channel matrix $\boldsymbol{H}$

ii) The QR decomposition of the channel matrix $\boldsymbol{H}$

The complexity of the first part is shown in Section 3.4.1. The QR decomposition used for regular sphere decoder is simple, and slightly differs from SQRD described of Section 3.4.5, in that it doesn't involve any sorting (no norm computation and the minimum search among the norms). The detailed description of the QR decomposition of any given matrix is provided in Appendix (B). Hence, following similar procedure as in the Section 3.4.5, the total complexity of the QR decomposition is obtained to be $4N_t^2N_r - 2N_tN_r - N_t^2$ (R_{ADDs}) and $4N_t^2N_r + N_t$ (R_{MULs}).

Thus, the total complexity of the preamble processing for SDAs is as shown below

$$4N_t^3 + 12N_t^2N_r - 3N_t^2 - 4N_tN_r\ (R_{ADDs}) \cdots\cdots\cdots\cdots\cdots\cdots\cdots\cdots (4.19)$$

$$4N_t^3 + 12N_t^2N_r + N_t\ \ (R_{MULs}) \cdots\cdots\cdots\cdots\cdots\cdots\cdots\cdots\cdots\cdots\cdots\cdots (4.20)$$

Considering layer reordered k−best SD the complexity of the preamble processing is slightly different due to SQRD of the channel matrix $\boldsymbol{H}$. Thus, using the complexity of the SQRD in Equations (3.30) and (3.31), the complexity of preamble processing for layer reordered k−best is:

$$4N_t^3 + 12N_t^2N_r - \frac{3}{2}N_t^2 - 2N_tN_r - \frac{5}{2}N_t\ (R_{ADDs}) \cdots\cdots\cdots\cdots\cdots\cdots\cdots\cdots (4.21)$$

$$4N_t^3 + 12N_t^2N_r + N_t^2 + 2N_tN_r\ (R_{MULs}) \cdots\cdots\cdots\cdots\cdots\cdots\cdots\cdots\cdots\cdots\cdots (4.22)$$

b) **Complexity of the payload processing**

Before starting the tree search, SDAs perform the ZF estimation as given by equation (4.5). In section 3.4.1, this is shown to have the complexity of $4N_tN_r - 2N_t\ R_{ADDs}$ and $4N_tN_r\ R_{MULs}$.

As detailed in section 4.3.1, the complexity of SDAs is directly related to the number of nodes visited during the tree traversal. Therefore, to determine the complexity of SDAs, it suffices to know the number of nodes visited and the amount of complexity associated with each node at any given layer. The number of nodes depends on the type of tree search; therefore analysis must be made independently for DF SD and k-best SDA

I. Complexity of the payload processing for DF SDA

At root node only equation (4.9) modified as, $e_{N_t}\left(\boldsymbol{s}^{(N_t)}\right) = \left|r_{N_t,N_t}\left(\hat{s}_{N_t} - s_{N_t}^{m}\right)\right|^2$ is computed. This equation has a computational complexity of 5 (R_{ADDs}) and 6 (R_{MULs}). Since there are M root nodes and the sphere constraint test must be performed for each, totally we would have $6M$ (R_{ADDs}) and $6M$ (R_{MULs}). After this step, all nodes satisfying the sphere constraint become parent nodes. Equation (4.10) is computed for any parent node, while Equations (4.9) and (4.11) are computed for any child node. Since a parent node has M children, we can add the complexity of these children nodes to the complexity of parent nodes and by doing so we obtain the total complexity associated with any parent node as follows:

$$4(N_t - i + 1) + 8M \ \ (R_{ADDs}) \ \cdots\cdots\cdots\cdots\cdots\cdots\cdots\cdots\cdots\cdots\cdots\cdots\cdots\cdots (4.23)$$

$$4(N_t - i + 1) + 6M(\ R_{MULs}) \cdots\cdots\cdots\cdots\cdots\cdots\cdots\cdots\cdots\cdots\cdots\cdots\cdots\cdots (4.24)$$

Hence, knowing the number of parent nodes at each layer is sufficient to determine the complexity of SDA. Unfortunately, for DF SDA, the number of nodes that can become parent nodes at a given layer is not deterministic as it varies with parameters such as search radius and SNRs. For this reason, the average number of parent nodes for DF SDA can only be known from simulation. However, assuming P_{i+1} is the number of parent nodes at layer $i+1$, the total computational complexity of payload processing for DF SDA is obtained to be

$$4N_tN_r - 2N_t + 6M + \sum_{i=1}^{N_t-1}(4(N_t - i + 1) + 8M)\, P_{i+1}\ (\ R_{ADDs}) \ \ \cdots\cdots (4.26)$$

$$4N_tN_r + 6M + \sum_{i=1}^{N_t-1}(4(N_t - i + 1) + 6M)\, P_{i+1}\ (\ R_{MULs}) \ \cdots\cdots\cdots\cdots\cdots (4.27)$$

Considering the additional complexity of the radius setting technique introduced in this thesis, the complexity comes from the computation of Equations (4.11) and (4.12). Equation (4.11) has a

complexity of $N_t \log_2 M$ (R_{ADDs}) and Equation (4.12) adds a computational complexity of $2N_t^2 + 4N_t - 1$ (R_{ADDs}) and $2N_t^2 + 4N_t$ (R_{MULs}).

II. Complexity of the payload processing for k−best SDA

The computational complexity of the payload processing for k−best SDA is determined in the same way as for DF SDA. The difference between the two is that for k−best SDA; there are always k parent nodes while the number of parent nodes is variable for DF SDA as stated above. Moreover, the k−best SDA employs sorting algorithms in order to obtain the k parent nodes with the smallest PEDs among the available nodes at a given layer. However, unlike the DF SDA, k−best SDA doesn't perform the sphere constraint test. Considering these differences, the computational complexity of the payload processing for k−best SDA is determined to be:

$$4N_tN_r - 2N_t + Mk^2N_t + 2kN_t^2 + 7MkN_t + \frac{3}{2}KN_t + \frac{1}{2}k^2 + 5M - \left[\frac{1}{2}k^2N_t + 2MK^2 + 5Mk + \frac{7}{2}k + 1\right](R_{ADDs}) \cdots\cdots\cdots\cdots (4.28)$$

$$4N_tN_r + 6M + k[2N_t^2 + 6MN_t + 2N_t - (6M + 4)](R_{MULs}) \cdots\cdots\cdots (4.29)$$

Note: The sorting algorithm employed for the k-best SDA is bubble sorting algorithm for its simplicity even though there are others which have lower complexity.

4.6 Summary of Complexity Analysis

It can be concluded from the complexity analyses made in Chapter 3 that the complexity of MIMO detection schemes such as ZF, MMSE, ZF−SIC, MMSE−SIC, ZF−SQRD and MMSE−SQRD predominantly depend on the number of transmit antennas N_t, and linearly and logarithmically dependent on the number of receive antennas N_r and the constellation size M, respectively. Also in this chapter, we have seen that the complexity of MLD is exponential in N_t and/or M; whereas the complexities of sphere decoders (both DF and BF) are polynomial in N_t and linear in both M and N_r. Besides, the complexity DF SDA and k−best SDA depend on the size of the search radius C and the value of k chosen, respectively.

In order to compare the complexities of MIMO detection algorithms, we have to express the complexity in terms of single number, for example, number of equivalent additions. To do so we have to know the number of additions equivalent to a single multiplication for our particular implementation. In some literatures, such as [34], algorithms are assumed to be implemented with 8−bit operations. Also in this thesis the same assumption is made. Based on this assumption, a single 8−bit multiplication is assumed to be as complex as ten 8−bit additions. With these considerations, the complexity can now be expressed as single number in terms of equivalent additions. Tables 4.1 and 4.2 summarize the complexities of preamble processing and payload processing, respectively, real additions (R_{ADDs}) and real multiplication (R_{MULs}), and equivalent additions (E_{ADDs}) where $1R_{MULs} = 10E_{ADDs}$

Table 4.1 Summary of the complexity of preamble processing for MIMO detection schemes

Detection Technique	Complexity of preamble processing		
	Number of R_{ADDs}	Number of R_{MULs}	Number of E_{ADDs}
ZF	$4N_t^3 + N_t^2(8N_r - 2) - 2N_tN_r$	$4N_t^3 + 8N_t^2N_r$	$44N_t^3 + 88N_t^2N_r - 2N_t^2 - 2N_tN_r$
MMSE	$4N_t^3 + N_t^2(8N_r - 2) - 2N_tN_r + N_t$	$4N_t^3 + 8N_t^2N_r$	$44N_t^3 + 88N_t^2N_r - 2N_t^2 - 2N_tN_r + N_t$
ZF-SIC	$\frac{1}{6}N_t(6N_t^3 + 8N_t^2(1 + 2N_r) + 3N_t(1 + 6N_r) + 2N_r - 5)$	$N_t^2(N_t + 1)^2 + \frac{4}{3}N_rN_t(N_t + 1)(2N_t + 1)$	$11N_t^4 + \frac{88}{3}N_t^3N_r + \frac{64}{3}N_t^3 + 43N_t^2N_r + \frac{21}{2}N_t^2 + \frac{41}{3}N_tN_r - \frac{5}{6}N_t$
MMSE-SIC	$\frac{1}{3}N_t(3N_t^3 + 4N_t^2(2N_r + 1) + 3N_t(3N_r + 1) + Nr - 1)$	$N_t^2(N_t + 1)^2 + \frac{4}{3}N_tN_r(N_t + 1)(2N_t + 1)$	$11N_t^4 + \frac{88}{3}N_t^3N_r + \frac{64}{3}N_t^3 + 43N_t^2N_r + 11N_t^2 + \frac{41}{3}N_tN_r - \frac{1}{3}N_t$
ZF-SQRD	$4N_t^2N_r + \frac{1}{2}(N_t^2 - 5N_t)$	$4N_t^2N_r + N_t^2 + 2N_tN_r$	$44N_t^2N_r + \frac{21}{2}N_t^2 + 20N_tN_r - \frac{5}{2}N_t$
ML	$2M^2N_r\frac{M^{N_t-1}-1}{M-1} + 2MN_rN_t$	$4MN_rN_t$	$2M^2N_r\frac{M^{N_t-1}-1}{M-1} + 42MN_rN_t$
DF SD	$4N_t^3 + 12N_t^2N_r - 3N_t^2 - 4N_tN_r$	$4N_t^3 + 12N_t^2N_r + N_t$	$44N_t^3 + 132N_t^2N_r - 3N_t^2 - 4N_tN_r + 10N_t$
Regular k-best	$4N_t^3 + 12N_t^2N_r - 3N_t^2 - 4N_tN_r$	$4N_t^3 + 12N_t^2N_r + N_t$	$44N_t^3 + 132N_t^2N_r - 3N_t^2 - 4N_tN_r + 10N_t$
Layer reordered k-best	$4N_t^3 + 12N_t^2N_r - \frac{3}{2}N_t^2 - 2N_tN_r - \frac{5}{2}N_t$	$4N_t^3 + 12N_t^2N_r + N_t^2 + 2N_tN_r$	$44N_t^3 + 132N_t^2N_r + \frac{17}{2}N_t^2 + 18N_tN_r - \frac{5}{2}N_t$

Table 4.2 Summary of the complexity of payload processing for MIMO detection schemes

Detection Technique	Complexity of payload processing		
	Number of R_{ADDs}	Number of R_{MULs}	Number of E_{ADDs}
ZF	$2N_tN_r + 2N_t(N_r - 1) + N_t log_2 M$	$4N_tN_r$	$44N_tN_r - 2N_t + N_t log_2 M$
MMSE	$2N_tN_r + 2N_t(N_r - 1) + N_t log_2 M$	$4N_tN_r$	$44N_tN_r - 2N_t + N_t log_2 M$
ZF−SIC	$2N_t(4N_r - 1) + N_t log_2 M$	$8N_tN_r$	$88N_tN_r - 2N_t + N_t log_2 M$
MMSE−SIC	$2N_t(4N_r - 1) + N_t log_2 M$	$8N_tN_r$	$88N_tN_r - 2N_t + N_t log_2 M$
ZF−SQRD	$2N_t^2 + 4N_tN_r - 4N_t + N_t.log_2 M$	$2N_t^2 + 4N_tN_R$	$22N_t^2 + 44N_tN_r - 4N_t + N_t.log_2 M$
ML	$(4N_rM^{N_t} - 1)$	$2N_rM^{N_t}$	$24N_rM^{N_t} - 1$
DF SD	$4N_tN_r - 2N_t + 6M + \sum_{i=1}^{N_t-1}[4(N_t - i + 1) + 8M]\,P_{i+1}$	$4N_tN_r + 6M + \sum_{i=1}^{N_t-1}[4(N_t - i + 1) + 6M]\,P_{i+1}$	$44N_tN_r - 2N_t + 66M + \sum_{i=1}^{N_t-1}[44(N_t - i + 1) + 68M]\,P_{i+1}$
k−best	$4N_tN_r - 2N_t + Mk^2N_t + 2kN_t^2 + 7MkN_t + \frac{3}{2}KN_t + \frac{1}{2}k^2 + 5M - \left[\frac{1}{2}k^2N_t + 2MK^2 + 5Mk + \frac{7}{2}k + 1\right]$	$4N_tN_r + 6M + k[2N_t^2 + 6MN_t + 2N_t - (6M + 4)]$	$44N_tN_r + 20kN_t^2 + Mk^2N_t + 60MkN_t + \frac{43}{2}kN_t + \frac{1}{2}k^2 - [65M(k - 1) + 2Mk^2 + \frac{1}{2}k^2N_t + 2N_t + \frac{87}{2}k + 1]$

Chapter 5

Simulation Results and Discussion

5.1 Introduction

In this chapter, the MIMO detection schemes which are described in Chapters 3 and 4 are programmed in MATLAB and simulations are performed to obtain BER characteristics. These characteristics are used to compare the performances of the different MIMO detection algorithms. There are also simulations included to compare the throughput and computational complexities of these algorithms based on the complexity figures of Tables 4.1 and 4.2.

5.2 Simulation Setup

In all simulations, it is assumed that the channel is perfectly known at the receiver and unknown at the transmitter. Hence, the total transmission power is uniformly allocated across all the transmitter antennas (and all the sub−carriers for MIMO−OFDM system). Besides, in order to make a fair comparison between MIMO and SISO systems, the total transmit power is fixed irrespective of the number of transmitters and for convenience, the total power is normalized to unity.

The BER performance is obtained by averaging over 50,000 channel realizations and unless otherwise mentioned, for a packet length of 256 bits per channel realization, making the transmission of 12,800,000 bits at a given SNR. Moreover, an indoor like environment is assumed, and since the objects and/or the transceivers in such an environment move slowly, the Doppler shift is negligible. For this reason, quasi-static channel described in Section 2.3.2 is assumed in all simulations. Besides, since an indoor environment is characterized by large scattering, the channel matrix elements are Rayleigh fading. Unless otherwise mentioned, sufficient antenna spacing ($\geq \lambda_c/2$) is assumed both at the transmitter and receiver sides and hence resulting in uncorrelated channel coefficients. Thus, the channel matrix elements are i.i.d Rayleigh fading. Although, the channel is assumed static during a packet transmission, independent channel realizations are used for different packets (see Section 2.3.2).

Since we are considering point−to−point communication (single user MIMO) systems, it is assumed that all the transmit antennas are co−located and the same holds for the receive antennas. With this, it is reasonable to consider equal number of delays for all spatial channels with the same average power at a given tap. Finally, it is assumed that these delays are uniformly spaced in time with exponentially decaying power delay profiles as shown by Equation (2.15).

Since the objective of the thesis is to compare the performance of different MIMO detection algorithms, for simplicity, most of the simulations are performed for narrowband systems, where the number of channel tap is 1, which are special cases of wideband systems. With this, the channel has turned out to be frequency flat Rayleigh fading as described in Subsection 2.3.3. Finally, the performance of the MIMO detection schemes in wideband systems is evaluated in combination with OFDM technique. Besides, the BER performance comparisons are made without channel coding in all simulations. Figure 5.1 shows basic simulation set up for the computation of BER in MIMO systems.

Table 5.1 Basic simulation parameters for narrowband MIMO systems

Channel Model	Discrete time, Quasi-static, i.i.d., Rayleigh fading coefficients
Packet size	256 bits
Modulation type	BPSK, QPSK, and 16−QAM
Transmit power	Total power is normalized, equally shared among all antennas
Channel coding	Only un-coded system is considered
MIMO configuration	Symmetric, i.e. $N_t = N_r$, linear array arrangement
Antenna spacing	$\geq \lambda_c/2$
Correlation Model	Kronecker, $H = {R_{RX}}^{1/2} h_{i.i.d} \left({R_{TX}}^{1/2}\right)^*$

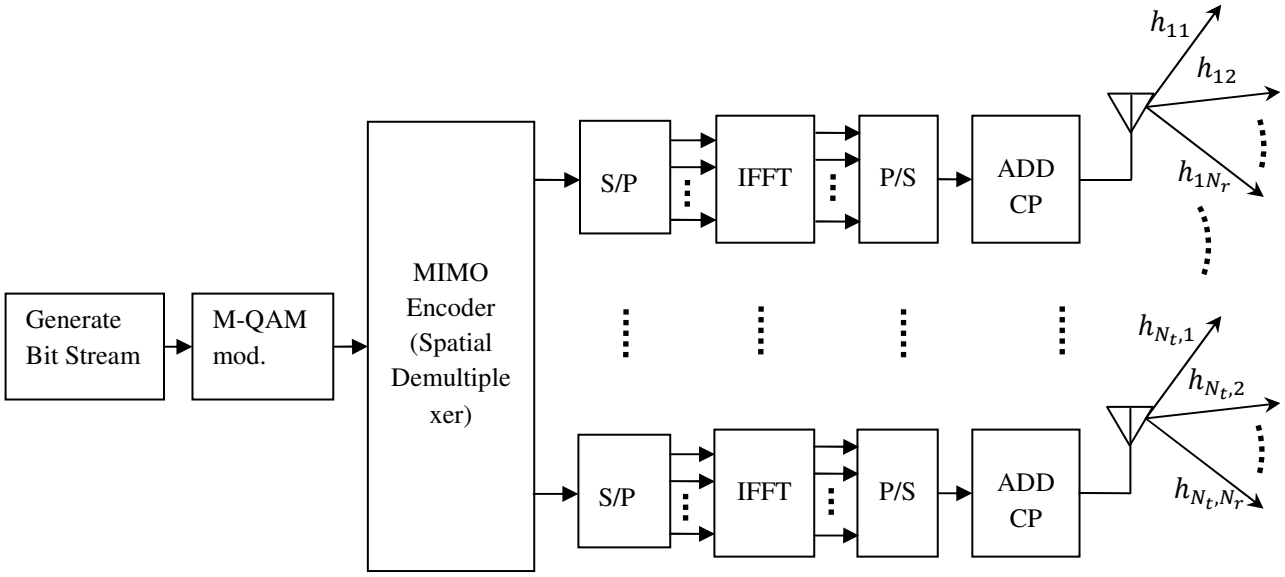

a) Transmitter Block Diagram

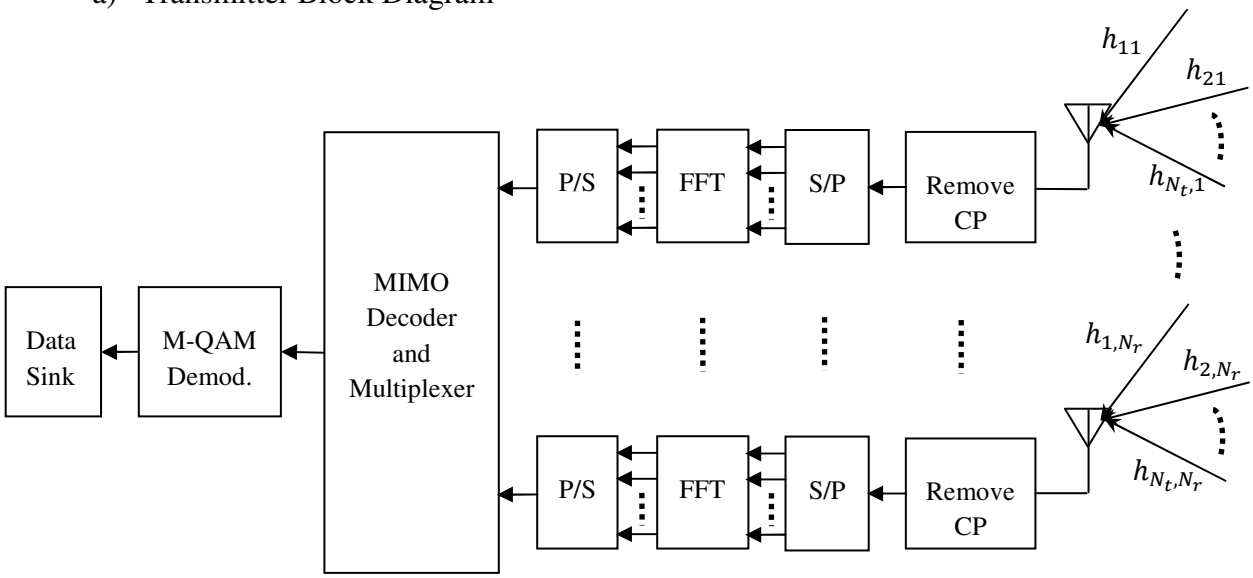

b) Receiver Block Diagram

Figure 5.1 Simulation Setup for MIMO−OFDM Systems

5.3 Performance Comparison for Conventional MIMO Detection Schemes

Figure 5.2 shows the BER characteristics of the conventional MIMO detection techniques against average SNR per receive antenna for a 2 X 2 system that operates in a flat Rayleigh fading environment. A QPSK modulation scheme is used and there is no channel coding applied. The BER performance of 1 X 1 system is included as a reference to compare the MIMO systems with SISO systems.

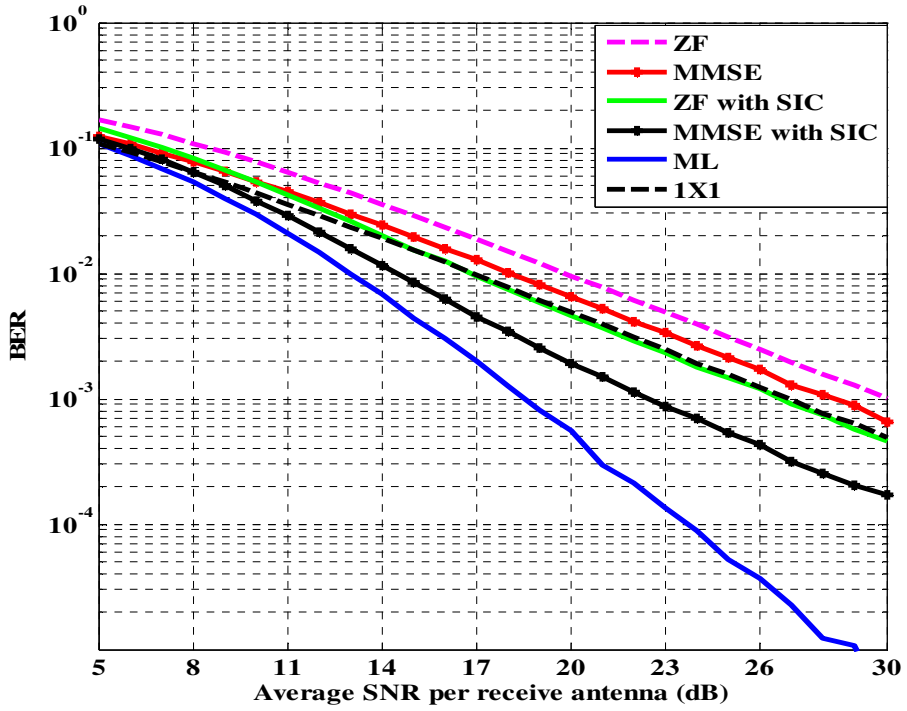

Figure 5.2 BER performances of conventional MIMO detection schemes for 2X2, QPSK modulation

From Figure 5.2, it can be seen that the linear detection schemes (ZF and MMSE) have the poorest performance among the MIMO detection techniques. The ZF has the poorest performance due to error amplification in its detection process and the MMSE improves this performance by suppressing the error amplification. Another reason for poor performance of the linear detection schemes is that these methods have lower diversity order which tends to be $N_r - N_t + 1 = 1$ for symmetric$(N_t = N_r)$ systems.

The MLD outperforms all the detection schemes by far because it has a diversity order equal to $N_r = 2$ and independent of N_t. For SIC schemes the diversity order increases, per detection layer, from $N_r - N_t + 1$ for the first layer to N_r for the last detection layer (from 1 to 2 for this particular case). Thus, these detection schemes have better performance than the linear detection schemes but poorer than that of MLD. Moreover, SIC in combination with MMSE detection significantly outperforms the other detection techniques except the MLD.

The other important point worth observing from Figure 5.2 is the performance comparison of MIMO systems with SISO systems. It is clearly seen that the non linear MIMO detection schemes have even better performance than 1 X 1 systems due to their higher diversity order. However, the diversity order of the linear MIMO detection methods for symmetric systems is the same as that of SISO systems (1 X 1) and since there is interference among the layers in MIMO systems; the linear detection schemes have poorer performance than the SISO systems. This fact is more conspicuous in Figure 5.3 shown below.

Figure 5.3 depicts the performance results of the same MIMO detection schemes as Figure 5.2, but this time for 4 X 4 system. From these results it can be seen that the performance of the ZF detection scheme is getting worse whereas the performance of all the non linear detection schemes is getting better. The main reason for this is that the diversity order of the ZF detection technique remains the same (equal to one) for both systems (2 X 2 and 4 X 4) while the interference among the layers has been increased for a 4 X 4 system, thus resulting in performance degradation. However, for non linear detection schemes, for instance, for MLD the diversity order is increased from 2 to 4 and hence the BER curve falls off rapidly for 4 X 4 system. This verifies the fact that the BER performance of the MLD increases with increasing number of antennas as discussed in Section 4.2. Similarly, it can also be seen that the BER performances of the SIC schemes are increased for 4 X 4 systems, even though the rate is not as rapid as that of MLD, due to the fact that diversity order for SIC schemes range from 1 to 4 for 4 X 4 system from the first detection layer to the last layer. The SISO performance is provided as a reference in order to clearly show this fact.

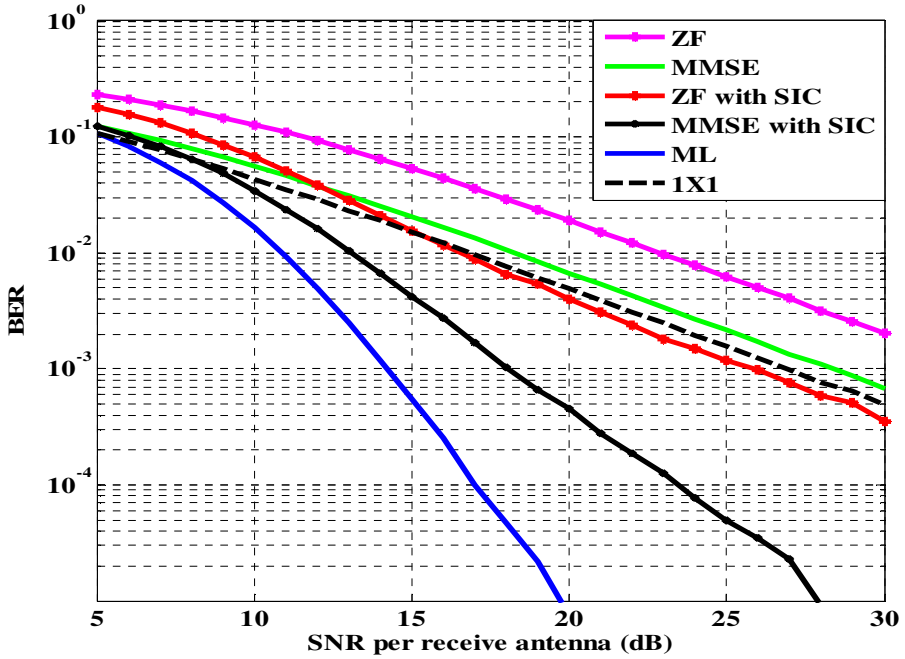

Figure 5.3 BER performances of conventional MIMO detection schemes for a 4 X 4, QPSK modulation

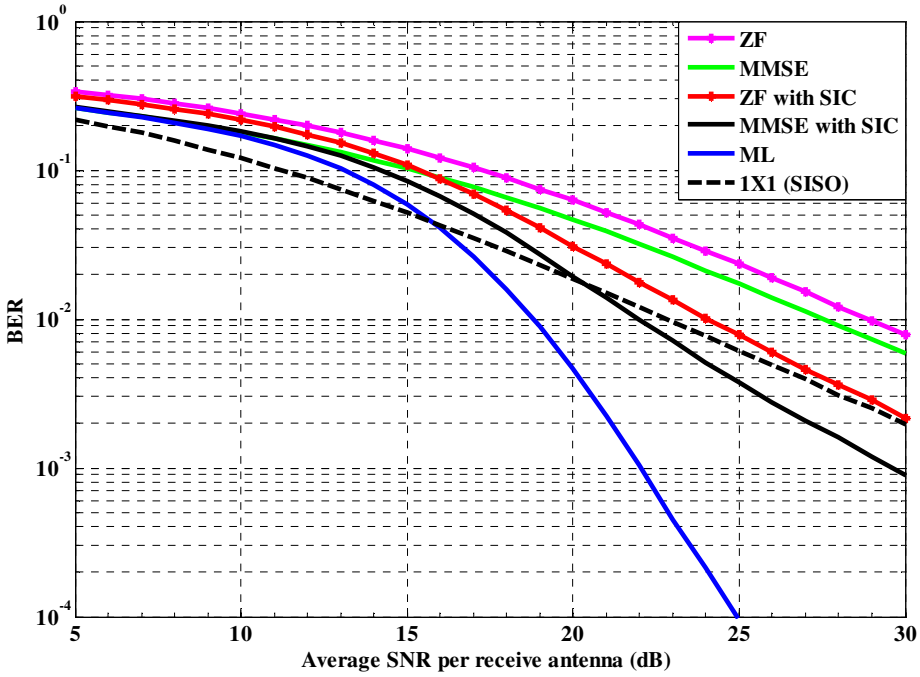

Figure 5.4 BER performances of conventional MIMO detection schemes for a 4 X 4, 16−QAM modulation

Figure 5.4 shows the effects of employing higher constellation order (16−QAM) on the performances of the conventional MIMO detection schemes. As it can be seen from this figure, the performance of MMSE with SIC drops considerably compared to the MLD and, so do the performances of the other schemes. Furthermore, the performance of MMSE and ZF schemes, as well as ZF with SIC and MMSE with SIC get closer to one another. Therefore, from Figures 5.3 and 5.4 we can conclude that the conventional MIMO detection schemes do not work well for large number of antennas and large constellation sizes. This can be explained by the fact that the higher constellation orders are more vulnerable to noise, resulting in performance loss.

5.3.1 Effect of Spatial Correlation

Moreover, the performance of the conventional MIMO detection schemes deteriorates further as compared to the MLD under ill conditioned MIMO channels. One of the impairments of MIMO channel is the spatial correlation between the channel matrix elements which results from lack of sufficient antenna spacing and/or lack of sufficient scattering objects in the channel environment. To see the effects of spatial correlation, simulations are performed with spatial correlation model introduced in Section 2.4. Figure 5.5 shows the BER characteristics of the conventional MIMO detection schemes (only ZF, MMSE with SIC and MLD are shown for clarity) for a 4 X 4 system with equal transmit and receive side correlation $r = r_{T_X} = r_{R_X} = 0.6$ and 16−QAM modulation. In order to show performance penalty introduced due to correlation, the performances of the same detection schemes under uncorrelated channel condition are included (the smooth curves). From this figure, it can be seen that the performance penalty strongly depends on the detection algorithm, SNR and the correlation coefficient r. Thus, the performance penalty of the MLD is small as compared to the other detection schemes while the penalty of ZF detection scheme is large. To explain the dependence of the performance penalty on SNR and r, Figure 5.6 depicts the BER performance of MMSE with SIC and MLD as a function of correlation coefficient r at average SNR per receive antenna values of 10 dB and 30 dB. Note that, from Figure 5.6 we can compare the BER penalties of the two schemes at a given SNR by a vertical shift (constant correlation coefficient) of the performance point. Thus, we can conclude that the performance difference between the two schemes is large at higher SNRs and vice versa. Similarly, the

horizontal shift (at fixed BER) of performance point at a given SNR shows the performance degradation as a function of the correlation coefficient r.

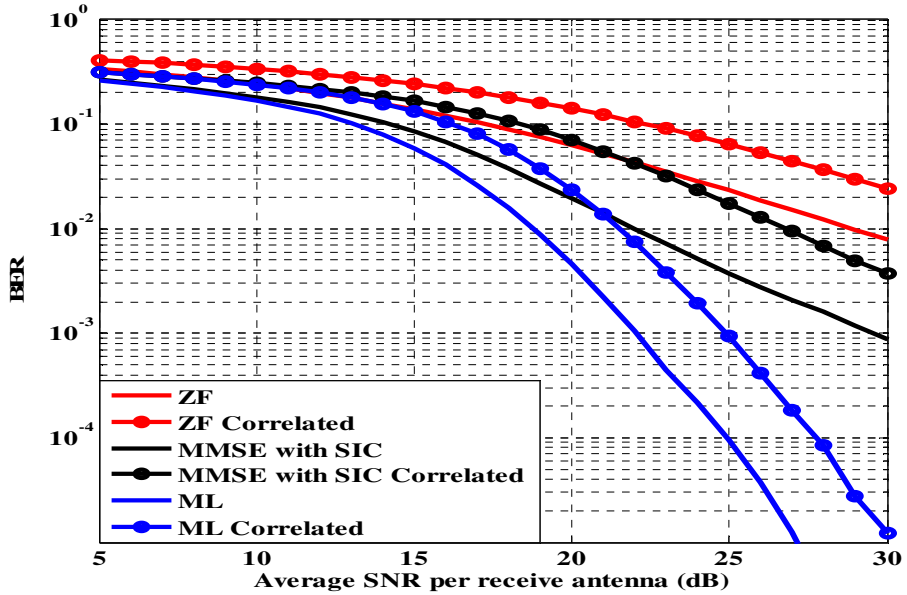

Figure 5.5 BER performance of conventional MIMO detection schemes for a **4 X 4**, operating in a correlated (r=0.6), flat Rayleigh fading, 16−QAM modulation

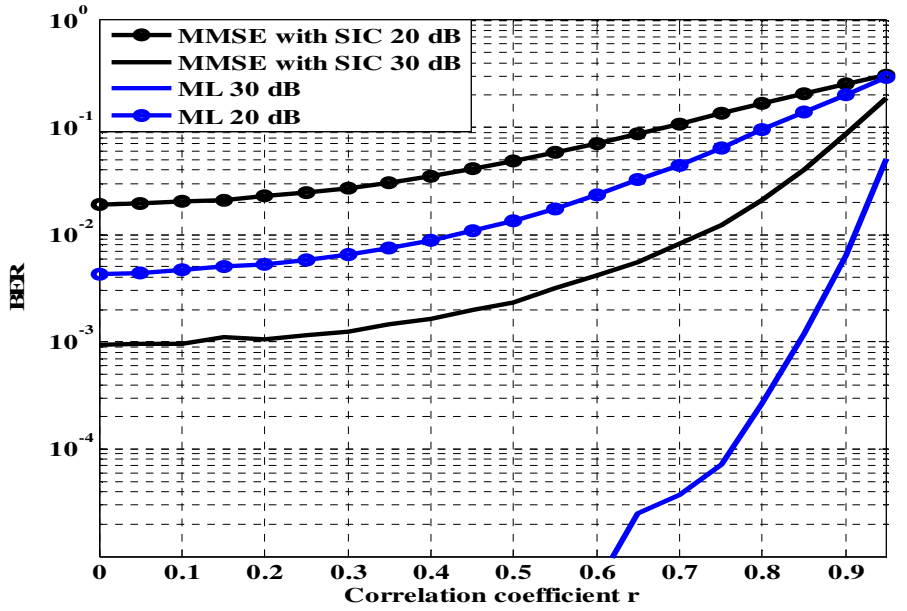

Figure 5.6 BER versus correlation coefficient r of MMSE with SIC and MLD for a 4 X 4, 16−QAM, and flat Rayleigh fading at 20 and 30 dB

5.3.2 Complexity Comparison

So far we have considered comparison of MIMO detection schemes based on BER performance, as a result of which the MLD is found to be optimal in any case. However, MIMO detection schemes can also be compared in terms their computational complexities. The complexity figures shown in Tables 4.1 and 4.2 are general and are not suitable for comparison as one of the detection schemes may have lower complexity during preamble processing and higher complexity during payload processing, or vice versa, when compared to the others. Thus, for a fair comparison we have to compute the overall complexity i.e. the sum of the complexity of the preamble processing and the payload processing for a given packet length. In this section it is assumed that the packet length is 1024 bits. Moreover, the complexity associated with packet detection, time and frequency synchronization and channel estimation does not depend on the chosen MIMO detection technique; therefore, we do not take it into account. Based on these assumptions, the average computational complexity per transmitted symbol vector in E_{ADDs} is given as:

$$Average\ complexity = PL + (N_t \log_2 M) * \frac{PA}{1024}\ (E_{ADDs}) \quad \cdots\cdots (5.1)$$

where PA is the complexity of preamble processing and PL is the complexity of payload processing in E_{ADDs} given in Tables 4.1 and 4.2 respectively.

Hence, using this fact, Figure 5.7 shows the complexity comparison of conventional MIMO detection schemes for BPSK modulation. It can be seen from this figure that the complexity of ZF and MMSE almost coincide and, so do the complexities of ZF with SIC and MMSE with SIC. Obviously, the performance improvement of the schemes with SIC is paid by the complexity increase compared to the linear detection schemes. Moreover, the complexity of SIC based on SQRD is lower than the complexity of SIC based on V−BLAST while their performance is the same. Another important point to note from this figure is that the complexity of MLD is less than or equal to the complexity of the SIC based on V−BLAST for number of antennas up to $N_t = 4$. However, for larger number of antennas and higher constellation sizes, the complexity of the MLD diverges rapidly from the complexity of the other schemes. For 16−QAM constellations this is shown in Figure 5.8. (Note: the Y-axis scale is logarithmic scale that is why ML grows linearly)

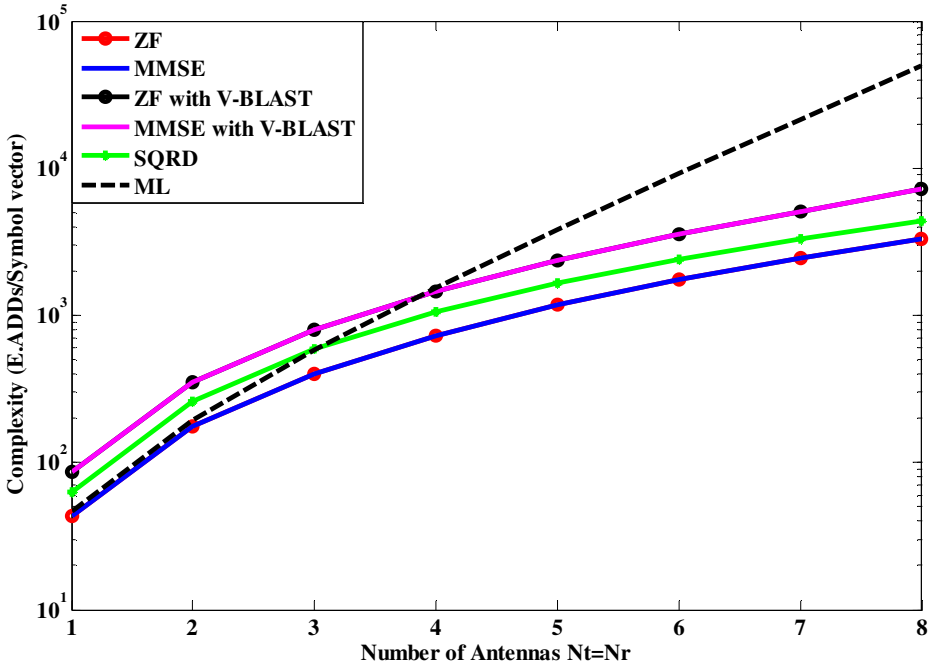

Figure 5.7 Complexity (E_{ADDs}/symbol) of conventional MIMO detection schemes versus number of antennas ($N_t = N_r$), for BPSK, 1024 bit packet length

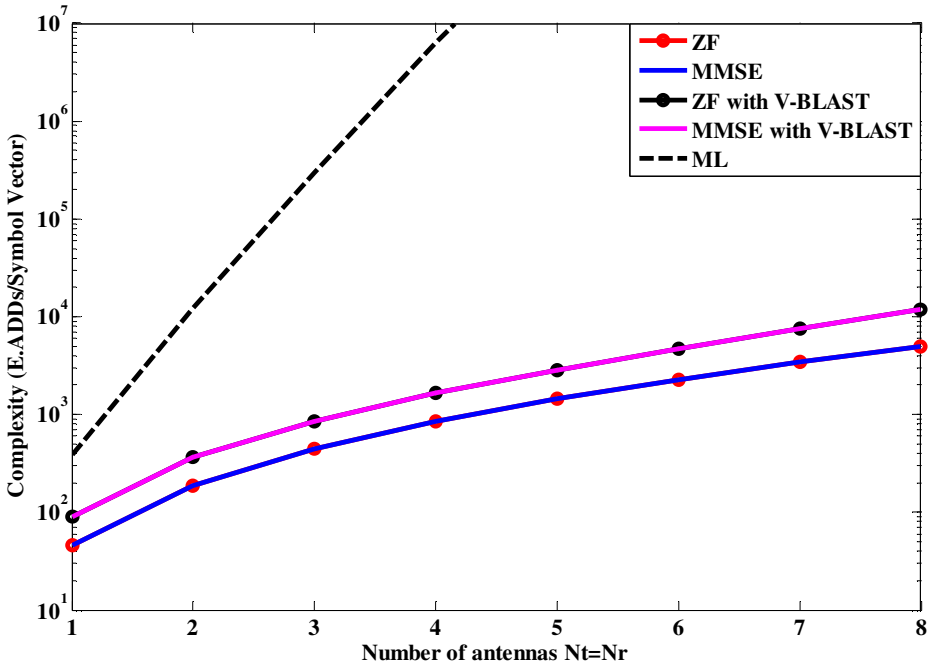

Figure 5.8 Complexity (E_{ADDs}/Symbol Vector) comparisons of conventional MIMO detection schemes versus number of antennas, for 16−QAM

5.4 Performance Comparison for the State−of−the Art MIMO Detection Schemes

From the discussions of the last section, we can deduce that the MLD has optimal performance; but it has the main drawback of computational complexity whereas the conventional MIMO detection schemes have manageable computational complexity while their performances are far lower than that of MLD. Thus, we have to look for the other detection schemes which have performance near that of MLD while their complexity is near that of the conventional MIMO detection schemes. These are the Sphere Decoder schemes discussed in chapter 4.

5.4.1 Performance of DF SDA

Theoretically, it is shown in Section 4.3.2 that the DF SD can guarantee the ML solution and this is verified in Figure 5.9 through simulations where the BER curve of the two schemes exactly coincide. However, DF SD has the main drawback that its complexity is dependent on the search radius which is difficult to determine.

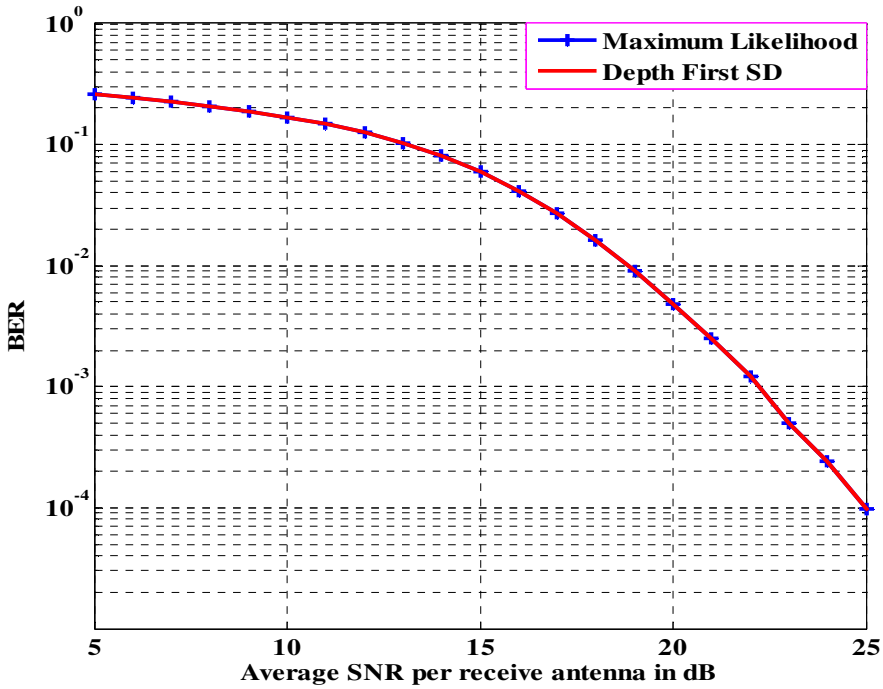

Figure 5.9 BER performance versus SNR per receive antenna of DF SD and MLD for a **4 X 4**, 16-QAM modulation

One solution to the problem of the search radius is to set the initial radius to infinity and then update in the mean time. In fact this can reduce the computational complexity, however, in order to reduce the computational complexity further, radius setting technique is proposed in this thesis.

With the proposed radius setting, enormous saving in computational complexity is achieved while the additional complexity to determine the initial radius is negligible. This is shown in Figure 5.10 where the complexity is expressed in terms of the average number of parent nodes per transmit vector at a given SNR. However, it is clearly seen from this figure that the number of parent nodes varies with SNRs for both radius setting strategies. Thus, the DF SD has variable computational complexity and as a result, it has variable throughput which is undesirable feature. The complexity of 8−best SD is provided as a reference to show that the complexity of DF SD is even lower than the k−best SDAs for high SNRs.

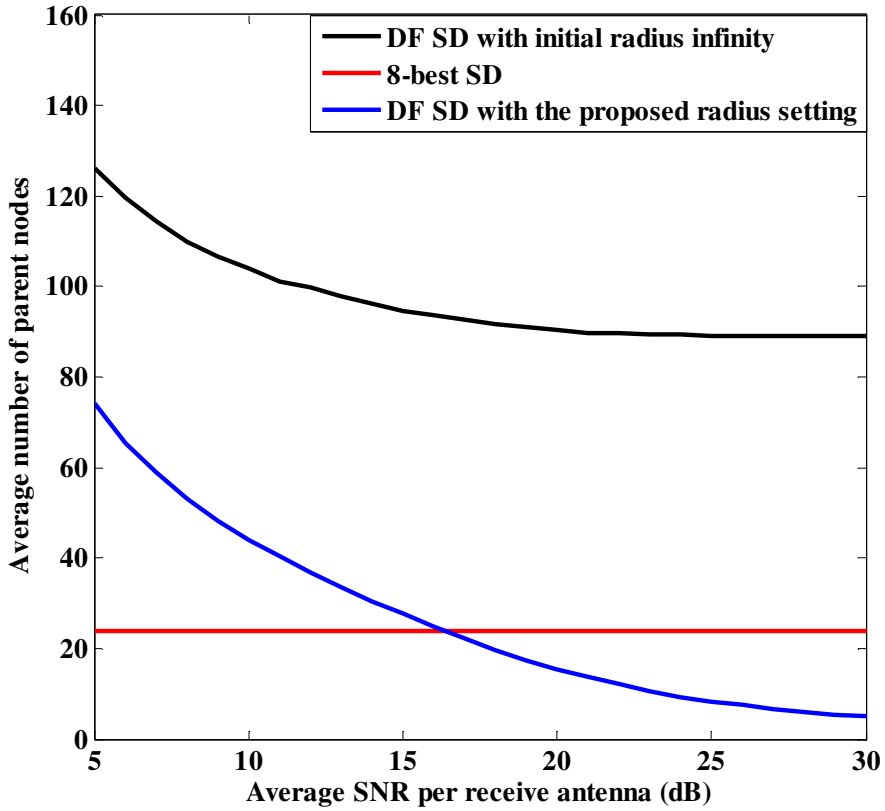

Figure 5.10 Complexity of DF SD (Number of parent nodes) versus SNR per receive antenna for the two radius setting strategies

5.4.2 Performance comparison for k−best SDA

In order to avoid the variable throughput of the DF SD, k−best SDAs are used. With the k−best SDA fixed throughput is achieved; however, this scheme has performance degradation when compared to MLD as it can be seen from Figure 5.11. Nevertheless, the performance of the k−best SD can be improved by increasing the k value as depicted in the figure for k=6, 8 and 10. But this will introduce large complexity due to increased number of parent nodes and additional sorting. For instance, increasing the k value from 6 to 8 improves the performance (about 2 dB at BER of 10^{-3}) while the number of parent nodes increase by 25% and the sorting complexity increases by 57.3%. Thus, increasing the k value to improve the performance is not a feasible approach. The performance of the MMSE with SIC and MLD are included as a reference to show that SDAs perform better than all the conventional detection schemes.

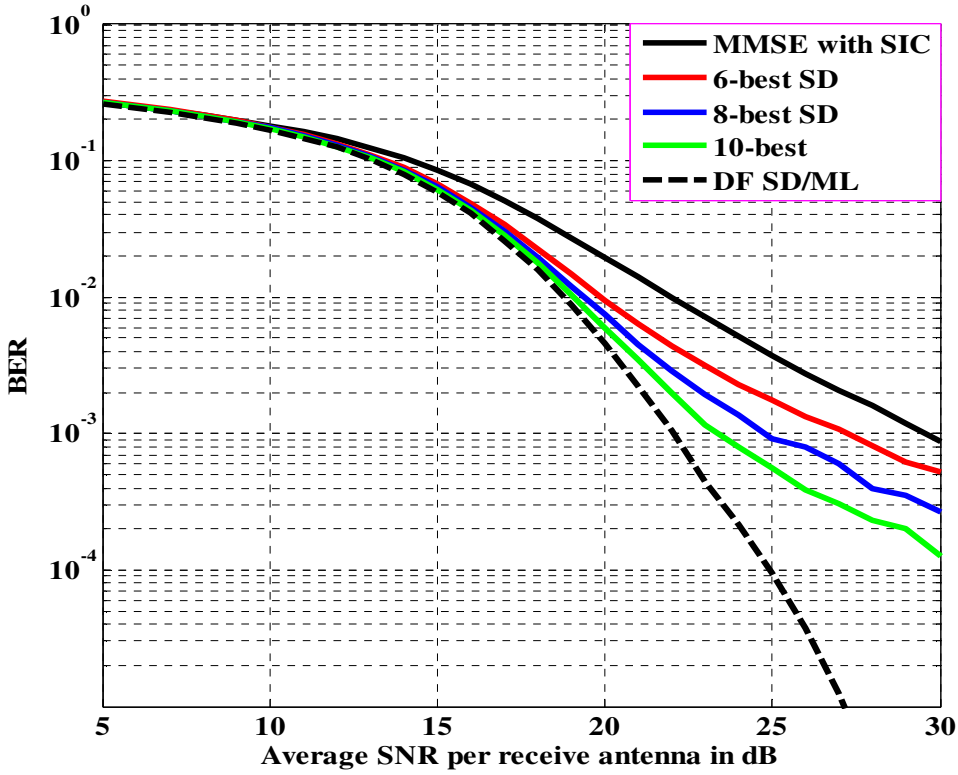

Figure 5.11 BER performance of k−best SDA (k=6, 8 and 10) for a 4 X 4, 16−QAM, flat Rayleigh fading channel (MMSE with SIC and DF SD are included as a reference)

5.4.3 Performance Comparison for Layer Reordered k−best SD

One approach to improve the performance of the k−best SD, without using large k values, is by applying layer reordering introduced in section 4.3.3. The simulation results obtained by applying layer reordering to the k−best SDA are shown in Figure 5.12. From this figure, we can see that by applying the layer reordering to the 6−best SDA, similar performance to normal 8−best SDA is obtained which is about to 2dB gain compared to normal 6−best SDA. In other words, by applying layer reordering which has negligible complexity, 25% increase in number of parent nodes and 57.3% increase in sorting complexity is saved. Similarly, it can be seen from this figure that layer reordered 8−best SDA achieves the same performance as normal 10−best SD, thus saving 20% parent nodes and 64.1% increase in sorting complexity.

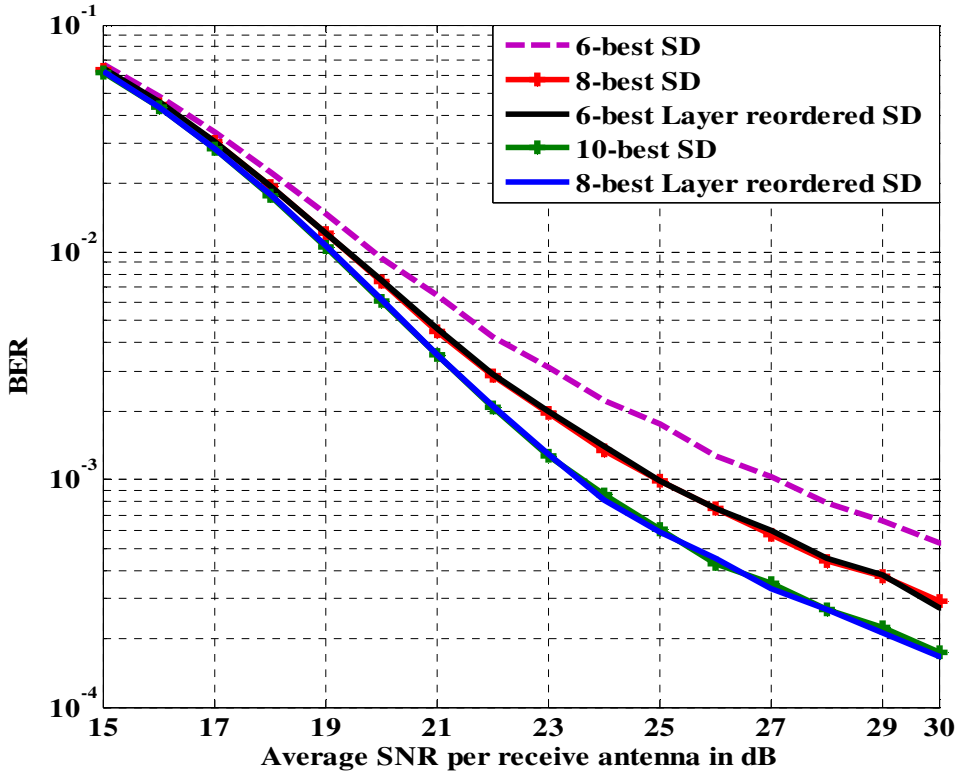

Figure 5.12 BER comparison of normal k−best SDA and layer reordered k-best SDA for a 4 **X** 4, 16−QAM, flat fading Rayleigh channel

Computational complexity comparison in terms of average number of Equivalent additions per transmitted symbol vector for k−best SDAs (both normal and layer reordered) as compared to the conventional detection schemes are provided in Figure 5.13. Clearly, the figure depicts that the computational complexity of normal k−best and layer reordered k−best are almost the same. Furthermore, unlike the MLD the complexity of k−best SDAs is not exponential with the number antennas albeit it is larger than the computational complexities of conventional detection schemes represented by MMSE with SIC in this figure. Obviously, it can be seen that the computational complexity of the k−best SDAs increase with increasing k values.

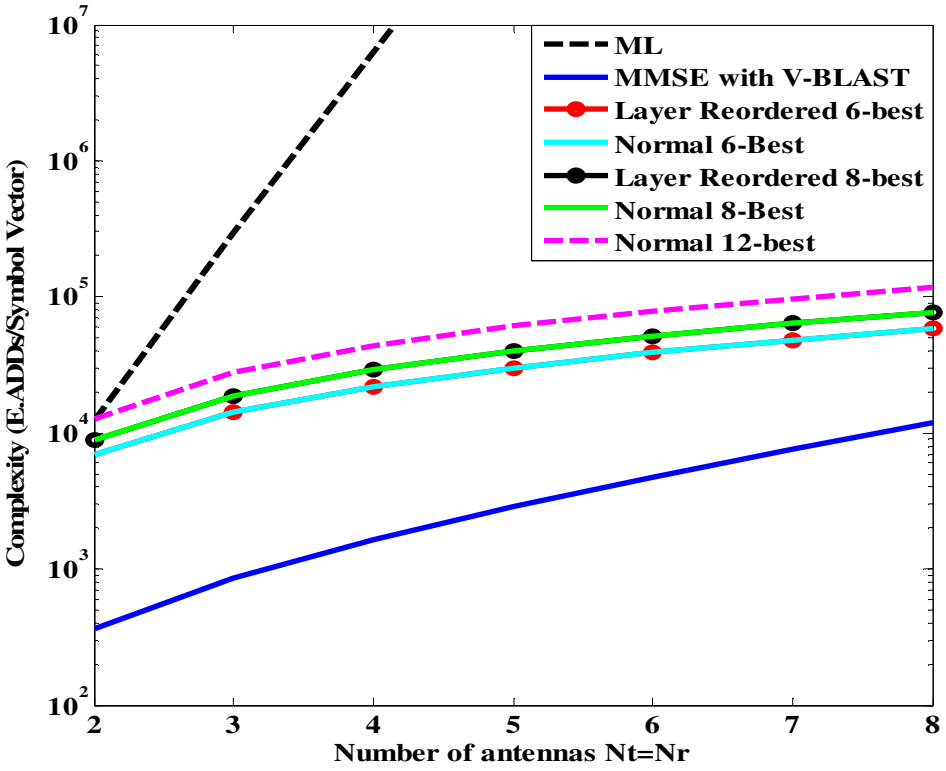

Figure 5.13 Computational complexity comparisons (E_{ADDs}/Symbol vector) for k−best SDA (k=6, 8 and 10), MLD and MMSE with SIC as a function of number of antennas.

5.4.4 Performance Comparison for Dynamic k−best SD

Another scheme to improve the performance of k−best SDA without increasing the complexity is by varying the value of k dynamically at different decoding levels (see Section 4.3.3). Figure 5.14

shows simulation results obtained by applying dynamic k-best SDA as compared to the normal and layer reordered k−best SDAs. Thus, by applying dynamic k−best (average k=8), significant performance improvement (about 3dB) as compared to normal 8−best SDA, which is even better than layer reordered 8−best SDA, is obtained. Dynamic k−best SDA does not introduce any additional computational complexity, but it has the problem of how to determine the appropriate k values at each decoding levels. However, this can be solved through number simulations using different values of k at each simulation. Moreover, dynamic k−best SDA can be combined with layer reordered k−best in order to obtain further performance enhancement. This is shown in Figure 5.14 which is labeled as combined k−best. Clearly, the combined k−best SDA can replace the normal k-best SDA to obtain performance closer to MLD at a reduced computational complexity.

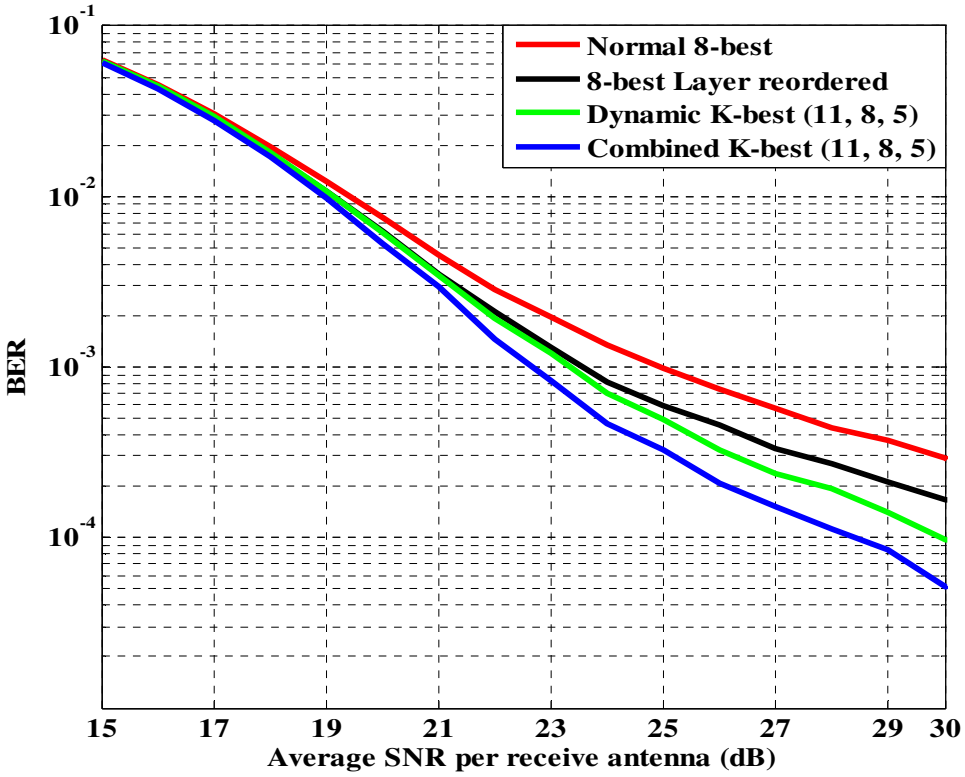

Figure 5.14 BER comparison of normal k-best, dynamic k−best, layer reordered k−best and combined k−best SDAs for a 4X4, 16−QAM modulation

5.5 Performance Comparison for the Proposed Hybrid SD

So far we have looked at the schemes that can improve the performance of k−best SDAs without increasing the computational complexity. A scheme that can significantly reduce the computational complexity of the k−best SDAs without affecting the performance is proposed in this thesis. This is the hybrid SDA described in section 4.4. The scheme uses k−best SDA to detect the first L layers and then DF SDA, with the proposed radius setting technique, to detect the remaining $N_t - L$ layers. In Figure 5.15, simulation results of the proposed scheme in comparison with k−best SDAs is depicted with $L = 2$.

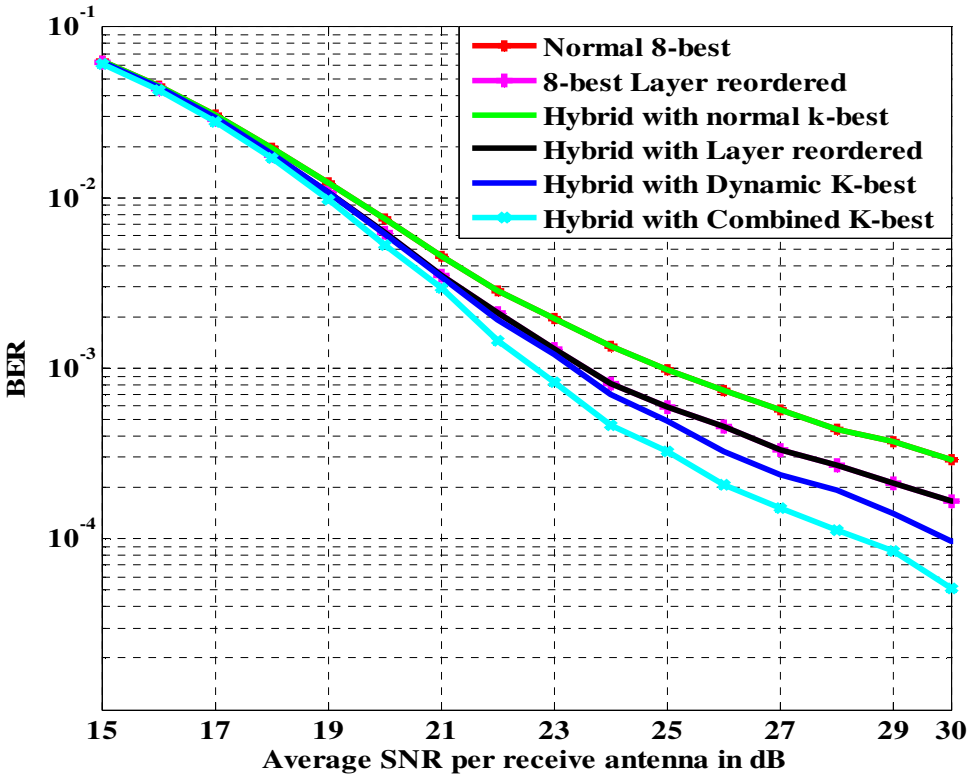

Figure 5.15 BER performance comparison of hybrid SD scheme with k-best SD schemes for a 4X4, 16-QAM (k=8 for normal and layer reordered, and k=11, 8 and L=2 for hybrid schemes)

From this figure it can be seen that the proposed hybrid scheme maintains the performance of the k−best SDA. Furthermore, the schemes used to enhance the performance of the k−best SDAs can be introduced in to the proposed scheme for the same purpose. Thus, as it is shown in the figure,

by introducing layer reordering to the hybrid SD scheme the same performance as layer reordered k−best SDA is achieved. Similarly, dynamic k−best SDA can also be incorporated in to the proposed detection scheme as depicted in the same figure.

From Figure 5.15 we can generalize that the proposed hybrid scheme can at least maintain the performance of k−best SDAs. However, when we compare the proposed scheme in terms of computational complexity with the k−best SDAs, the former has much reduced complexity as this can be verified from Figure 5.16. For simplicity, the number of parent nodes in the first L layers, which are detected using k−best SDAs, is not included in the comparison as it is the same for both cases (hybrid and k−best).

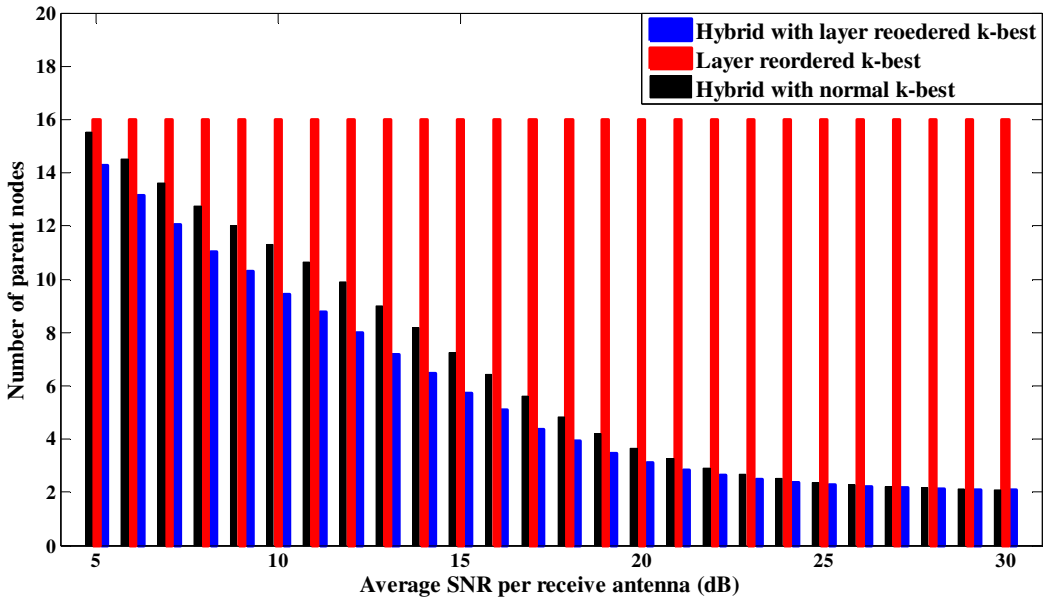

Figure 5.16 Average number of parent nodes for the proposed scheme as compared to the number of parent nodes for k−best SDAs for a 4X4, 16−QAM modulation

It can be seen from this graph that the hybrid scheme has lower average number of parent nodes than the k−best SDAs. Particularly, for medium to high SNRs the proposed scheme has significant complexity difference from the k−best SDAs. Moreover, the number of nodes reduces further for low to medium SNRs when layer reordering is used in the hybrid scheme. Thus, layer

reordering introduces both performance enhancement and complexity reduction as we can see from Figures 5.15 and 5.16. Henceforth, we will use layer reordering in all simulations.

Another important observation from Figure 5.16 is the variation of the number of parent nodes with SNRs which was stated as undesirable feature in the earlier discussions. However, the variation of parent nodes in the proposed scheme is upper bounded (loose upper bound) by the number of parent nodes in the k−best SDAs, unlike the regular SDAs where the corresponding number may be is very large at low SNRs. This fact is further elaborated using throughput as shown in Figure 5.17.

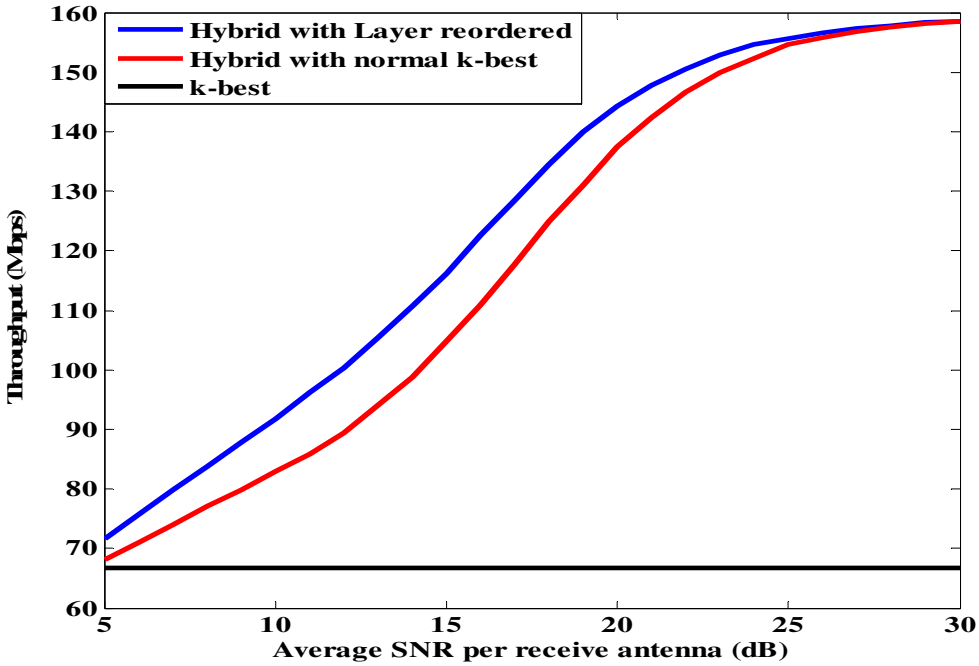

Figure 5.17 Throughput versus SNR per receive antenna of the proposed hybrid scheme and the conventional k−best SDA for a 4X4, 16−QAM systems.

Figure 5.17 depicts the throughput (Mbps) comparison of the hybrid sphere decoding both with and without layer reordering and the traditional k−best SDAs. The throughput is computed based on equation 4.13 assuming operating clock frequency of 100MHz and, one clock cycle per one parent node. Clearly, it can be seen from the figure that the throughput of the proposed scheme is superior to the traditional k−best SD even at low SNRs. At higher SNRs, the proposed scheme has

throughput more than twice of the throughput of the k−best SDAs which is fixed to about 66.6 Mbps for k is equal to eight. Besides, the proposed detection scheme enables us to choose between k−best SDA and DF SDA by setting the parameter L to N_t and 0, respectively.

Figure 5.18 shows the effect of varying the design parameter L on the system performance. As it can be seen from the figure, for fixed k value (k=8 in this particular case) there is no significant difference in BER performance obtained as a result of varying the parameter L from 1 to 3. However, there is a considerable difference in computational throughput for various values of L. This is clearly illustrated in Figure 5.19 that, in general, the throughput increases with decreasing L. For L=2 and 3, the throughput is better than the k−best SDA for all SNRs and the variation of throughput for these values of L with SNRs is smooth especially for L=3.

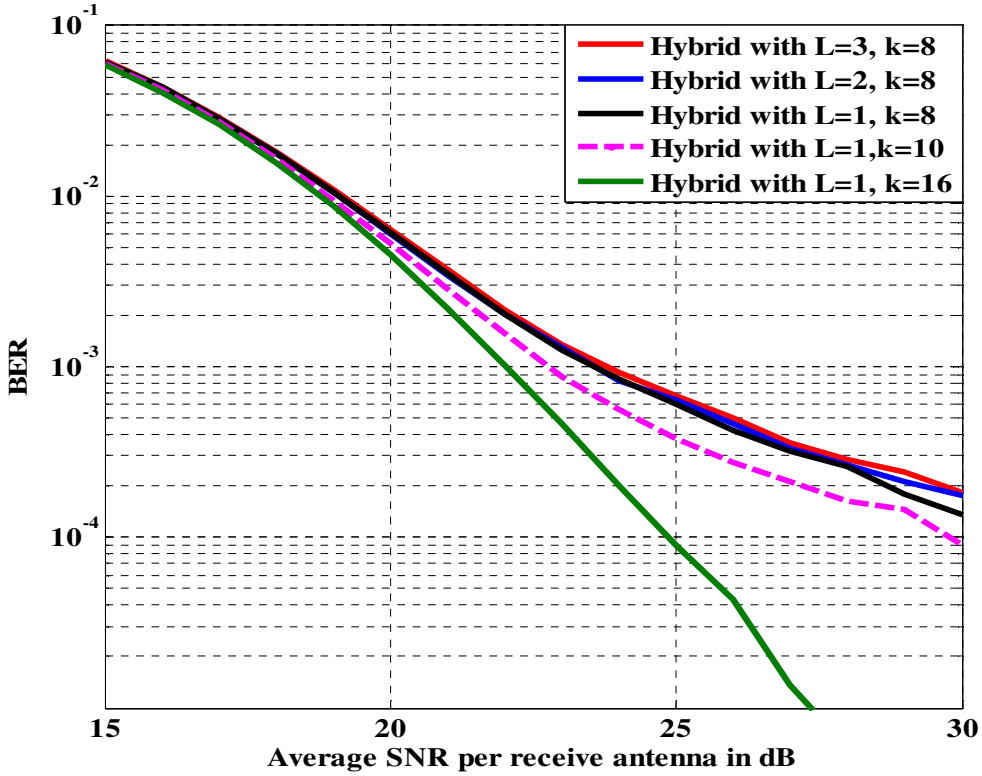

Figure 5.18 performance comparison of hybrid SDA for different values of parameter L and k for a 4X4, 16-QAM system

But for $L = 1$, the throughput is slightly lower than that of k−best SDA for SNRs of less than about 10dB. Nevertheless, the throughput for L=1 increases almost linearly for medium to high SNRs, thus, overtaking the throughput of L=2 and 3 at about 15dB. From these results we see that the throughput can be controlled by varying the parameter L where small value of L must be chosen for medium to high SNRs and vice versa to maintain the throughput above that of the k−best SDAs.

Another important property of the hybrid sphere decoding scheme is that its computational complexity is not as sensitive to the chosen k value as the pure k−best SDA, especially for small values of L. This is clearly seen from Figure 5.19 that the computational throughput for $k = 8$ and $k = 16$ almost coincide when $L = 1$, with negligible difference at low SNRs. However, there is significant performance difference between $k = 8$ and $k = 16$ as shown in Figure 5.18. With $k = 16$ and $L = 1$, similar performance with the optimal MLD is obtained. Hence, using the proposed scheme it is possible to achieve optimal performance with much reduced computational complexity.

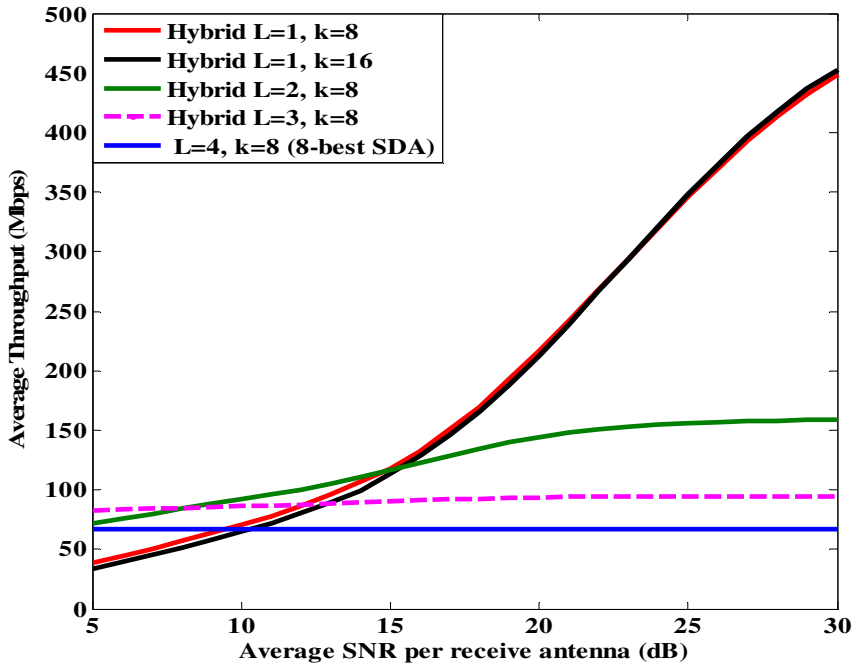

Figure 5.19 Average throughput (Mbps) comparison of the hybrid sphere decoding for different values of L for a 4X4, 16−QAM systems (The throughput of k-best SDA included for reference)

From all simulation results, we can conclude that the significant performance difference among the MIMO detection schemes is seen at high SNRs. Our proposed scheme has almost optimal performance with high throughput at these SNRs and hence it is feasible MIMO detection scheme. On the other hand, all MIMO detection schemes have more or less similar performance at low SNRs and in order to keep high throughput at all SNRs it is advisable to use the proposed detection scheme with large *L* and small k at low SNRs and vice versa.

5.6 Performance Comparison of MIMO Detection Schemes in Wideband Systems

So far, the MIMO detection algorithms are evaluated for narrowband systems, where there is no inter symbol interference (ISI). However, MIMO technology will predominantly be used in broadband systems that exhibit frequency selective fading and, therefore, ISI. OFDM transforms wideband frequency selective fading channel into a set of parallel flat fading channels and thus, robust against ISI. MIMO systems operating in wideband channels can be combined with OFDM systems for more spectral efficiency and higher performance.

MIMO detection schemes described in this thesis are implemented for wideband systems in combination with OFDM technique. Figure 5.20 shows the simulation results of some of the detection algorithms which are obtained based on parameters enumerated in Table 5.2.

Table 5.2 Main parameters of OFDM used in the simulation

MIMO size	4X4
Modulation scheme	16-QAM
Number of sub-carriers	52
Number of pilots	4
OFDM symbol duration	4μs
Guard interval	800ns
Sub-carrier spacing	312.5 kHz
Channel bandwidth	20MHz
RMS delay spread	100ns

The simulations results shown in Figure 5.20 are performed considering an ideal channel environment where the maximum delay spread $\tau_{max} = 500$ ns, which is reasonable for large building. Thus, the guard interval of 800ns is sufficient to combat the ISI resulting from such typical environment. Accordingly, the channel length (number of taps) under consideration is 10 with uniformly spaced exponentially decaying power delay profile described in chapter 2. As already pointed out at the beginning of the chapter, impairments associated with OFDM such as inter carrier interference (ICI), frequency offset, peak average power ratio (PAPR) problem, IQ imbalance and so on are assumed to have no effect. Besides, since the channel under consideration is quasi−static and perfect CSI is also available at the receiver, the pilot symbols are simply inserted to fulfill the requirement.

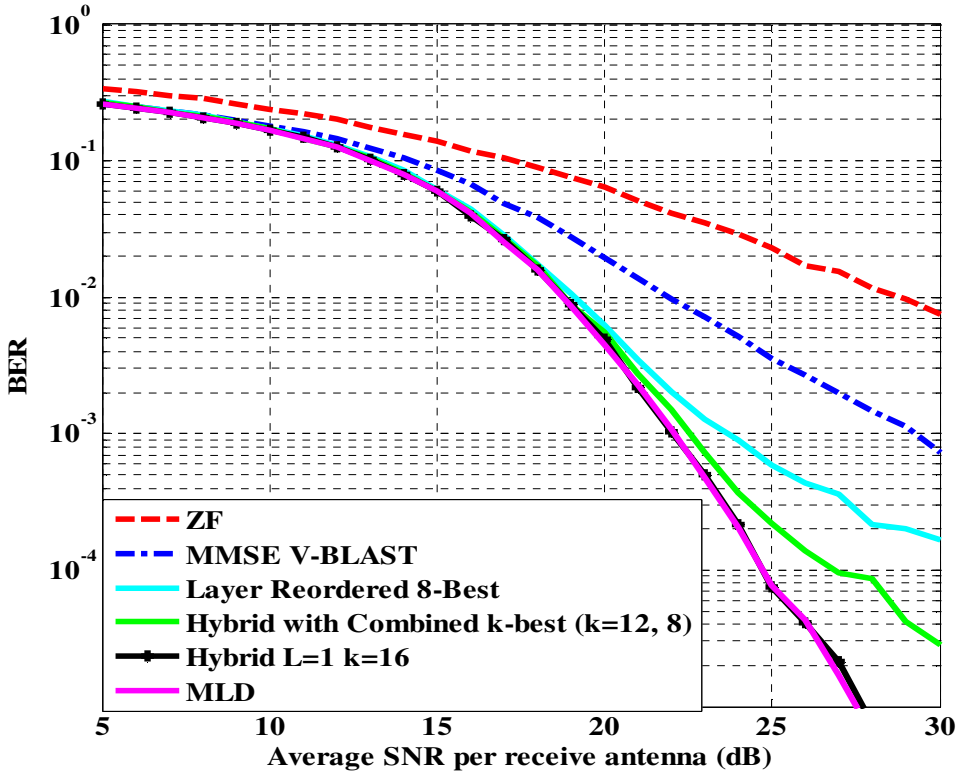

Figure 5.20 BER performance comparisons of MIMO−OFDM signal detection schemes for 4X4, 16−QAM systems and wideband Rayleigh fading channel

Simulations performed based on these assumptions are depicted in Figure 5.20 for different MIMO detection schemes. In general, it can be deduced that MIMO systems can be combined with OFDM techniques for high data rate wireless communications with performance even better than the narrowband systems (due to frequency diversity inherent in OFDM systems). Moreover, the proposed MIMO detection scheme can achieve similar performance as MLD with much reduced computational complexity as shown in the figure. Also in this case, the conventional detection schemes are shown that their performance is suboptimal.

Chapter 6

Conclusions and Recommendations for Future Work

6.1 Conclusions

MIMO−OFDM provides an attractive and practical solution for future high−speed indoor wireless data communications networks since it combines spectrally efficient MIMO systems with OFDM technique, which is robust against frequency selective fading.

In this thesis, plenty of MIMO detection schemes are extensively studied. As it is shown in the literature, the MLD is obtained to have optimal performance. Unfortunately, it is found from the complexity analysis that this scheme suffers from large computational complexity which grows exponentially with number of antennas and/or constellation points. Hence, the use MLD is practically limited to systems with low data rate per channel use (up to 8 bpcu) as shown in Figures 5.7 and 5.8.

The conventional MIMO detection schemes such as ZF, MMSE, ZF with SIC and MMSE with SIC (order put in increasing performance) are also evaluated in this work. Accordingly, it can be concluded that these schemes are suboptimal in performance when compared to MLD, even though they have manageable computational complexity. Moreover, the performance of these schemes is found to decline with larger MIMO sizes and/or larger constellation points.

So, it is necessary to find the MIMO signal detection schemes that can achieve performance closer to MLD and have computational complexity nearer to that of conventional detection schemes. To this end, sphere decoding algorithms (SDAs) are proposed in the literature and these are investigated thoroughly in this thesis. As a result, it is found that DF SD algorithm achieves similar performance as MLD (Figure 5.9), but with much reduced computational complexity. Furthermore, in order to reduce the complexity of DF SDA radius setting strategy is introduced in this thesis. With this, considerable reduction in computational complexity is achieved. However, there is significant variation of throughput with SNRs which is undesirable from hardware implementation point of view.

K−best SDAs are introduced in order to obtain fixed computational complexity and thus, fixed throughput. Even though k−best SDA can perform better than the conventional detection schemes as shown in Figure 5.11, it cannot guarantee the performance of MLD as DF SDA. To obtain performance very close to that of MLD large k value must be used which in turn introduces large computational complexity.

Some techniques such as layer reordering and use of dynamic values of k at different decoding layers are shown to enhance performance of k−best SDAs with negligible additional complexity. Layer reordering, which is obtained through the use of sorted QR decomposition of the channel matrix, introduces performance enhancement of more than 2dB at high SNRs. Dynamic k−best achieves performance even better than that of the layer reordered k−best SDA. Additionally, layer reordering and dynamic k−best are combined to achieve further performance enhancement more than 4 dB at high SNRs as depicted in Figure 5.14.

In this thesis, the two sphere decoding algorithms are hybridized effectively so that the desirable features of both schemes are exploited while the undesirable features of each scheme are suppressed. Accordingly, the first L layers are detected using k−best SDA while the remaining $N_t - L$ layers are detected using DF SD with the introduced radius setting strategy. It is verified through simulations that the proposed hybrid scheme can at least maintain the performance of the corresponding k−best SDA, but with much lower computational complexity.

Moreover, the hybrid scheme can accommodate the layer reordered and dynamic k−best SDAs and hence, performance enhancement is obtained at a reduced complexity. Thus, with the proposed hybrid scheme significant throughput enhancement more than twice of the fixed throughput of k−best SDAs is achieved particularly for medium to high SNRs. Besides, by varying the parameter L, target throughput can be achieved at specific SNR even with better performance. It is seen from simulation results that, throughput is maximized by reducing L for medium to high SNRs and, increasing L and decreasing k for low SNRs. Hence, it can be concluded that, the proposed hybrid scheme achieves much better performance and computational throughput than the traditional k−best SDAs.

The described MIMO detection techniques are implemented for wideband systems in combination with OFDM and the simulation results show that the proposed MIMO detection scheme works well even in wideband channel.

6.2 Recommendations for Future Work

Here are list of recommendations to the possible extensions of the works of this thesis research:

- MIMO−OFDM detection schemes considered in this thesis are hard-decision detectors without any sort of channel coding. Further works can extend these schemes for soft-decision decoding by designing appropriate coding schemes capable of utilizing outer channel coding and inner space time coding.
- Perfect channel state information at the receiver is assumed in this work. However, obtaining CSI is another challenge of MIMO−OFDM systems under practical situations. Thus, it would be beneficial to design simple and efficient channel estimation and tracking techniques for MIMO−OFDM systems
- Realistic wireless channels are time varying which implies time varying system capacity. Therefore, it is preferable to study and incorporate adaptive resource allocation techniques by supplying CSI at the transmitter
- The indoor environment with Rayleigh fading channel, where there is no line of sight (NLOS) component, is assumed in this work. However, practically there might be line-of-sight (LOS) component even in an indoor environment. Thus, it is desirable to develop channel model particular to MIMO systems under such an environment and evaluate the proposed detection schemes for such models. Furthermore, the models should consider the spatial correlation which are inevitable in MIMO systems
- The proposed detection scheme has high performance with very high computational throughput for medium to high SNRs. Thus, we recommend further works focusing on how to measure SNRs at the receiver. With this, the proposed scheme can be made adaptive through the variation of the design parameter L and hence maintain the target throughput and performance.

- In the proposed detection scheme, the distance of a candidate vector is measured using l_2 −norm, which is relatively complex, and hence, it is desirable to investigate the performance complexity tradeoff of this scheme using other, low complex, norm computations.
- Further reduction in computational complexity can be achieved with the proposed scheme if appropriate enumeration techniques, which work directly on complex constellations, are found. With this, the computational complexity associated with large MIMO sizes can be kept reasonable. Thus, we recommend future works focus on these issues.
- It is assumed that the impairments associated with OFDM systems such as time and frequency synchronization, PAPR, IQ imbalance and DC offset are negligible. Practically, these problems are inevitable and therefore, it is necessary to study appropriate techniques to combat these impairments and incorporate into the system
- It would better if theoretical error rate performances of different MIMO detection methods are developed. This would enable the researcher focus on his/her objectives. Moreover, theoretical results provide simpler benchmark for simulation results.

Appendix A

General Rules of Complexity Analysis

In this section, basic rules used in the complexity analysis such as complexity of matrix multiplication, conversion from complex complexity figures to real complexity figures, the complexity of slicer and the complexity of finding a minimum value from a set of values are provided.

1) Complexity of Matrix product: consider matrices $\boldsymbol{A}$ and $\boldsymbol{B}$ (real or complex) with dimension C X D and D X E, then the $(i,k)^{th}$ element of the their product matrix is given by:

$$\boldsymbol{a}^{i}\boldsymbol{b}_{k} = \sum_{l=1}^{D} a_{i,l}b_{lk} \quad \ldots\ldots\ldots\ldots\ldots\ldots\ldots\ldots\ldots\ldots\ldots\ldots\ldots\ldots\ldots\ldots\ldots\ldots\ldots\ldots\ldots\ldots (A.1)$$

Where $\boldsymbol{a}^{i}$ is the i^{th} row of matrix A

b_k is the k^{th}column of matrix B

Thus in order to obtain one element of the product matrix $D-1$ additions and D multiplications need to be performed. The resulting matrix is C X E dimensional and therefore, a total of $C(D-1)E$ additions and CDE multiplications are needed. Since in complex addition the real and imaginary parts are added independently, there are two real additions for each complex addition.

$$1C_{ADDs} = 2R_{ADDs} \quad \ldots\ldots\ldots\ldots\ldots\ldots\ldots\ldots\ldots\ldots\ldots\ldots\ldots\ldots\ldots\ldots\ldots\ldots\ldots\ldots\ldots\ldots (A.2)$$

Similarly, a complex multiplication consists of the following operations:

$$1C_{MUL} = 4R_{MULs} + 2R_{ADDs} \quad \ldots\ldots\ldots\ldots\ldots\ldots\ldots\ldots\ldots\ldots\ldots\ldots\ldots\ldots\ldots\ldots\ldots\ldots\ldots\ldots (3)$$

2) Complexity of slicer: is minimal in terms of additions and/or multiplications. M−PSK or M−QAM constellation schemes require $log_2(M)$ comparisons. The complexity of one comparison is equivalent to the complexity of one real addition. Henceforth, the slicing of N_t dimensional vector $\boldsymbol{s}_{est}$ requires at most $N_t.log_2(M)\ R_{ADDs}$. To find a minimum of N numbers, the complexity is equivalent to $N-1\ R_{ADDs}$.

Appendix B

B.1 QR Decomposition Algorithm

The QR decomposition of a matrix $\boldsymbol{H}$ is a factorization that results two output matrices namely, the orthogonal matrix $\boldsymbol{Q}$ and the upper triangular matrix $\boldsymbol{R}$. It can be computed using several algorithms such as Householder reflections, Givens rotations or Gram-Schmidt process. In this thesis, Modified Gram-Scmidt (MGS) process is used for its relatively numerical stability. The following algorithm shows the basic MGS process

Let $\boldsymbol{q}_k$ denote the k^{th} column of matrix $\boldsymbol{Q}$, ${\boldsymbol{q}_k}^H$ the Hermitian transpose of $\boldsymbol{q}_k$ and $r_{k,j}$ the element in the k^{th} row and j^{th} column of $\boldsymbol{R}$. Assume $N_r \mathrm{X} N_t$ channel matrix $\boldsymbol{H}$

$$\boldsymbol{R} = \boldsymbol{0}; \boldsymbol{Q} = \boldsymbol{H}$$
$$for\ k = 0{:}\, N_t - 1$$
$$r_{k,k} = \|q_k\|$$
$$\boldsymbol{q}_k = \boldsymbol{q}_k / r_{k,k}$$
$$for\ j = k + 1{:}\, N_t - 1$$
$${r_{k,j}} = {\boldsymbol{q}_k}^H . \boldsymbol{q}_j$$
$$\boldsymbol{q}_j = \boldsymbol{q}_j - \boldsymbol{q}_k . r_{k,j}$$
$$end$$
$$end$$

Algorithm B.1 Modified Gram-Schmidt Procedure

B.2 Sorted QR Decomposition Algorithm

The MGS algorithm can be extended to compute the sorted QR decomposition [8] which attempts to sort the elements in the main diagonal of $\boldsymbol{R}$ decreasingly in the order they are used by the decoding algorithm, i.e. from bottom right corner to top left corner. This order is backwards to that which these elements are calculated by the MGS algorithm. Therefore the SQRD algorithm attempts, at each iteration, to minimize the element in the main diagonal of $\boldsymbol{R}$ being calculated by swapping the k^{th} column in the $\boldsymbol{Q}$ with the smallest norm still not used. The permutation vector $\boldsymbol{p}$ is used to keep track of the exchanges performed, information required later in the decoding process. Let $conj$ denote the complex conjugate of a value. The MGS algorithm extended to compute the SQRD is shown below

$$\boldsymbol{R} = \boldsymbol{0}; \boldsymbol{Q} = \boldsymbol{H};\ \boldsymbol{p} = [0 \quad 1 \quad \cdots \quad N_t - 1]$$
$$for\ k = 0{:}\,N_t - 1$$
$$norm(k) = \|\boldsymbol{q}_k\|^2$$
$$end$$
$$for\ k = 0{:}\,N_t - 1$$
$$i = \arg \min_{j=k:N_t-1} norm(j)$$
$$Exchnage\ columns\ k\ and\ i\ in\ \boldsymbol{Q}, \boldsymbol{R}, \boldsymbol{p}\ and\ norm$$
$$r_{k,k} = \|\boldsymbol{q}_k\|$$
$$\boldsymbol{q}_k = \boldsymbol{q}_k / r_{k,k}$$
$$for\ j = k + 1{:}\,N_t - 1$$
$$r_{k,j} = \boldsymbol{q}_k{}^H . \boldsymbol{q}_j$$
$$\boldsymbol{q}_j = \boldsymbol{q}_j - \boldsymbol{q}_k . r_{k,j}$$
$$norm(j) = norm(j) - Conj(r_{k,j}) . r_{k,j}$$
$$end$$
$$end$$

Algorithm B.2 The SQRD Algorithm

References

[1] G. J. Foschini and M. J. Gans, "On Limits of Wireless Communications in a Fading Environment When Using Multiple Antennas", *Wireless Personal Communications*, Vol. 6, no. 3, 1998, pp. 311-335.

[2] G. J. Foschini, "Layered space-time architecture for wireless communication in fading environment when using multiple antennas," *Bell Laboratories Technical Journal*, Vol.1, no 2, autumn, 1996, pp. 41-59.

[3] G. L. Stüber, J. R. Barry, S. W. Mclaughlin, Ye (Geoffrey) Li, M. A. Ingram and T. J Pratt, "Broadband MIMO-OFDM Wireless Communications", *Proceedings of the IEEE,* Vol.92, no.2*,* Feb. 2004, pp. 271-294.

[4] Hongwei Yang, "A Road to Future Broadband Wireless Access: MIMO-OFDM-Based Air Interface", *IEEE Communications Magazine*, Vol. 43, No. 1, Jan. 2005 pp. 53-60.

[5] Helmut Bölcskei, "MIMO-OFDM wireless systems: Basics, perspectives, and Challenges", *IEEE Wireless Communications,* Vol. 13, No. 4, Aug. 2006, pp. 31-37.

[6] A. Van Zelst and T.C. W. Schenk, "Implementation of MIMO OFDM based wireless LAN system", *IEEE Transaction on Signal Processing*, Vol. 52, No. 2, Feb. 2004, pp. 483-94.

[7] P. W. Wolniansky, G. J. Foschini, G. D. Golden, and R. A. Valenzuela, "V-BLAST: an architecture for realizing very high data rates over the rich-scattering wireless channel," in *Proc. International Symposium on Signals, Systems, and Electronics (ISSSE '98)*, Sept. 1998, pp. 295–300.

[8] D. W¨ubben, R. B¨ohnke, V. K¨uhn, and K.−D. Kammeyer, "MMSE extension of V-BLAST based on sorted QR decomposition," in *Proc. IEEE 58th Vehicular Technology Conference (VTC '03)*, vol. 1, Oct. 2003, pp. 508–512.

[9] D. Wübben, R. Böhnke, J. Rinas, V. Kühn, and K.−D. Kammeyer, "Efficient algorithm for decoding layered space-time codes," *Electronics letters*. Vol. 37, No. 22, Oct. 2001, pp. 1348-1540.

[10] A. van Zelst, "Space division multiplexing algorithms", in *proc. Of the 10th Symposium on Communications and Vehicular technology in the Belenux (STVT 2003)*, Vol. 13, Nov. 2003, pp. 1218-1221.

[11] R. van Nee, A. van Zelst and G. A. Awater, “Maximum Likelihood Decoding in a Space Division Multiplex System”, *51st IEEE Veh. Tech. Conf. (VTC) 2000-Spring*, Japan, Vol. 1, May 2000, pp. 6-10.

[12] D.W¨ubben, R. B¨ohnke, V. K¨uhn, and K.−D. Kammeyer, “Near-maximum-likelihood detection of MIMO systems using MMSE-based lattice reduction,” in *Proc. IEEE Int. Conf. on Commun. (ICC ’04)*, Paris, France, Vol. 2, June 2004, pp. 798-802.

[13] A. van Zelst, R. van Nee and G. A. Awater, “Space Division Multiplexing (SDM) for OFDM systems”, *51st IEEE Veh. Tech. Conf. (VTC) 2000-Spring Proceedings*, Japan, vol. 2, May 2000, pp. 1070-1074.

[14] Geert Awater, Allert van Zelst and Richard van Nee “Reduced Complexity Space Division Multiplexing Receivers,” *51st IEEE Veh. Tech. Conf. (VTC) 2000-Spring Proceedings*, Tokyo, Vol. 1, May 2000, pp. 11-15.

[15] A.A.M. Saleh and R.A. Valenzuela, “A statistical model for indoor multipath propagation,” *IEEE J. Select. Areas Commun.*, vol. 5, 1987, pp. 128-137.

[16] Q. H. Spencer, et al., “Modeling the statistical time and angle of arrival characteristics of an indoor environment,” *IEEE J. Select. Areas Commun.*, vol. 18, no. 3, March 2000, pp. 347-360.

[17] G. German, Q. Spencer, L. Swindlehurst, and R. Valenzuela, “Wireless indoor channel modeling: Statistical agreement of ray tracing simulations and channel sounding measurements,” *in proc. IEEE Acoustics, Speech, and Signal Proc. Conf.*, vol. 4, 2001, pp. 2501-2504.

[18] A. van Zelst, "MIMO OFDM for wireless LANs", Ph.D. dissertation, Department of Electrical Engineering, Eindhoven University of Technology, April 2004.

[19] Erceg, V. et al. “TGn Channel Models.” Doc. IEEE802.11-03/940r4

[20] Schumacher, L., Pedersen, K. I., Mogensen, P.E., "From antenna spacing to theoretical capacities - guidelines for simulating MIMO systems", *13th IEEE Int. Syymp. on Personal, Indoor and Mobile Radio Communications, 2002*, vol.2, Sept. 2002, pp. 587-592.

[21] John G. Proakis, *Digital Communications*, Fourth Edition, New York, McGraw-Hill, 2000, McGraw-Hill Series in Electrical and Computer Engineering

[22] Rappaport, T. S., *Wireless Communications. Principles and Practice*, Prentice Hall, New Jersey, 1996

[23] Jakes, W.C., *Microwave Mobile Communications*, New York: Wiley, 1974

[24] A. Van Zelst and J. S. Hammerschmidt, "A single coefficient spatial correlation model for multiple input multiple output (MIMO) radio channels", in *Proc. of the* 27^{th} *General Assembly of the International Union of Radio Science (URSI),* Maastricht, The Netherlands, Aug 2002

[25] A. Van Zelst, "A compact Representation of spatial correlation in MIMO radio channels", Submitted to *International Conference on Communications (ICC) 2004,* Paris, June 2004

[26] P. Kyritis, D. C. Cox, "Correlation Properties of MIMO Radio Channels for Indoor Scenarios", *IEEE Conference on Signals, Systems and Computers*, Pacfic Grove, CA, vol. 2, Aug. 2002, pp 994-998.

[27] Da-Shan Shiu, G. J. Foschini, M. J. Gans and J. M. Kahn, "Fading correlation and its effect on the capacity of multi-element antenna systems", *IEEE Transactions on Communications*, vol. 48, no. 3, March 2000, pp. 502-513.

[28] K.−D. Kammeyer, J. Rinas and D. Wübben: Architectures for Reference-Based and Blind Multilayer Detection, Chapter in Book*: Smart Antennas in Europe -- State-of-the-Art*, Hindawi, 2005

[29] A. Benjebbour, H. Murata, and S. Yoshida, "Comparison of Ordered Successive Receivers for Space-Time Transmission", in *Proc. IEEE Vehicular Technology Conference (VTC)*, Atlantic City, NJ , USA, Vol. 4, Fall 2001, pp. 2053-2057.

[30] U. Fincke and M. Pohst, "Improved methods for calculating vectors of short length in a lattice, including a complexity analysis", *Mathematics of Computation*, vol. 44, no. 4, April 1985, pp. 463-471.

[31] C. P. Schnorr and M. Euchner, "Lattice basis reduction: improved practical algorithms and solving subset sum problems", *Mathematical Programming*, vol. 66, no. 2, Sept. 1994, pp. 181-191.

[32] E. Viterbo and J. J. Boutros, "A universal lattice decoder for fading channels," *IEEE Transaction on Information Theory*, vol. 45, no. 5, Jul. 1999, pp. 1639–1642.

[33] B. Hassibi and H. Vikalo, "on the sphere-decoding algorithm I. expected complexity", *IEEE Transaction on Signal Processing*, vol. 53, Aug. 2005, pp. 2806-2818.

[34] Y. L. de Jong and T. J. Willink, "Iterative tree search detection for MIMO wireless systems," *Proc. IEEE 56th Veh. Tech. Conf.*, Vol. 2, Sept. 2002, pp. 1041-1045.

[35] M. O. Damen, H. El Gamal, and G. Caire, "On maximum-likelihood detection and the search for the closest lattice point," *IEEE Trans. Inf. Theory*, Vol. 49, No. 10, Oct. 2003, pp. 2389–2402.

[36] E. Agrell, T. Eriksson, A. Vardy, and K. Zeger, "Closest point search in lattices," *IEEE Trans. Inf. Theory*, Vol. 48, No. 8, Aug. 2002, pp. 2201–2214.

[37] A. Burg, M.Wenk, M. Zellweger, W. Fichtner, and H. Bolcskei, "VLSI Implementation of MIMO Detection Using the Sphere Decoding Algorithms", *IEEE J. of Solid State Circuits,* Vol. 40, No. 7, July 2005, pp. 1566-1576.

[38] Zhan Guo and P. Nilsson, "Algorithm and implementation of the K-best sphere decoding for MIMO detection", *IEEE J. Select. Areas Commun.*, Vol. 24, No. 3, March 2006, pp. 491-503.

[39] Qingwei Li and Zhongfeng Wang, "Improved K-Best sphere decoding algorithms for MIMO systems", *Proc. IEEE Int. Symp. on Circuits and Systems,* Kos, Greece, Sept. 2006, pp. 1159-1162.

[40] Qingwei Li and Zhongfeng Wang, "New sphere decoding architecture for MIMO Systems." *Proc. IEEE 13th NASA Symposium on VLSI Designs,* Post Falls, Idaho, June 2007

[41] Qingwei Li and Zhongfeng Wang, "Early-Pruning K-Best sphere decoder for MIMO systems." *Proc. IEEE Workshop on Signal Processing Systems (SiPS 2007)*, Shanghai, Oct. 2007, pp. 40-44.

[42] A. M. Chan and I. Lee, "A new reduced complexity sphere decoder for multiple antenna systems", *Proceedings of IEEE International Communications Conference*, New York, USA, April 2002, pp. 460-464

[43] K. W. Wong, C. Y. Tsui, R. S. K. Cheng, and W. H. Mow, "A VLSI architecture of a K-best lattice decoding algorithm for MIMO channels," *IEEE ISCAS 02,* Vol. 3, Aug. 2002, pp. 273-276.

[44] Johanna Ketonen, Markku Juntti and Joseph R. Cavallaro**, "**Performance-Complexity Comparison of Receivers for a LTE MIMO-OFDM System," *IEEE transactions on signal processing*, Vol. 58, No. 6, June 2010, pp. 3360-3372.

[45] Pankaj Bhagawat, Gwan Choi, "Staggered Sphere Decoder", *Technical Report TAMU-ECE*, March 2007

[46] H. L. Chiang and S. G. Chen, "An Efficient Hybrid Sphere Decoding Algorithm for MIMO Systems", *IEEE 10th international Symposium on Spread Spectrum Techniques and Applications, ISSSTA '08*, Bologna, Italy, Aug. 2008, pp 339-343

[47] L. Barbero and J. Thompson, "Rapid Prototyping of a Fixed-Throughput Sphere Decoder for MIMO Systems", IEEE *International Conference on Communications (ICC '06)*, Istanbul, Jun. 2006, pp. 3082-3087.

[48] B Hochwald and S. ten Brink, "Achieving near-capacity on a multiple-antenna channel", *IEEE Transactions on Communications*, Vol. 51, No. 3, March 2003, pp. 389 – 399

[49] M. Wenk, M. Zellweger, A. Burg, N. Felber, W. Fichtner, "K-Best MIMO detection VLSI architectures achieving up to 424 Mbps", *Proc. IEEE-ISCAS'06*, May 2006, pp. 1151-1154.

[50] T. Fujita, T. Onizawa, W. Jiang, D. Uchida, T. Sugiyama and A. Ohta, "A New Signal Detection Scheme Combining ZF and *K*-best Algorithms for OFDM/SDM," *IEICE Technical Report, RCS2003-266*, January. 2004.

[51] A. Wiesel, X. Mestre, A. Pages, and J. R. Fonollosa, "Efficient implementation of sphere demodulation", *IEEE Workshop on Signal Processing Advanced in Wireless Communications*, 2003, pp. 36-40.